CONTROL OF THE TEXTURE OF GEL-SILICA BY AGING

BY

SHUYUAN LIU

A DISSERTATION PRESENTED TO THE GRADUATE SCHOOL
OF THE UNIVERSITY OF FLORIDA IN PARTIAL FULFILLMENT
OF THE REQUIREMENTS FOR THE DEGREE OF
DOCTOR OF PHILOSOPHY

UNIVERSITY OF FLORIDA

1991

To my wife, Rounan, with gratitude
for her patience and support

ACKNOWLEDGMENTS

I would like to express my sincere gratitude to Dr. Larry L. Hench, chairman of my supervisory committee, for his guidance, support and encouragement.

I also wish to express my appreciation to the other members of the committee, Dr. D.E. Clark, Dr. F. Ebrahimi, Dr. E.D. Whitney and Dr. K.B. Wagener, for their patience, understanding and helpful comments.

My special thanks goes to Dr. J.K. West for suggestions and discussions during this research.

I wish to thank Guy P. La Torre at the AMRC for his assistance during the work.

Further, I wish to thank Dr. R. Ochoa and Dr. J. Simmons for skillful assistance in the laser test.

Financial support from the Air Force Office of Scientific Research under contract #F49620-88-C-0073 is gratefully acknowledged.

TABLE OF CONTENTS

Page

ACKNOWLEDGMENTS iii

LIST OF TABLES vii

LIST OF FIGURES ix

ABSTRACT xvii

CHAPTERS

I INTRODUCTION 1

- 1.1 Silica Glasses 1
  - 1.1.1 Traditional Types 2
  - 1.1.2 Two New Types Derived from the Sol-Gel Processing 8
- 1.2 Objectives 11

II SOL-GEL PROCESSING 15

- 2.1 Historical Review 15
- 2.2 Aqueous and Alcohol Gels 19
- 2.3 Processing Steps for Making Alcohol Gel-Silica 26

III CONTROL OF THE TEXTURE OF GEL-SILICA 38

- 3.1 Introduction 38
- 3.2 Textural Control by Catalysts 39
- 3.3 Textural Control by Densification 43
- 3.4 Textural Control by Aging 47
  - 3.4.1 Introduction 47
  - 3.4.2 Aging Concepts 48
  - 3.4.3 Changes during Aging 49
    - 3.4.3.1 Condensation 50
    - 3.4.3.2 Syneresis 51
    - 3.4.3.3 Coarsening 52
    - 3.4.3.4 Properties 53
  - 3.4.4 Aging Parameters which Affect the Texture 56

IV AGING TREATMENTS OF ALCOHOL GEL-SILICA MONOLITHS..... 62

4.1 Experimental Procedures.......................... 62
    4.1.1 Gel Preparation......................... 62
    4.1.2 Aging Treatment......................... 65
    4.1.3 Drying.................................. 70
    4.1.4 Stabilization and Densification.......... 72
4.2 Texture Measurement............................ 74
    4.2.1 BET Theory.............................. 74
    4.2.2 BET Equipment........................... 82
4.3 Property Characterization...................... 84
    4.3.1 Density................................. 84
    4.3.2 Microhardness........................... 85
    4.3.3 UV-VIS-NIR Spectra...................... 85
    4.3.4 pH Measurement.......................... 86
    4.3.5 Si Ion Concentration Measurement......... 86

V TEXTURE AND PROPERTY CHANGES OF GEL-SILICA........... 87

5.1 Textural Changes............................... 87
    5.1.1 Surface Area, Pore Volume and Pore Radius........................ 87
    5.1.2 Pore Shape and Pore Size Distribution........................... 119
5.2 Property changes...............................133
    5.2.1 Appearance and Dimension.................133
    5.2.2 Density..................................139
    5.2.3 Mechanical Strength......................143
    5.2.4 Densification Behavior...................155
    5.2.5 Optical Properties.......................176

VI POSSIBLE AGING MECHANISMS...........................194

6.1 Aging Mechanisms...............................194
6.2 Model for Aging Process........................206
    6.2.1 Model A................................. 210
    6.2.2 Model B................................. 213
6.3 Molecular Orbital Calculations.................216

VII APPLICATIONS OF GEL-SILICA TREATED BY NH_4OH..........233

7.1 Solid State Dye Laser..........................233
7.2 Experimental Procedures........................238
7.3 Results and Discussion.........................242
    7.3.1 Texture Effects......................... 242
    7.3.2 Dye Concentration Effects............... 247
    7.3.3 Impregnation Temperature Effects......... 256
7.4 Conclusion.....................................261

VIII SUMMARY AND CONCLUSIONS...........................262

REFERENCES..271

BIOGRAPHICAL SKETCH...288

LIST OF TABLES

Table		Page
1.1	Processing and impurity concentration of the different types of silica glasses.............	3
1.2	Properties of the different types of silica glasses...	4
2.1	Major differences between aqueous gels and alcohol gels.....................................	25
2.2	Characteristics and properties of Type VI gel-silicas.......................................	35
4.1	Recipe of gel-silica samples......................	64
5.1	Textural change of gel-silica samples.............	99
5.2	Textural change as a function of aging time for gel-silica samples aged in a 0.01 N NH_4OH solution at 25°C...........................	104
5.3	Textural change as a function of NH_4OH concentration for gel-silica samples aged in NH_4OH solution at 25°C for 1 day...............	115
5.4	The effect of atmosphere in drying chamber on gel textures....................................	117
5.5	Variation of microhardness as a function of aging time for gel-silica samples aged in a 1 N NH_4OH solution at 25°C then dried at 180°C..................................	151
5.6	Contraction of gel-silica samples after aging, drying and stabilization.........................	156
5.7	Identification of molecular vibrations in gel-silica optical spectra.......................	178
5.8	Absorption peaks of the pore water and the surface hydroxyl groups of gel-silica monoliths.............................	179

5.9 Variation of texture as a function of heat-treatment temperature for gel-silica samples aged in a 0.25 N NH_4OH solution at 25°C for 24 hours 192

6.1 Variation of Si ion concentration in the solution as a function of aging time for gel-silica samples aged in NH_4OH solution at 25°C 203

6.2 Heteroatom parameters 220

6.3 Some representative bond energies and k-parameters 223

6.4 Results of Huckel molecular orbital calculation for hydrolysis reactions 224

6.5 Results of Huckel molecular orbital calculation for condensation reactions 226

7.1 Different types of laser 234

7.2 Advantages of solid state dye lasers 236

7.3 Texture characterization of gel-silica aged in a 0.5 N NH_4OH solution at 25°C for 4 days 245

7.4 Texture effects on lasing characteristics of 4PyPO-MePTS impregnated (at 25°C) gel-silica specimens 246

7.5 Texture effects on lasing characteristics of 4PyPO-MePTS impregnated (at 45°C) gel-silica specimens 257

7.6 Lasing characteristics of 4PyPO-MePTS impregnated (at 45°C) 90 Å gel-silica specimen 258

LIST OF FIGURES

Figure Page

1.1 Optical transmission of different types of vitreous silica.................................. 7

1.2 Sol-gel processing steps........................... 10

2.1 Effect of surface curvature on OH coverage and hydrogen bonding............................... 23

3.1 Hydrolysis rate of (a) TEOS with HCl catalysis (b) TMOS with HCl catalysis and (c) TMOS with NH_3 catalysis................................ 41

3.2 Variation of average pore radius of 12 Å gel-silica samples as a function of densification temperature....................... 44

3.3 Variation of the surface area of pores per unit volume (Sv) and the volume fraction of pores (Vv) of 12 Å gel-silica samples as a function of densification temperature......... 46

3.4 Definition of positive and negative radii of curvature.................................... 54

4.1 Flowchart of experiments A, B and C................ 63

4.2 Schematic illustration of gelation and aging schedules for experiment A................... 66

4.3 Schematic illustration of gelation and preaging schedules for experiment B................ 67

4.4 Schematic illustration of drying schedule for gel-silica samples............................ 71

4.5 Schematic illustration of stabilization and densification schedules for gel-silica samples.. 73

4.6 Five types of adsorption isotherms................. 78

4.7 de Boer's five types of hysteresis loops........... 80

4.8 Three important types of hysteresis loops.......... 81

5.1 Variation of surface area of gel-silica samples aged in pore liquid at various temperatures as a function of time................. 88

5.2 Variation of surface area of gel-silica samples aged in pore liquid for various times as a function of temperature................. 89

5.3 Variation of pore volume of gel-silica samples aged in pore liquid at various temperatures as a function of time................. 90

5.4 Variation of total pore volume of gel-silica samples aged in their pore liquid for various times as a function of temperature................. 91

5.5 Variation of average pore radius of gel-silica samples aged in pore liquid at various temperatures as a function of time.. 92

5.6 Variation of average pore radius of gel-silica samples aged in pore liquid at various times as a function of temperature................................. 93

5.7 Variation of slope (S) of pore size vs time plots as a function of temperature.. 95

5.8 Log S vs. 1/T.................................... 97

5.9 Time effect on surface area of gel-silica samples aged in NH_4OH solution with various concentrations at 25°C................ 100

5.10 Time effect on total pore volume of gel-silica samples aged in NH_4OH solution with various concentrations at 25°C................ 101

5.11 Time effect on average pore radius of gel-silica samples aged in NH_4OH solution with various concentrations at 25°C................ 102

5.12 Temperature effect on the surface area of gel-silica samples aged in NH_4OH solution with various concentrations for 1 day.............. 105

5.13 Temperature effect on the total pore volume of gel-silica samples aged in NH_4OH solution with various concentrations for 1 day.............. 106

5.14 Temperature effect on average pore radius of gel-silica samples aged in NH_4OH solution with various concentrations for 1 day.............. 107

5.15 Concentration effect on surface area of gel-silica samples aged in NH_4OH solution at different temperatures for 1 day................ 108

5.16 Concentration effect on total pore volume of gel-silica samples aged in NH_4OH solution at different temperatures for 1 day................ 109

5.17 Concentration effect on average pore radius of gel-silica samples aged in NH_4OH solution at various temperatures for 1 day.................. 110

5.18 Concentration effect on surface area of gel-silica samples aged in dilute NH_4OH solution at different temperatures for 1 day.. 112

5.19 Concentration effect on total pore volume of gel-silica samples aged in dilute NH_4OH solution at different temperatures for 1 day....... 113

5.20 Concentration effect on average pore radius of gel-silica samples aged in dilute NH_4OH solution at different temperatures for 1 day.. 114

5.21 Variation of nitrogen sorption hysteresis as a function of time for gel-silica samples aged in a 1 N NH_4OH solution at 25°C 123

5.22 Variation of nitrogen sorption hysteresis as a function of time for gel-silica samples aged in a 0.01 N NH_4OH solution at 25°C... 125

5.23 Variation of nitrogen sorption hysteresis as a function of NH_4OH concentration for gel-silica samples aged in NH_4OH solution at 60°C for 1 day................................ 126

5.24 Variation of pore size distribution as a function of time for gel-silica samples aged in a 1 N NH_4OH solution at 25°C.............. 129

5.25 Variation of pore size distribution as a function of time for gel-silica samples aged in a 0.01 N NH_4OH solution at 25°C............ 130

5.26 Variation of pore size distribution as a function of NH_4OH concentration for gel-silica samples aged in NH_4OH solution at 60°C for 1 day................................ 132

5.27 Variation of contraction as a function of aging temperature for wet gel-silica samples aged in their pore liquid for various times........ 135

5.28 Variation of contraction as a function of aging time for wet gel-silica samples aged in their pore liquid at various temperatures....... 136

5.29 Variation of contraction as a function of aging temperature for wet gel-silica samples aged in a 14 N NH_4OH solution for various times................................ 137

5.30 Variation of contraction as a function of aging time for wet gel-silica samples aged in a 14 N NH_4OH solution at various temperatures..................................... 138

5.31 Variation of bulk density as a function of aging temperature for wet gel-silica samples aged in their pore liquid for various times.. 141

5.32 Variation of bulk density as a function of aging time for wet gel-silica samples aged in their pore liquid at various temperatures..................................... 142

5.33 Theoretical relationship between volume fraction of porosity, bulk density and total pore volume of gel-silica samples................. 144

5.34 Variation of bulk density as a function of time for gel-silica samples aged in a 14 N NH_4OH solution at 45°C.................. 145

5.35 Variation of microhardness as a function of time for wet gel-silica samples aged in the pore liquor at different temperatures.......... 147

5.36 The appearance of gel-silica samples aged in their pore liquid at various temperatures for different periods of time...................... 149

5.37 Variation of microhardness after drying at 180°C as a function of temperature for gel-silica samples aged in dilute NH_4OH solution with various concentrations for 1 day... 152

5.38 Variation of microhardness as a function of concentration of NH_4OH for gel-silica samples aged in NH_4OH solution at various temperatures for 1 day............................. 153

5.39 Variation of microhardness as a function of concentration of NH_4OH for gel-silica samples aged in dilute NH_4OH solution at various temperatures for 1 day............................. 154

5.40 Contraction with densification temperature for gel-silica samples aged in a 0.25 N NH_4OH solution at 25°C for 1 day........................ 158

5.41 Variation of microhardness as a function of densification temperature for gel-silica samples aged in a o.25 N NH_4OH solution at 25°C for 1 day.................................. 161

5.42 Variation of surface area of 90 Å average radius gel-silica samples as a function of processing temperature............................ 163

5.43 Variation of total pore volume of 90 Å average radius gel-silica samples as a function of processing temperature............................ 164

5.44 Variation of average pore radius of 90 Å average radius gel-silica samples as a function of processing temperature................. 165

5.45 Cylindrical geometric model....................... 169

5.46 Variation of surface area per unit volume (Sv) as a function of processing temperature for 90 Å average radius gel-silica samples............................... 171

5.47 Variation of volume fraction of porosity (Vv) as a function of processing temperature for 90 Å average radius gel-silica samples.................................. 172

5.48 Variation of number of branches (Bv) of 90 Å average radius gel-silica samples as a function of processing temperature................. 173

5.49 Variation of number of branches (Bv) as a function of processing temperature for gel-silica samples with 12 Å, 32 Å and 90 Å average radius..................................... 174

5.50 UV-VIS-NIR spectrum of 90 Å gel-silica samples dried at 180°C............................. 180

5.51 UV-VIS-NIR spectrum of 90 Å gel-silica samples heat-treated at 400°C...................... 181

5.52 UV-VIS-NIR spectrum of 90 Å gel-silica samples heat-treated at 600°C...................... 182

5.53 UV-VIS-NIR spectrum of 90 Å gel-silica samples heat-treated at 800°C...................... 183

5.54 UV-VIS-NIR spectrum of 90 Å gel-silica samples heat-treated at 1000°C..................... 184

5.55 UV-VIS-NIR spectrum of 90 Å gel-silica samples heat-treated at 1100°C..................... 185

5.56 UV-VIS-NIR spectrum of 90 Å gel-silica samples heat-treated at 1150°C..................... 186

5.57 UV-VIS-NIR spectrum of 90 Å gel-silica samples heat-treated at 1200°C..................... 187

5.58 UV-VIS-NIR spectrum of (a) 90 Å gel-silica samples heat-treated at 1200°C for 4 hours and (b) commercial fused silica (Type III) cuvette.. 189

5.59 UV-VIS-NIR spectrum of 90 Å gel-silica samples heat-treated at 1000°C, then placed in open air for different times................... 191

5.60 UV cutoffs for Types II and III optical silica, Type V fully dens gel-silica and Type VI porous optical matrices.................... 193

6.1 Variation of pH as a function of NH_4OH concentration.. 196

6.2 Variation of pH as a function of initial concentration of NH_4OH solution in which the gel-silica samples were aged for 1 day at different temperatures................ 197

6.3 Variation of pH as a function of initial concentration of initial NH_4OH solution (dilute) before and after aging at different temperatures for 24 hours.......................... 198

6.4 Solubility of amorphous silica versus pH at different temperatures.......................... 200

6.5 Variation of Si ion concentration in solution as a function of aging time for gel-silica samples aged at 25°C in (a) 0.10 N and (b) 0.25 N NH_4OH.................... 201

6.6 Variation of Si ion concentration in solution as a function of aging temperature for gel-silica samples aged in a 0.10 N NH_4OH for 4 days................................. 202

6.7 Dissolution and reprecipitation cause growth of necks between particles 205

6.8 Proposed model of textural evolution during aging for gel-silica samples aged in their pore liquor.. 208

6.9 Proposed model of textural evolution during aging for gel-silica samples aged in an NH_4OH solution................................209

6.10 Schematic illustration of bond formation resulting in shrinkage of the gels................. 212

6.11 UV spectrum of D.I. water......................... 222

6.12 Schematic illustration of proposed step 1 of condensation reaction: two trisiloxane rings encounter each other........................ 227

6.13 Schematic illustration of proposed step 2 of condensation reaction: the formation of pentacoordinated intermediate state................ 228

6.14 Schematic illustration of proposed step 3 of condensation reaction: the formation of hydrogen bonded water.................................. 229

6.15 Schematic illustration of proposed step 4 of condensation reaction: the formation of Si-O-Si bond and the removal of water.............. 230

6.16 Variation of Huckel molecular energy as a function of reaction steps 232

7.1 4PyPO-MePTS laser dye............................... 240

7.2 UV spectra for (a) 6 x 10^{-3} M 4PyPO-MePTS dye solution, (b) porous gel-silica matrix with 100 Å average pore radius and (c) gel-silica matrix (100 Å) impregnated with 6 x 10^{-3} M 4PyPO-MePTS dye solution with dye solution.................................. 243

7.3 UV spectrum of 1 x 10^{-2} M 4PyPO-MePTS dye solution....................................... 248

7.4 UV spectrum of 1 x 10^{-3} M 4PyPO-MePTS dye solution....................................... 249

7.5 UV spectrum of 1.875 x 10^{-4} M 4PyPO-MePTS dye solution....................................... 250

7.6 UV spectrum of 1.1718 x 10^{-5} M 4PyPO-MePTS dye solution....................................... 251

7.7 Variation of total output energy as a function of concentration of dye solution.......... 254

7.8 Variation of peak ratio as a function of concentration of dye solution................... 255

7.9 Schematic illustration of surface structure........ 260

Abstract of Dissertation Presented to the Graduate School of
the University of Florida in Partial Fulfillment of the
Requirements for the Degree of Doctor of Philosophy

CONTROL OF THE TEXTURE OF GEL-SILICA BY AGING

By

Shuyuan Liu

December, 1991

Chairman: Dr. Larry L. Hench
Major Department: Materials Science and Engineering

A novel approach to control the texture of gel-silica monoliths has been investigated. The gel texture can effectively be controlled by an aging treatment rather than by changing catalysts and other processing parameters.

Two different mechanisms which may dominate the aging process are proposed: one is a chemical condensation reaction and the other Ostwald ripening. The dominating mechanism depends upon the nature of the aging medium.

After aging treatments in NH_4OH solutions (concentration varied from 1 x 10^{-3} N up to 14.5 N) at certain temperatures (from 5 to 80°C) for certain periods of time (from 5 minutes up to 60 days), the surface area, the total pore volume and the average radius of dried gel-silica samples can be controlled in the range of 770 m^2/g to 200 m^2/g, 0.50 cm^3/g to 1.15 cm^3/g and 12 Å to 135 Å respectively. Very narrow distributions of pore sizes around the mean pore radius can be obtained using controlled aging treatments. Gas adsorption isotherm hysteresis loops show that ink-bottle necked pores inside gel-silica monoliths can also be changed into cylindrical pore cross sections by aging treatment.

Dried porous gel-silica monoliths with aging controlled textures are easy to stabilize at temperature ranging from 700°C to 1100°C. The resultant stabilized monoliths are strong, optically transparent, and capable of being impregnated with a large volume fraction of organic molecules to make a unique class of optical composites. Another remarkable feature of this kind of large pore size gel-silica is that it can be fully densified at 1150°C, within 40 hours in an open air box furnace without any chemical dehydration treatment such as chlorination or gas flow, and without foaming which is a common problem in the densification of gel-silica monoliths.

Gel-silica with controlled texture, especially larger size pores, larger volume fraction of porosities and cylindrical pore shapes, has many potential applications. Solid state dye lasers made by using the aging controlled gel-silica matrices (average pore radius > 90 Å, total pore volume > 1.00 cm^3/g) and impregnated with laser dye 4PyPO-MePTS showed good lasing characteristics.

CHAPTER I
INTRODUCTION

1.1 Silica Glasses

Silica, a short convenient designation for "silicon dioxide" (SiO_2) in all its crystalline, amorphous, and hydrated or hydroxylated forms, is by far the major component of the crust of the earth. It has been found that oxygen and silicon account for 50% and 26% of the elements in the earth's crust respectively [1]. Since SiO_2 is inexpensive, hard, chemically stable, and relatively infusible and has the ability to form glasses, it is widely used in most glasses, glazes, enamels, refractories, abrasives, and whiteware compositions.

Silica (SiO_2) glasses or vitreous silicas made by pure silica are desired for many optical systems because they have high purity, high-temperature stability, low coefficients of thermal expansion (CTE), high thermal shock resistance, very low electrical conductivity and dielectric loss, very high chemical durability, and a wide range of high optical transparency; they are isotropic and can be fabricated and polished to high standards.

1.1.1. Traditional Types

Four traditional types of silica glasses have been available commercially, each with its own manufacturing method (Table 1.1) and characteristic properties (Table 1.2) [2-4].

The most common process for producing silica glasses involves the melting of naturally occurring silica at the temperature above its liquidus (1713°C), usually 1800 to 2000°C. Although there are a variety of mineral forms in which silica naturally occurs, the most important as a raw material is quartz. The glasses resulting from this process are called Type I and II [2] silica glasses, commonly called fused quartz. Type I is obtained by electric arc melting of natural quartz crystals, whether chunks or grains, under vacuum or in an inert or reducing atmosphere as indicated by eq. (1.1)

$$SiO_2 \text{ (quartz)} \xrightarrow[\text{vacuum}]{\text{heat}} SiO_2 \text{ (glass)} \qquad (1.1)$$

while Type II is made by flame fusion of natural quartz:

$$SiO_2 \text{ (quartz)} \xrightarrow[O_2+H_2]{\text{heat}} SiO_2 \text{ (glass)} \qquad (1.2)$$

Since Types I and II silica glasses are melted from crushed natural crystalline quartz powders of mixed particle

Table 1.1
Processing and impurity concentration
of the different types of silica glasses

Type	Method of manufacture	Maximum impurity concentration (ppm)								
		Al	Fe	Ca	Mg	K	Na	Li	Cl	OH
I*	Electrical fusion of quartz crystal	150	7	12	7	4	12	12	50	4
II*	Flame fusion of quartz crystal	Similar to I								400
III*	Flame hydrolysis of $SiCl_4$	10	6	4	3	2	2	1	60	1200
IV*	Vapor phase oxidation of $SiCl_4$	Similar to III							500	low
V**	Dense Gel-silica	Total cation: 1-2							0-1000	<1
VI**	Porous Gel-silica	Similar to V							>2000	0

* [2]

** [3]

Table 1.2
Properties of the different types of silica glasses

	Properties				
Type	UV (50% trans.) (nm)	TEC (cm/cm) x 10^6	Refractive index n_D	Dispersion v_D ($Å^{-1}$)	Density (g/cc)
I	212-223	0.54	1.458	67.8±0.5	2.21
II	210-220	0.55	1.458	67.8±0.5	2.21
III	165-188	0.55 to 0.57	1.458	67.8±0.5	2.20
IV	165-180	0.55	1.458	67.8±0.5	2.20
V	165-168	0.2	1.458 to 1.463	67.8 to 66.4±0.5	2.20
VI	250-300	-	1.28 to 1.45	-	1.30 to 2.10

Source: [3]

size well above micrometers in diameter, they have numerous deficiencies including considerable cation impurities (Type I), hydroxyl impurities (Type II), inhomogeneities, seeds, bubbles, inclusions, and microcrystallites [5]. The relative extent of these defects depends on the grade of the products, with a corresponding increase in cost for the better grades.

Type III (flame hydrolysis of silicon tetrachloride) optical silica is made by vapor-phase hydrolysis of pure silicon tetrachloride carried out in a flame [2]:

$$SiCl_4 + O_2 + 2H_2 \rightarrow SiO_2 \text{ (glass)} + 4HCl \qquad (1.3)$$

Type IV (vacuum plasma oxidation of silicon tetrachloride) optical silica is made by oxidation of pure silicon tetrachloride which is subsequently fused electrically or by means of a plasma:

$$SiCl_4 + O_2 \rightarrow SiO_2 \text{ (glass)} + Cl_2 \qquad (1.4)$$

Both Types III and IV silica glasses are usually termed synthetic fused silica. The cation impurity content of fused silica is substantially lower than in Types I and II, because of the high purity of $SiCl_4$ used in the processing of Types III and IV [4]. However, it is difficult for the reactions indicated in eqs. 3 and 4 to go to completion.

Consequently, water contents of several thousand ppm are present in Type III silica, and Cl ion in a few hundred ppm is retained as an unreacted residual in both Types III and IV silica [3].

The variations in impurity content of Type I-IV silica significantly affect optical transmission. The optical transmission of Types I and III silica from 0.16 to 5 µm is shown in Figure 1.1 [6]. Type I fused quartz offers excellent transmission in the visible and near IR but gives rise to a UV cutoff at longer wavelengths and UV absorption due to cation impurities. IR absorption of Type II fused quartz can also occur due to residual OH ions in the glass. Type III fused silica has excellent UV transmission but substantial absorption in the NIR and IR due to OH ions in the glass. Type IV silica has good NIR and IR transmission with the UV cutoff and absorption dependent upon processing. There is relatively little variation in the coefficient of thermal expansion (CTE), hardness, density, refractive index, or dispersion of Type I-IV vitreous silica [3]. However, because of the differing manufacturing methods there are significant differences in structural features such as striae, residual strain, bubbles, inclusions, and index inhomogeneity. All these shortcomings limit the use of Types I-IV silica glasses in specific applications.

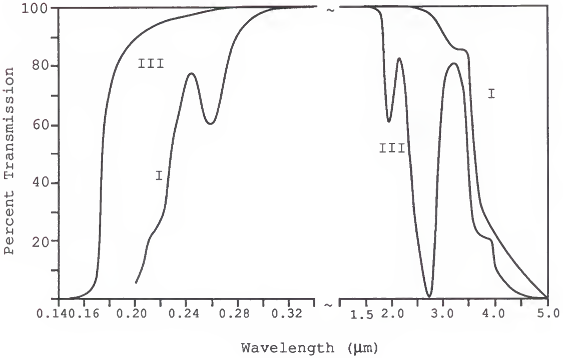

Figure 1.1 Optical transmission of different types (see Table 1.1) of vitreous silica [6].

1.1.2 Two New Types Derived from the Sol-Gel Processing

The sol-gel processing for making silica glasses has been receiving increased attention because of the recognized advantages inherent in the processing. The outstanding features of the resultant silicas, including very high homogeneity, very high purity, extremely low optical loss, near net shape casting including the ability to form desired internal cavities using a lost wax process, and relatively low processing temperature, make them potentially applicable to a wide range of optical products such as lenses, mirrors, and optical fibers. In addition, sol-gel processing offers hope that sufficient structural manipulation is possible on an extremely fine scale, within the nanometer range for ease of chemical doping, thereby allowing production of a new generation of silica materials which can be used in the following fields [3]:

1. Integrated optoelectronics.
2. Host for atoms and molecules.
3. Matrices for doping or impregnation.
4. Lenses with graded refractive indices.
5. Planer waveguides and multiplexers.
6. Fast radiation hard scintillators.
7. Transpiration cooled optical component.
8. Pure silica matrix glass laser.

9. Tunable solid state dye laser.
10. Optical filters.
11. Wavelength shifters
12. Non-linear optical elements of compounds, etc.

During the last few years two new types of silica glasses called gel-silica glasses: Type V and Type VI have been developed using sol-gel processing [7-9]. The process schedule for those two types is shown schematically in Figure 1.2. The properties of Type I and Type II fused quartz optics and Types III and IV synthetic fused silica optics have been compared with the new metalorganic sol-gel derived (Types V and VI) gel-silica glasses (for detail see ref.3).

Fully dense (Type V) gel-silica has excellent optical transmission throughout the vacuum UV, UV, VIS, NIR, and IR (wavelengths from 165 to 4000 nm) with no OH absorption peaks. Other physical properties and structural characteristics of Type V gel-silica are generally equivalent or superior to the best grades of Type I-IV optical silicas and offer the advantages of near net shape casting, including internal cavities, lower OH content, lower dispersion, and a lower coefficient of thermal expansion of 0.2×10^{-6} cm/cm compared with 0.55×10^{-6} cm/cm for Types I-IV [3].

Optically transparent porous gel-silica, termed Type VI, has substantial quantities of interconnected porosity of a size smaller than that which scatters visible light, and

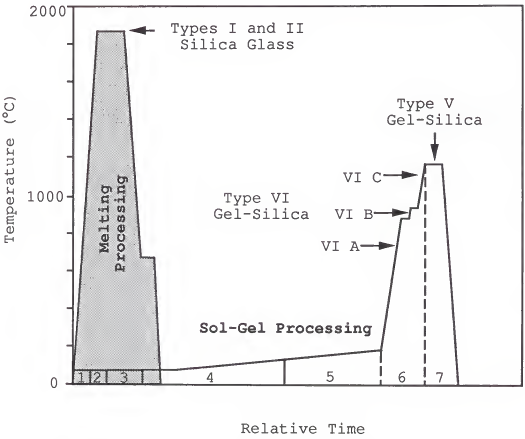

Figure 1.2 Sol-gel processing steps:
1.mixing, 2.casting, 3.gelation, 4.aging,
5.drying, 6.stabilization 7.densification.

even in some grades UV light. This type of gel-silica glass has a UV cutoff ranging from 250-300 nm and a density as low as 60% of Types I-V silica and can be impregnated with up to 30 to 40% by volume of a second-phase, optically active organic or inorganic compound [3].

The sol-gel process of producing fully dense (Type V) and optically transparent porous (Type VI) gel-silica glasses has recently been commercialized. The initial commercial interest was in fully dense (Type V) gel-silica glasses but has expanded into the production of porous (Type VI) gel-silica glass monoliths. The interests in porous monoliths stem from a unique combination of properties including its excellent ultraviolet, visible and near infrared transmission qualities and its interconnecting porosity. With controllable texture including surface area, volume fraction of porosity, average pore radius, pore size distribution, and the pore shape of the porous network, Type VI gel-silica glasses have opened up more different application interests than Type V gel-silica glasses.

1.2. Objectives

Type VI optically transparent porous gel-silica has been used in advanced optical applications, as described by Hench [10] and Hench et al. [3,11] for years. However, the relatively narrow range of texture, mainly characterized by the surface area, the total pore volume and the average pore radius, (as described in the previous section, the maximum average pore radius of Type VI gel-silica is about 12 Å and the maximum volume fraction of porosity is less than 50%) greatly limits the potential applications of currently produced Type VI gel-silica materials. In order to meet various stringent requirements of special applications, the range of texture as well as other properties of Type VI gel-silica need to be expanded. This need has led to the main objective of the research which is to establish a new, effective and reliable approach for producing Type VI gel-silica with a wider range of controllable textures and improved properties.

In addition, despite the remarkable progress that has been made in the area of sol-gel processing, the principal chemical and physical mechanisms of texture control are still not clearly understood [12-15]. An atomic and molecular level of understanding of many steps of sol-gel processing is still lacking. Thus the other objectives of this study are:

1) To study the effects of the aging process and aging parameters, such as aging temperature, time and the pH of the solution, etc., on the texture and properties of Type VI gel-silica.

2) To achieve an understanding of the mechanisms of the aging stage in the sol-gel processing and lay down a basis for further investigation of other scientific aspects of aging treatment.

In Chapter II, the history and development of the sol-gel processing is reviewed. Another purpose of Chapter II is to emphasize that there exist two different categories of sol-gel processing and correspondingly two groups of gel-silicas, namely, aqueous gel-silica and alcohol gel-silica. The main differences between those two groups of gels are discussed. The alcohol gel-silica made from controlled hydrolysis and condensation reactions of alkoxides is different from the aqueous gel-silica made from destabilization of inorganic sols in all aspects except the chemical composition. Alcohol gel-silica, e.g., Type V and Type VI gel-silicas, has more potential applications but has been less scientifically understood than the aqueous process. The processing sequence for making alcohol gel-silica, especially Type VI gel-silica, is described in the same chapter.

Chapter III describes the various approaches to control the texture of monolithic gel-silica. The aging process, which has extensively been studied and used in aqueous gel-silica system, shows the possibility of being used in an alcohol gel-silica system as a method to control the texture.

In Chapter IV, two experiments which concern the control of texture of monolithic gel-silica by use of aging treatments are designed. In experiment A, gels are aged in their own pore liquor, while in experiment B NH_4OH is used as an aging medium instead of the pore liquor.

Chapter V presents the results of the aging experiments, which prove that the texture of Type VI gel-silica can be effectively controlled by proper aging treatments. The effects of aging temperature, time, and concentration of an aging medium on texture and other properties of gel-silica, such as contraction, density, microhardness, and UV transmission, are investigated and the topological properties of the gels are also discussed.

Chapter VI proposes possible mechanisms which predominant the aging process. A Huckel molecular orbital (HMO) calculation is conducted to provide complementary information about the textural evolution of gel-silica during the aging treatment. In Chapter VII, an application of monolithic gel-silica optical matrices with modified texture controlled by aging is demonstrated. General conclusions are presented in Chapter VIII.

CHAPTER II
SOL-GEL PROCESSING

2.1 Historical Review

The novel idea of making materials, mainly silica, by sol-gel processing originated in the mid-1800s. Manmade polysilicate gels synthesized from alkoxide precursors closely followed the first preparation of silicon tetrachloride ($SiCl_4$) in 1824 [16]. Ebelmen [17] reacted $SiCl_4$ with ethanol to form first tetraethoxysilane (TEOS) as early as 1845. His subsequent publications [18] document that the synthesized compound, TEOS, slowly converted into a glassy gel due to hydrolysis by atmospheric moisture at room temperature. Fibers could be drawn, even monoliths could be cast from the viscous gel and finally dried to yield optical elements such as lenses. Since an extremely long period, 1 year or more, was required for drying, the gel had no technological significance at that time [17,19]. Sir Thomas Graham [20] prepared silica by dialyzing dilute silica sols obtained by mixing an aqueous solution of sodium silicate with hydrochloric acid in 1864. He proposed a network structure theory that the silica gel consisted of a solid network with continuous porosity. This theory competed with existing theories of gel structure, which regarded the gel as a coagulated sol with each of the particles surrounded by a layer of bound water, or as an emulsion [20].

During the period from the late 1800s through the early 1900s, sol-gel processing remained in its infancy. Although many noted chemists, including Ostwald [21] and Lord Rayleigh [22] were stimulated by the process and investigated the phenomenon of Liesegang Rings formed from the gels, only descriptive literature resulting from these studies was published [23-25] and a relatively sparse understanding of the physical-chemical principles was reported [26].

Both scientific and technological progress in the sol-gel field were made in the 1930s. Geffcken et al. [27] reported that sol-gel processing could be used in the preparation of oxide films. The Schott glass company in Germany commercialized this process in the 1950s and studied its physics, which was well explained in the excellent reviews by Schroeder [28,29] and Dislich [30]. Graham's network structure theory of silica gel was finally accepted, largely through the work of Hurd [31]. Kistler [32], who invented the process of supercritical (or hypercritical) drying to produce aerogels around the same time, studied the gel structure and demonstrated the existence of the solid skeleton of the gel. Meanwhile, the sol-gel process was first applied by the mineralogists to the preparation of homogeneous powder for the use in their phase equilibria studies [33,34] and later introduced in the ceramic community by R. Roy and coworkers [35-38] for the preparation of colloidal gel powders with very high levels of chemical homogeneity of the oxides.

Further development of the sol-gel processing was achieved during the 1950s and 1960s. Iler's pioneering work in silica chemistry [39] led to the commercial development of colloidal silica powders, Du Pont's colloidal Ludox® spheres. Stober et al. [40] extended Iler's findings to show that using ammonia as a catalyst for the TEOS hydrolysis reaction could control both the morphology and size of the powders, yielding the so-called Stober spherical silica powder. Much more sophisticated work, both scientifically and technologically, was conducted in the nuclear-fuel industry, but it was not published until later [41,42].

The ceramics industry began to show interest in gels in the late 1950s and early 1970s. The sol-gel method was widely used to synthesize a large number of novel ceramic oxide compositions, involving Si, Al, Ti, Zr, etc., which could not be made using traditional ceramic powder methods [35-38]. Controlled hydrolysis and condensation of alkoxides for preparation of multicomponent glasses were independently

---

® Registered trademark, E.I. Du Pont de Nemours & Co. Wilmington, DE.

developed by Levene and Thomas [43] and Dislich et al. [30]. Both glass and polycrystalline ceramic fibers, including TiO_2-SiO_2 and ZrO_2-SiO_2 glass fibers [44], high purity SiO_2 waveguide fibers [45-47], Al_2O_3, ZrO_2, ThO_2, MgO, TiO_2, $ZrSiO_4$ and $3Al_2O_3 \cdot 2SiO_2$ fibers [48-51], have been prepared by using sol-gel processing on a commercial basis by several companies [52-54]. Abrasive grains based upon sol-gel-derived alumina are important commercial products [51]. A variety of coatings and films have also been developed by using sol-gel methods [12,55-57]. Of particular importance are the antireflection coatings of indium tin oxide (ITO) and related compositions applied to glass window panes to improve insulation characteristics [57-59].

During the past decade there has been an enormous growth in the interest in the sol-gel process. This growth has been stimulated by the following factors. On the basis of Kistler's early work [60], several teams produced very low density silica monoliths, called aerogels, using hypercritical drying [61]. Zarzycki et al. [62,63] demonstrated that hypercritical point drying of silica gels could yield large fully dense silica glass monoliths. Yoldas [64] showed that large monolithic pieces of alumina could be made by sol-gel methods. Hench et al. have developed two new types of silica optics [7-9]. These demonstrations of potentially practical routes for production of new materials with unique properties coincided with the growing recognition that powder processing of materials had inherent limitations in homogeneity due to difficulty in controlling agglomeration.

In addition, a series of international conferences [65-71], workshops [72], and other special conferences [61,73] on sol-gel processing were held and a large volume of papers and books were published during the same period of time which laid down a solid foundation for the further development of sol-gel processing.

2.2 Aqueous and Alcohol Gels

Generally speaking, sol-gel processing can be divided into two main categories [74]: (a) destabilization of an inorganic salt containing one or more metal ions in aqueous solutions in which the only liquid present is water, and (b) controlled hydrolysis and polycondensation of alkoxide precursors in nonaqueous solutions which contain solvents other than or in addition to water. Correspondingly, silica gels are classified into two groups [75]: (1) aqueous gels, usually called colloidal gels, and (2) alcohol gels depending upon the kind of the precursors (starting compounds) and the method from which they are produced.

The typical example of the first group is aqueous silica. Nowadays, aqueous silica gel, such as Ludox®, is manufactured commercially according to Patrick's process, which consists essentially of gelation of an alkali metal silicate by means of acid [76].

The second category comprises many gels, for instance Gelsil®, prepared in alcoholic solution through hydrolysis and polycondensation reactions of a metal alkoxide, which is the class of precursors most widely used in sol-gel research.

The particle size of gels of both groups are within the range of colloids. However, the gels are different in nature.

The structures of alkoxide-derived gels prepared in nonaqueous solvents (or mixed solvents) are unlike the structures of aqueous silicate gels described by Iler [39]. In an aqueous silica gel system fully hydrolyzed monomers condense in such a manner as to maximize the number of siloxane bonds and minimize the number of terminal silanols [39]. In addition, since silica exhibits partial solubility in water (increasing at elevated temperature and increasing pH), Ostwald ripening occurs, further biasing growth toward the formation of fully crosslinked (anhydrous) silica colloids.

® Registered trademark, Geltech Inc. Alachua, FL.

In contrast to aqueous systems, for most alkoxide syntheses condensation begins before hydrolysis is complete (as evidenced by ^{29}Si NMR and ^{1}H NMR [77]). Thus in all but the initial stage, condensation reactions occur between oligomeric species which cannot easily coalesce to a fully crosslinked state. Furthermore, the possible condensation sites can be limited by reducing the extent of hydrolysis. Computer simulations show that this results in highly ramified, fractal species (i.e., wispy structures whose density decreases with distance from the center of mass) rather than dense colloids [78].

Finally, because the solubility of silica in alcohol is much less than in water, there can be comparatively little rearrangement or ripening to more highly compacted states. Small-angle X-ray scattering (SAXS) experiments [79] confirm the polymeric structure and fractal nature of alkoxide-derived gels in a wide range of compositions, whereas Ludox is proven to consist of dense colloids. Due to the different structure of the particles, sometimes aqueous gels are also called particulate gels and alcohol gels are called polymeric gels.

The surface activities of aqueous gels and alcohol gels are also different. The nature of the silica gel surface has been reviewed by numerous authors [39, 80-87]. One topic all these reviews have in common is the emphasis on surface coverage of OH groups, presumably because surface coverage largely determines the adsorption behavior and consequently the surface reactivity. Surface curvature, which depends on the gel synthesis, has profound effects on OH coverage and hydrogen bonding (Figure 2.1). In general, particulate gels characterized by a small positive radius of curvature surface (small particles) should contain less hydrogen-bonded silanol groups on the surface and are less active than polymeric gels that are microporous, with extremely small negative curvatures.

It is now well established that the shrinkage behavior of aqueous gels differs markedly from that of metal alkoxide gels synthesized in alcoholic solutions [88]. The two groups of gels also have different densification behaviors. Colloidal gels (composed of a fully crosslinked skeleton) are analogous to porous glass. Their densification behavior can be accurately predicted by application of a viscous sintering model [89-91]. However, the densification of alkoxide-derived gels cannot be described on the basis of viscous sintering alone. The metastable nature of alkoxide-derived gels dramatically influences both the densification kinetics and thermodynamics. It is not appropriate to view the densification of colloidal gels (and porous glasses) as representative of the densification of alkoxide-derived gels. Since different precursors are used, a certain amount of

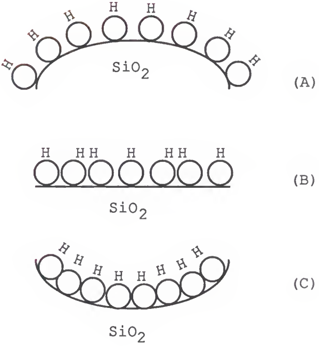

Figure 2.1 Effect of surface curvature on OH coverage and hydrogan bonding [93].
(A) Small positive radius of curvature (small paticles) has fewer hydrogen bonds.
(B) Large radius of cuvature (large particles flat surface) allow more hydrogen bonds.
(C) Small negative radius of curvature (small cylindrical pores or necks) has the most hydrogen bonding.

alkali ions, which may or may not be desirable, are usually found in the final aqueous gels. Obviously, certain properties of the gel result from the presence of these ions. For example, such gels have a strong tendency to crystallize during the heat treatment necessary for densification. Optical absorption also increases. The purity of the commercial grade of alkoxides is much higher than colloidal solutions of silica. Consequently, crystallization of alkoxide-derived gels is rarely observed during densification.

The major differences between aqueous gels and alcohol gels are listed in Table 2.1.

The chemistry and physics of aqueous silica gel has been extensively investigated by numerous researchers in many different ways [39,84,92]. In contrast, though the sol-gel processing for producing alcohol gels has been developed for many years, the technology always precedes the science, the chemical and physical principles of many fundamental aspects of the processing still lack understanding [12-15].

Our work will show in the following chapters that the aging behavior, including all the changes in texture and other properties, and the aging mechanism of these two groups of sol-gel materials are also different from each other.

It is one of the purposes of this work, as mentioned earlier, to study the textural and physical evolution of

Table 2.1
Major differences
between aqueous gels and alcohol gels

	Aqueous gels	Alcohol gels
Precursor	Inorganic salts	Organic alkoxides
Solvent	Water	Other than or in addition to water
Process	Destabilization	Controlled hydrolysis and condensation
Structure	Particulate, established by van der Waals forces	Polymeric, covalently linked
Applications	catalysts, adsorbents catalyst-carriers fillers selective adsorbents	high performance optical devices and composites

alkoxide derived silica-gel monoliths as the process proceeds.

From now on the term "sol-gel processing" will be used to refer to the processing of alcohol-based silica gels only, unless a special notation is made.

2.3 Processing Steps for Making Alcohol Gel-Silica

The steps of the processing for making alcohol gel-silica, such as Types V and VI gel-silica, are schematically illustrated in Figure 1.2.

(1) Mixing. This step is also called sol preparation. A silicon alkoxide, either tetramethylorthosilicate (TMOS) or tetraethylorthosilicate (TEOS), which are popular precursors (starting material) because they react readily with water, is mixed with water and undergoes simultaneous hydrolysis and polycondensation reactions resulting in the formation of SiO_2 [92]. The overall reaction consists of the following steps:

$$Si(OR)_4 + nH_2O \text{ -> } (HO)_nSi(OR)_{4-n} + nROH \qquad (2.1)$$

where $n \leq 4$, R represents a proton or other ligand (e.g., an alkyl), and ROH is an alcohol. Hydrolysis may go to completion ($n = 4$) depending upon the amount of water and catalyst present,

$$Si(OR)_4 + 4H_2O \rightarrow Si(OH)_4 + 4ROH \qquad (2.2)$$

or stop while the silicon is only partially hydrolyzed $(HO)_nSi(OR)_{4-n}$ $(n < 4)$.

Two partially hydrolyzed molecules can link together in a condensation reaction, such as

$$(OR)_{4-n}Si(OH)_n + (HO)_mSi(OR)_{4-m} \rightarrow$$
$$(OR)_{4-n}(HO)_{n-1}Si\text{-}O\text{-}Si(OH)_{m-1}(OR)_{4-m} + H_2O \qquad (2.3)$$

where $m \leq 4$ also, or

$$(OR)_{4-n}Si(OH)_n + (HO)_mSi(OR)_{4-m} \rightarrow$$
$$(OR)_{3-n}(OH)_nSi\text{-}O\text{-}Si(OH)_{m-1}(OR)_{4-m} + ROH \qquad (2.4)$$

In most cases, the above reactions are generally incomplete. Consequently, sufficient Si-O-Si bonds are formed in a region and respond cooperatively as a sol in which the dispersed phase consists of polymeric particles with diameter at the low limit of the colloidal range (< 1 nm) [93]. The size of the sol particles and the cross-linking within the particle depend upon the preparative conditions such as temperature, pH, catalysts and the *R* ratio ($R = [H_2O]/[Si(OR)_4]$) [94,95].

(2) Casting. Due to its low viscosity, the silica sol can be cast into molds which have required characteristics [96], such as appropriate composition to avoid adhesion of the gel and appropriate thermal properties compatible with the processing temperatures and so on. The shape of the gel, with dimension enlarged to allow for shrinkage during drying and densification [97], and the surface quality of the gel will be determined by the mold for casting. It has been reported that the sol-gel processing can offer the advantage of near net shape casting [98], including the ability to form internal cavities using a lost-wax process [3].

(3) Gelation. Silica gel is a form of matter intermediate between a solid and liquid [99]. It consists of a continuous solid, silica network, and a fluid, which is a mixture of alcohols and water, with the interconnected phases being of colloidal dimensions (within 1 μm). It is this interconnected three-dimensional network of silica particles that gives elasticity of the gels. The gelation point or gelation time, t_{gel}, is defined theoretically as the point where the sol can support a stress elastically. It can be easy to observe qualitatively but extremely difficult to measure analytically. The gelation point or gelation time changes significantly with the sol-gel chemistry [8,9,39,100,101].

According to Flory's theory of gel formation [102,103], the degree of polymerization (DP) obtainable in a system can be described by the following equation:

$$DP = 1/(1-pf/2) \tag{2.5}$$

where p is the percentage of reacted monomers as a fraction of the total concentration of initial monomers which are the reaction products from hydrolysis reaction, and f is the number of polymerization functional groups. For a completely hydrolyzed silica monomer, $Si(OH)_4$, f equals 4.

At the gelation point the degree of polymerization (DP) approaches infinity, therefore the term, (1-pf/2), must equal zero. In the case of f=4, the percentage of total concentration of monomer going into gel phase, p, must equal 50%. As mentioned earlier, in most cases both the hydrolysis and polycondensation reactions are incomplete in the alcohol gel-silica system so that p is usually higher than 50% but never reaches 100% at the gelation point.

The structure of gel-silica is assumed to be established at the time of gelation. Subsequent processes such as aging, drying, stabilization and densification all depend upon this structure.

(4) Aging. Aging is defined as the structural evolutions that occur with time after gelation and prior to

solvent evaporation and involves maintaining the cast object for a period of time completely immersed in its pore liquid. It has been reported [93] that four processes can occur, singly or simultaneously, during aging, including continuation of polycondensation reactions, syneresis (spontaneous shrinkage of the gel with expulsion of solvent), coarsening (increase in pore size and reduction in surface area through depolymerization and repolymerization), and segregation (phase transformation and crystallization). The gel structure is generally reinforced via the minimization of surface area. A properly aged gel can develop sufficient strength to resist cracking during drying.

The scientific principles of aging in aqueous gel-silica systems which have been investigated for a long time are already thoroughly understood [39] (the details will be reviewed in the next chapter). However, there is relatively little detailed knowledge of aging mechanisms and kinetics and even less quantitative analysis of the effects of aging on structure and properties of alcohol gel-silica systems, although extensive efforts have recently been made to use this system to make optical devices [104,105].

(5) Drying. A silica gel is defined as "dried" when the physically absorbed water is completely evacuated and no significant weight loss is observed at increased temperature [4].

Depending upon different drying methods, alcohol gels can be further classified into two subgroups: xerogels and aerogels. Drying by evaporation under ambient atmosphere gives rise to capillary pressure that causes shrinkage of the gel network. The resulting dried gel is called a xerogel, which is often reduced in volume by a factor of 5 to 10 compared to the original wet gel. If the gel is placed in an autoclave and dried under supercritical conditions, by removing the liquid from the pores above the critical temperature (T_C) and critical pressure (P_C) of the liquid, there is no interface between liquid and vapor, so there is no capillary pressure and relatively little shrinkage. This process is called supercritical drying, and the product is called an aerogel; it contains mostly air and a volume fraction of solid as low as ~1% [93].

Types V and VI gel-silica are xerogels. During drying, the liquid is removed from the interconnected pore network and the wet gel experiences progressive shrinkage and hardening. Since stress develops not only from differences in expansion coefficients due to variable water content, but also from the action of capillary forces which become operative when the pores start to empty and the liquid-air interface is present in the form of menisci distributed in the pores of the drying gel, this step is considered the most critical one in the process. A monolithic silica gel, of which the smallest dimension is greater than a few millimeters, can only be dried by certain precautions; otherwise the resulting product fractures into a "powder" consisting of small pieces or grains of various sizes.

The dried xerogel gel-silica is porous and contains interconnected and open micropores (radius < 20 Å) and macropores (radius > 2000 Å) [106]. Although the textural features of a gel, including surface area, pore size and its distribution, may differ considerably depending on processing method, a very high surface area (>400 m^2/g) remains for all xerogels gels. This surface is completely surrounded by residual hydroxyl groups [107].

Because few bridging bonds are broken and reformed during solvent removal, the structure of resulting porous xerogel bears some relation to the structure at the gel point.

The drying behavior of porous materials has been extensively studied by Sherwood [108-110], Keey [111], Mujumdar [112,113], Moore [114], Whitaker [115], Cooper [116], Ford [117], and Scherer [118-123]. Different drying models have been proposed based on the quantitative studies conducted on large pore (> 20 nm) gels by Kawaguchi et al. [124], Dwivedi [125], and Zarzicki [126] and on small pore xerogels (< 20 nm) by Wilson and Wilson and Hench [127,128].

Wilson and Hench's [128] work is the most relevant to this study of aging of gel-silica. Their results show that the drying behavior of acid-catalyzed alkoxide silica gel can also be described in terms of three stages which are consistent with that reported by other researchers investigating gel based systems [125]. However, the drying rate of acid-catalyzed alkoxide gels with pores < 20 nm during stage 1 is not constant but in fact decreases substantially, which illustrates the importance of pore size in drying behavior of gels.

(6) Stabilization. The large concentration of silanols on the surface of the pores, as just described, makes the gel-silica surface very active. Thus, after drying both thermal and chemical stabilization through heating are required for the gel-silica to be used in an ambient environment. Thermal stabilization involves reducing the surface area sufficient to enable the material to be used at a given temperature without reversible structural changes. Chemical stabilization involves removing the concentration of surface silanols below a critical level so that the surface does not rehydroxylate extensively in use where water vapor is present. The mechanisms of thermal and chemical stabilization are interrelated because of the extreme effects that surface silanols and chemisorbed water have on structural changes.

It is well known that gel-silica remains highly porous throughout a temperature range that is substantially higher than that required to produce a dried gel. This range extends up to 1100°C to 1250°C depending on the pore radii present [5]. By heating the dried gel-silica above a certain temperature (note that the lowest temperature of preparation of Type VI gel-silica is 600°C), stabilized Type VI optically transparent porous gel-silica is obtained. According to the stabilization temperature or the density of the gel, the stabilized gels can be divided into three sub-classes: Types VIA, VIB and VIC (Table 2.2) [3], which can be selected to be used as unique optical components when impregnated with optical active polymers such as dyes, fluors, wavequide shifters or nonlinear optical polymers [3,129].

(7) Densification. Heating the porous gel to higher temperatures causes densification to occur. At 1150°C, with a carbon tetrachloride treatment prior to pore closure to eliminate adsorbed water, the material no longer contains pores and has a surface area determined only by its external geometry. Type V gel-silica or a fully dense silica glass is finally obtained. Type V gel-silica has excellent optical transmission throughout the VV, UV, VIS, NIR, and IR [3]. Physical properties and structural characteristics of Type V gel-silica are generally equivalent or superior to the best grade of Types I-IV silica glasses [3].

Table 2.2
Characteristics and properties
of Type VI gel-silicas

Types	Temperature (°C)	Bulk density (g/cm3)	Pore volume (cm3/g)	Surface area (m^2/g)	Micro-hardness (VHN)	UV cutoff(nm) (50% trans.)
VI A	600-900	1.3-1.5	0.17-0.37	290-620	100-285	290-300
VI B	900-950	1.5-2.1	0.01-0.17	10-290	285-450	185-290
VI C	950-1150	2.1-2.2	0.00-0.01	0-10	450-680	165-185

Source: [3]

Densification is essentially a sintering process. The driving force for this process arises from the excess surface free energy of the gel. At least four mechanisms contribute to this process: (1) capillary contraction, (2) polycondensation, (3) structural relaxation, and (4) viscous sintering [130,131]. Mechanisms (1) and (2) are considered chemical processes which dominate at low and intermediate temperatures. Mechanisms (3) and (4), structural relaxation and viscous sintering, are physical processes and dominate at high temperatures [132].

The temperature range in which each of these mechanisms is dominant depends on the chemical and microstructural nature of the gel as well as the heating rate. An important stage is reducing or eliminating residual hydroxyl groups, termed dehydration, in the pores during the densification process. Although OH can be removed through polycondensation reactions, viscous sintering often starts before dehydration is complete, leading to bloating or foaming of the gel in the final stages of sintering. Even if sufficient hydroxyl content is removed so that sintering can occur without bloating, a subsequent heating of the consolidated gel to its softening point, for example, during fiber drawing or sealing, may cause bloating.

Thermal dehydration of silica gel has been extensively investigated. Hair [85] proved that OH groups are, in general, gradually lost with increasing temperature, but some single hydroxyl groups are still unable to escape from the surface before commencement of viscous sintering. Thus thermal dehydration is often not sufficient to avoid foaming in silica gels. Consequently, chemical dehydration procedures, primarily employing halogens, have been widely investigated [133]. An optically clear, bubble-free, and OH-free silica glass prepared by employing a halogen treatment followed by annealing in oxygen and sintering in He was reported by Matsuyama et al. [134]. The chemical and microstructural evolution during the densification of dried gels has been described by James [135]. Hench and Wang describe the dehydration steps involved in making Type V gel-silica optics [136].

CHAPTER III
CONTROL OF THE TEXTURE OF GEL-SILICA

3.1 Introduction

The texture of porous gel-silica can be characterized mainly by the specific surface area, the pore volume, and the average pore radius.

As mentioned in the previous chapters, there are two main reactions involved in the sol-gel processing: hydrolysis and polycondensation which are not separated in time but take place simultaneously [137]. It has been believed that the texture of the gel is determined by the relative rates of these two reactions [92]. So, any processing variables, such as reaction temperature, nature and concentration of catalysts (acid, base), nature of the solvent, and type of alkoxide precursor, which influences the rates will consequently influence the gel texture [93,138].

Controllable texture is an important feature of sol-gel processing. By controlling the variables in different steps of the processing it is possible to change and control the texture of gel-silica for various specific applications.

Optimizing processing to produce a specific and highly reproducible texture is essential to make high quality Type VI gel-silica optical matrices.

3.2 Textural Control by Catalysts

During the first step of sol-gel processing, mixing, the size of sol particle and the cross-linking within the particle depends upon the pH, the catalyst and the R ratio (R = $[H_2O]/[Si(OR)_4]$). The texture of a gel may change appreciably with the preparative conditions [94,95]. For instance, it has been observed [94] that under high pH and high water content, highly branched clusters and then textures with high porosity are developed, while under the conditions of low pH and low water content, linear or random branches and consequently low porosity textures are formed.

Hydrolysis is most rapid and complete when catalysts are employed [139]. Aelion et al.[140,141] observed that the rate and extent of the hydrolysis reaction was most influenced by the strength and concentration of the acid or base catalyst. Temperature and solvent were of secondary importance. They found that all strong acids behaved similarly, whereas weaker acids required longer reaction times to achieve the same extent of reaction.

Figure 3.1 [142] compares the hydrolysis of TEOS and TMOS under acidic and basic conditions, which tells us that the rate of hydrolysis is very fast in sol-gel processing, especially when TMOS is used as precursor. Figure 3.1 shows that the hydrolysis reaction is complete within 500 seconds using HCl as catalyst even in a low R ratio solution. It has been well established that the presence of H_3O^+ in the solution increases the rate of the hydrolysis reaction, whereas OH^- ions increase the condensation reaction [143].

In currently produced Type VI gel-silica, HNO_3 is used as catalyst. By replacing part of HNO_3 with hydrofluoric acid (HF) as catalyst, the following results have been reported [96,144]:

1. A very small amount of hydrofluoric acid was found to increase the average pore radius as well as the total pore volume dramatically. A specific pore radius of 32 Å, 46 Å, 62 Å, 79 Å and 88 Å could be reproducibly generated by using a specific concentration of HF as a catalyst.

2. With increasing addition of HF, thermal stability of the gel generally increases due to the decrease of chemical potential of the surface.

3. Pore radius has very little effect on the optical properties of Type VI silica. Increasing pore radius causes a moderate shift of the UV cutoff to higher wavelengths.

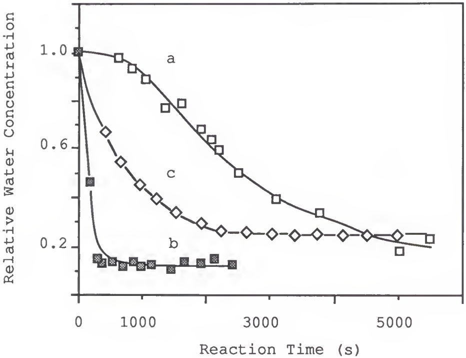

Figure 3.1 Hydrolysis rate of (a) TEOS with HCl catalysis (b) TMOS with HCl catalysis and (c) TMOS with NH3 catalysis [142].

The mechanism of HF affecting the texture of gel-silica has not been well investigated. Pope and Mackenzie [95] showed that F^-, the most notable conjugate base, has an effect on the gel time. Corriu et al. [145] believe that F^- is about the same size as OH^- and has the ability to increase the coordination of silicon above four, for example in $R_3SiF_2^-$. Many of the properties of HF-catalyzed gels are similar to those of base-catalyzed gels, which suggests that the roles of OH^- and F^- are similar. Andrianov [146] proposes that the catalytic effect of F^- involves the displacement of an OR^- via a bimolecular nucleophilic (S_N2-Si) mechanism in which the nucleophile, F^-, attacks Si followed by preferential hydrolysis of the Si-F bond. However Corriu and coworkers [147] have shown that the first step is fast reversible formation of a pentavalent intermediate that stretches and weakens the surrounding Si-OR bonds. The subsequent rate-determining step is the nucleophilic attack of water on the hypervalent silicon leading to nucleophilic substitution by proton transfer and elimination of ROH.

The main problem of controlling the texture of a gel using HF as a catalyst during the mixing stage mentioned above is apparent. The hydrofluoric acid is very corrosive and hazardous so that specific precautions must be taken not only for operating personnel but also for processing equipment.

In addition, all parameters of the processing steps may have to be adjusted or completely changed when HF is added. For instance, the sharp decrease in gelation time with increasing HF concentration usually introduces problems in controlling subsequent steps and makes the preparation of a uniform gel very difficult. The drying schedule for HF-catalyzed gel-silica has to be adjusted to be longer than 130 hours [144] while almost twice as long the normal schedule used for xerogel optics. Any other methods to increase the porosity of the gels during the mixing sol-formation step, such as increasing pH, or using a base as catalyst, will cause similar problems.

3.3. Textural Control by Densification

It is a well established fact that gel-silica remains highly porous at temperatures significantly higher than those required to produce a dried rigid gel [148]. Even after heating to much higher temperatures, extensive porosity remains. This gives an opportunity for control of the texture of the gels during the last step of the processing---densification. It is interesting to note that subsequent heat treatments of the rigid gel do not change the average pore size profoundly as long as the heating is below a certain temperature (<1000°C) (Figure 3.2). However, heat

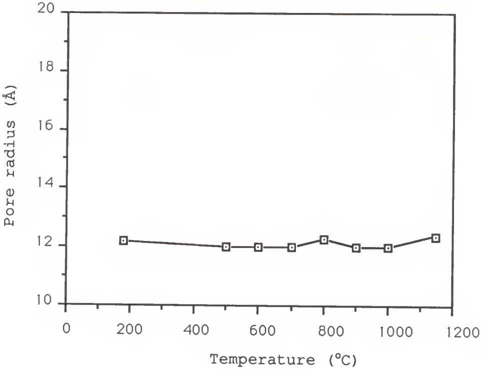

Figure 3.2 Variation of the average pore radius of 12 Å gel-silica samples as a function of densification temperature [96].

treatments do change the volume fraction of porosity and the surface area (Figure 3.3). Types VIA, VIB and VIC gel-silica with controllable texture and surface chemistry are now routinely produced using this method.

Unfortunately, the texture of the gel-silicas changes only in one direction during densification. The average pore radius and total pore volume always decrease with increasing processing temperature. The process is irreversible. For currently produced regular Type VI gel-silica, the controllable range of the texture is relatively narrow due to its initial texture, e.g., the range of average pore radius is only from 12 Å to zero as shown in Table 2.2, which imposes a strict limitation on the application of the method.

A brief description about densification mechanisms has already been made in Chapter II. Vasconcelos [96] and Vasconcelos et al. [149] have attempted to understand the textural evolution of the gel-glass transition using topological concepts. It has been shown that application of topological modeling to the densification of sol-gel derived nanometer scale structures reveals the same principles as determined for the sintering of larger scale powder structures. The topological evolution of the texture can be related to physical properties and presents potentially useful information which is complementary to the traditional metric parameters.

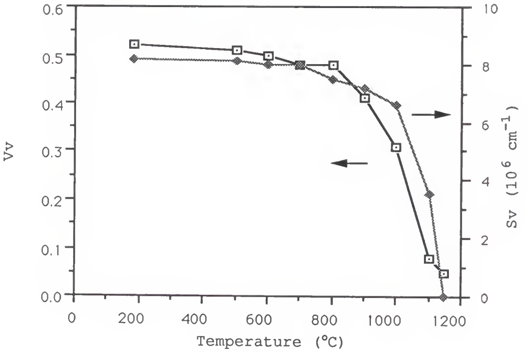

Figure 3.3 Variation of the surface area of pores per unit volume (Sv) and the volume fraction of pores (Vv) of 12 Å gel-silica samples as a function of densification temperature [96].

3.4 Textural Control by Aging

3.4.1 Introduction

The gel texture can also be controlled in the intermediate steps of the processing, such as aging and even drying.

Besides using the so called hypercritical drying method mentioned in Chapter II, the texture of acid catalyzed alcohol silica gels can be altered using a special designed drying chamber [127]. Samples of slightly larger pore size and larger initial (dried) volume fraction than those made using Teflon® containers were obtained. The internal volume of the drying container and the total external surface area of the gels inside the drying chamber seem to affect the drying process. This effect may be associated with changes in the equilibrium vapor pressure of the chemical components of the gel inside the drying container.

As a part of our work, the results presented in Chapter V will show that the atmosphere in the drying chamber was found for the first time have a drastic effect on the gel texture.

Aging plays an important role in sol-gel processing. Using aging treatments to increase the strength of the gel has been listed as one of the effective ways to avoid cracking of the gel during drying. However, for a long period of time, aging has not been considered as important in controlling gel texture as the other early steps of the processing. The initial principal objective of our work also was not to control the texture of the gels by aging. Instead, the original purpose was to achieve an understanding of the aging process of alcohol-derived gel-silica in order to make the production of dried gel-silicas more rapid and reliable. However, the preliminary results of the research quickly proved that not only the strength but also the texture of the alcohol gel-silica can be changed as well as controlled by aging parameters in which the nature of the aging medium plays the most important role. Consequently, our focus started to shift to the present topic of controlling gel texture by means of aging treatments.

3.4.2 Aging Concepts

The aging stage begins from the time of the gel point, at which the viscosity becomes infinite and the meniscus of a sol in a container no longer remains horizontal when the container is tilted, and lasts as long as the gel is still kept in the liquid.

Previously, most people believed that the texture of a gel is established at the time of gelation with subsequent processing steps such as aging, drying, stabilization, and densification all closely dependent upon the initial texture that formed at the gelation point [39].

Brinker et al. [94] argued that the rapid increase in viscosity which accompanies gelation essentially freezes in a particular polymer structure at the gel point. At this point gelation may be considered a rapid solidification process. This "frozen in" structure may change appreciably with time, depending on the temperature, solvent and pH conditions or upon removal of solvent.

Scherer [118] further pointed out that the chemical evolution of the system is essentially unaffected by gelation. The composition, the structure, and the properties of the gel continue to change with time during aging. The subsequent drying of the gel is strongly influenced by the structure developed during aging.

Obviously, the gel point does not indicate completion of the formation of the gel structure.

3.4.3 Changes during Aging

A wide variety of chemical and physical changes can occur after gelation. This is true even when evaporation is prevented. There are four major changes possible: condensation (chemical compositional change), syneresis (physical dimensional change), coarsening (textual change) and a change of physical properties of the gel during aging.

3.4.3.1 Condensation

Usually, the chemical hydrolysis reaction is fast; it is completed in the early stage of sol preparation especially when the sol is acid catalyzed. For gel-silicas synthesized in alcoholic solutions i.e. made by controlled hydrolysis and condensation of alkoxides, it has been shown by nuclear magnetic resonance (NMR) [150] and Raman spectroscopy [151] that the number of bridging bonds increases long after gelation. The condensation reaction continues to occur, because of the large concentration of silanol (Si-OH) groups. The result is a change in composition (loss of hydroxyls) accompanied by an increase in connectivity of the gel network resulting in a decrease in flexibility as new bonds are formed.

Since the chemical reaction is faster at higher temperature, aging can be accelerated by a hydrothermal treatment. That means the temperature can affect the condensation reaction and then affect the aging process.

3.4.3.2 Syneresis

The spontaneous shrinkage of the gel and the resulting expulsion of liquid from the pores is called syneresis [152]. Syneresis in an alcohol gel system is generally attributed to formation of new bonds through condensation reactions. As the condensation reaction proceeds, the increase in bridging bonds causes contraction of the gel network. In aqueous gel systems or particulate gels, the structure is controlled by the balance between electrostatic repulsion and attractive van der Waals forces. Therefore, the extent of shrinkage is controlled by additions of electrolyte. Vysotskii and colleagues [153,154] have shown that the rate of contraction of silica gel during syneresis has a minimum at the isoelectric point (IEP). For pure silica this point is at a pH of 2 at which the silicate species are uncharged.

It has also been suggested by Scherer [119] that contraction of a gel is driven by the tendency to reduce the huge solid/liquid interfacial area of the gel. This might be accomplished by flexure of the solid phase thereby bringing surfaces into contact, in which case it would be indistinguishable from the reaction driven mechanism. That means the chemical potential of the gel is reduced by both chemical reactions (since a condensation reaction is exothermic) and the reduction in solid/liquid interfacial area. But the latter suggestion is not supported by experimental results [119].

It has been shown that the syneresis contraction rate increases with concentration of silica in the sol [155] and with the temperature [156]. The rate of syneresis decreases with time. This could result from the increasing stiffness of the network as more bridging bonds are formed. Ponomareva et al. [156] found that the total syneresis strain is greater at lower temperatures, although the contraction rate is slower. They argued that at higher temperature the condensation reaction is faster, so the gel becomes stiff faster and shrinkage is prevented. If this is so, it implies that the shrinkage is not proportional to the scale of reaction. They conclude each bond does not cause a certain amount of strain. The other factor that may affect the rate of contraction is the permeability of the gel to the flow of liquid in the pores.

3.4.3.3 Coarsening

Another process, called coarsening or "Ostwald ripening" is discussed at length in the excellent book by Iler [39]. Since convex surfaces are more soluble than concave surfaces, if a gel is immersed in a liquid in which it is soluble, dissolved material will tend to precipitate into regions of negative curvature. That means that necks between particles will grow (Figure 3.4) and small pores may be filled in, resulting in an increasing in the average pore size of the gel, and a decrease in the specific surface area.

Thus, the study of aging mechanism and kinetics of silica gel, the textural changes (i.e. surface area, total pore volume and average pore sizes) are of great importance.

Iler [39] provides a number of references concerning the change in the texture of a gel during aging. The reduction in surface area is produced by dissolution and reprecipitation. The large pore size and high pore volume result because the stiffer gel produced by aging does not shrink as much under the influence of capillary pressure.

3.4.3.4 Properties

During aging, there are changes in most physical properties of the gel. With respect to drying behavior, it is the change in mechanical properties during aging that is most important. Inorganic gels are viscoelastic materials responding to a load with an instantaneous elastic strain and a continuous viscous deformation. As condensation reactions create additional bridging bonds, the stiffness of the gel network increases, so the elastic modulus and viscosity both rise [157]. Similar data were obtained by Pardenek, et al.

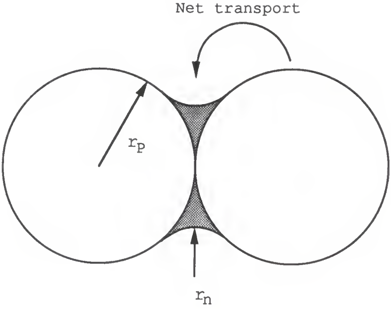

Figure 3.4 Definition of positive and negative radii of curvature.
The radius of the neck, r_n , is negative because the center of curvature is outside phase; the redius of the particle r_p , is positive.
Materal tends to dissolve from surfaces with positive curvature and deposit in regions with negative curvature. The growing neck (shaded) strengthens the gel [93].

[158] for polymeric gels as well as particulate or colloidal gels made from fused silica. Dumas, et al. [159] followed the shear modulus for 9 months in gels made from TEOS and found that the modulus continued to increase. The strength of the gel also increase with aging. For that reason, it is advised to age gels before drying to reduce the chance of cracking. The great stiffness of the aged gel reduces the shrinkages during drying as mentioned before, especially if the aging treatment is performed under hydrothermal conditions.

The effect of temperature and time during aging of silica gels made from TMOS have been evaluated [160]. Improvement in the physical properties of the wet gel have shown to be well correlated to their aging temperature and time. The modulus of rupture, MOR, of the gel aged at 105 °C for 40 days is about 400 Pa.

During aging, separation may occur into mixtures of solid-liquid, liquid-liquid, or solid-solid phases. Such phase separation can also affect physical properties. However, there is no data to describe the magnitude of this variable.

3.4.4 Aging Parameters which Affect the Texture

It has been found that time, temperature and pH are principal parameters which can effectively alter the texture of aqueous gels during aging.

Iler [39] recognized that once the aqueous gel structure has been formed it can be further modified in the wet state by treatment to (a) strengthen the structure without greatly affecting the pore structure (sometimes referred to as gel reinforcement) or (b) enlarge the pore size and reduce the surface area by a process of dissolution and redeposition of silica, coarsening the gel texture.

Reinforcement is most commonly carried out without much change of the colloidal gel structure by heat-aging the wet gel. When it is carried further in the aging process a coarsened structure develops. Depending on the character of the initial gel and the temperature, time, and pH of aging, the gel structure can go through the stages described by Iler [39]. Sheinfain et al.[161] recognized the first two distinct stages in the heat-aging process. The more extensive the wet aging, the subsequently dried gel shrinks less and the pore volume and diameter are greater, but there is very little change in surface area. Secondly, upon further aging the surface area begins to decrease while the pore size continues to increase. However, there is then little further change in pore volume. The first stage involves only an increased coalescence or bonding between the ultimate particles which strengthens the gel so that it shrinks less upon drying.

Heating the aqueous gel in water until the specific surface area has been reduced by 10-50% can strengthen the weak gel structure. Heating the gel in water at 80-100°C generally brings about reinforcement but does not modify the pore structure. It is interesting that at 80°C there was no effect unless the gel had a surface area greater than 200 m^2/g.

Prolonged aging of colloidal silica gel with an initial surface area of 920 m^2/g, in water at pH 6.8 at room temperature, was carried out by Sheifain, Stas, and Neimark [162]. The surface area dropped from 725 to 420 m^2/g while the pore radius increased from 9 to 43 Å. However, the porosity also increased from 0.31 to 0.90 cm^3/g. The structure was thus strengthened so that shrinkage upon drying was reduced. The reinforcement was most striking when samples were first washed with acetic acid and then dried. Since the surface tension of acetic acid is only one-third that of water, the reinforced gel had a much higher pore volume of 2.36 cm^3/g, which is quite a low density gel.

The rate of coarsening of colloidal silica increases with temperature and pressure. Heat aging in water above 100°C under pressure in an autoclave brings about far greater structural changes than can be obtained at 100°C. Van der Grift et al. [163] prepared silica gels by neutralization of alkali silicate solutions and aged them in an autoclave in water at various temperatures. When the temperature is above the boiling point of water, the sample is exposed to steam at high pressure, and the process is called hydrothermal aging. Obviously the aging temperature and the time affect both neck formation and condensation.

The pH plays a very important role during aging in an aqueous gel-silica system. The rapidity of change increases with pH and the process is governed by the factors that influence the rate of deposition and dissolution of silica.

It must be understood that the simple step of washing the pore liquor out of a aqueous gel is also an "aging" step and the pH of the wash water is critical in the case of gels made from acids and silicate solutions. The final properties of such gels depend on both pH at which the gel was formed and the pH in which it was washed (aged) before drying.

Okkerse, et al. [164] heated a series of aqueous silica gels for 1-4 days at 80°C in water, acid, and potassium chloride solutions and found that if the gel had a specific surface area greater than about 200 m^2/g, then it underwent a decrease in surface area. There was little effect at pH 2, but in neutral or alkaline solution, especially in the presence of salt, the gel texture was markedly coarsened. For example, surface area decreased from 752 to 452 m^2/g while pore radius increased from 13 to 22 Å but the pore volume remained at 0.5 cm^3/g.

Soaking a colloidal silica gel in dilute ammonium hydroxide solution at 50-85°C resulted in drastic coarsening of the gel texture. Girgis [165] reported that even soaking gel at pH 10-11 for 1 day at 20°C caused the surface area to drop from 650 to 467 m^2/g with corresponding increase in pore radius.

In the aqueous gel-silica system, the effect of ammonia concentration on the rate of decrease in surface area (430 to 126 m^2/g) and increase in pore diameter (85 to 397 Å) has been disclosed by Jenkins and Schwartz [166]. Similar effects of pH, salts, acids and alkalis on the aging process have been reported by a number of investigators.

It might be thought that since silica does not dissolve at low pH, acids would have no effect on wet aging other than to adjust pH. However, Sheifain, et al. [39] found that treating the aqueous gel-silica with strong acids, HCl, HNO_3, or concentrated H_2SO_4 before drying, increases the pore volume of the dried gel without lowering the surface area. This can only be because the acid promotes coalescence between particles without particle growth and coarsening of the texture. On the other hand, 8 N H_2SO_4 caused a drop in area from 700 to 300 m^2/g and at the same time increased the pore volume. The difference may be that silica is actually more soluble in 8 N H_2SO_4 than in the other acids. The observed difference is only a matter of the degree of modification of gel structure. In any case, strong acids (pH below 2) promote heat-aging of silica gel, but unlike alkali as a promoter, cannot dissolve the gel if added in excess.

It is seen that aging and thermal treatments result in a one-way process in aqueous gel-silica system: loss of specific surface area and increase in pore size. The pore size can be enlarged also by dissolving away some of the silica. Neimark et al. [167] reported that treating a colloidal silica gel with 0.5 N KOH or dilute HF can enlarge pores from 7 to 37 Å. If silica were dissolved away evenly from all the surface, there should be an increase in specific surface. However, it is probably that regions of lower radius of curvature will dissolve more rapidly so that the specific area may actually decrease.

Unfortunately, almost all the work on aging cited in this section were focused on the aqueous gel systems. For alcohol gel systems, the aging stage has been considered only as an auxiliary stage of processing. The main application of aging was confined to increasing the mechanical strength (some examples have already been mentioned in the preceding section) and avoiding cracking of the gel during drying. Other than a few small studies [168], aging has not been used for controlling the texture of monolithic gel-silica. It should emphasized here that until now the aging of alcohol-based gels has not been attracted proper attention. Consequently a molecular level of understanding of the aging process is still lacking and the mechanism and effects of aging kinetics of alcohol-based gel-silica monoliths are not well understood.

Our work discovered that the aging treatment provides more flexibility to control the texture of gel-silica than other methods previously described. By changing aging parameters only and keeping other parameters almost constant, a wide range of gel textures can be obtained. Ammonium hydroxide, the aging medium, used in our work, is a weak alkali which is much less corrosive and hazardous than HF mentioned above and also it will not introduce any harmful impurities to the gel system.

CHAPTER IV
AGING TREATMENT OF ALCOHOL GEL-SILICA MONOLITHS

4.1 Experimental Procedures

4.1.1 Gel Preparation

Figure 4.1 is the flowchart of the experiments specifically designed to prepare alcohol-based xerogel silica monoliths in this study.

The regular recipe (Table 4.1) of acid catalyzed silica gel (*R* ratio = 16, pH = 1), which is routine for production of Type V and Type VI gel-silica, has been used. In order to form highly homogeneous gel monoliths the following specific procedures have been used. At first, water and nitric acid were mixed in a beaker and covered. A specific amount of TMOS, which has a higher solid yield and higher rate of hydrolysis than TEOS, was gradually added to the above mixture. During the whole mixing reaction a magnetic stirring bar at moderate speed was applied. After half an hour, the stirring was stopped and the solution was kept quiet for a period of time until no bubbles could be seen. The solution was then filtered and cast into plastic containers. After being tightly sealed, the containers were placed into the

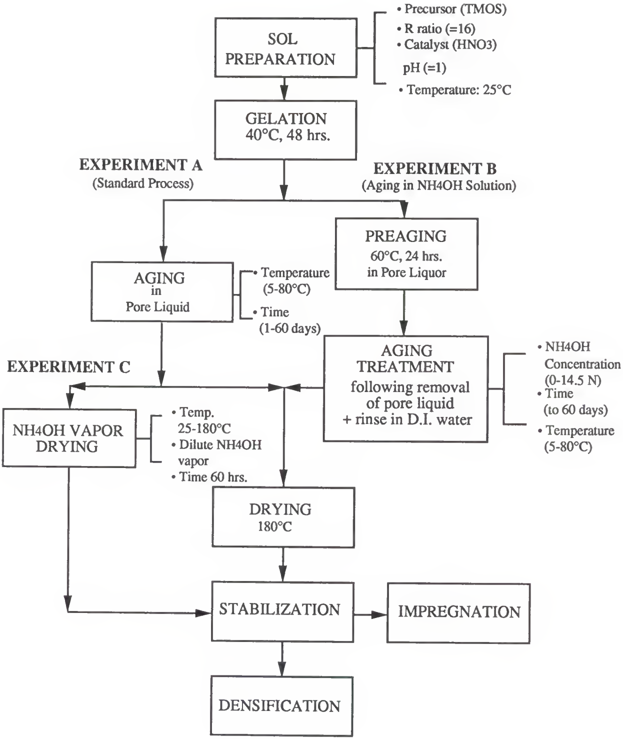

Figure 4.1 Flowchart of experiments A, B and C.

Table 4.1
Recipe of gel-silica samples

	Volume (ml)	Molecular weight (g)	Specific density (g/cm^3)	Weight (g)
D.I. Water	664.47	18.015	1.000	664.47
TMOS	327.17	152.220	1.052	344.28
HNO_3(70%)	8.36	63.012	1.420	11.87
Total	1000.00		1.021	1020.62

oven at 40°C for 48 hours which proved sufficient for gelation to complete. After gelation, three different experiments, A, B and C, were conducted.

4.1.2 Aging Treatment

In experiment A, the gel-silica samples were kept in the same container and placed into an oven for aging at various temperatures (5, 25, 45, 60, and 80°C) for different periods of time (from 1 day to more than 60 days) respectively (Figure 4.2). While in experiment B, before the gel samples being taken out for further treatment, a so-called "preaging" stage was required, otherwise the wet gel-silica would be too weak to be handled in the following step. After preaging in the pore liquor at 60°C for another 24-48 hours, the gel-silica samples were cooled down to room temperature (Figure 4.3) and transferred into the TEF containers which were filled with solutions other than pore liquor with different concentrations. The containers were then well sealed and placed into the oven for treatment at different temperatures (i.e. 5, 25, 45, 60 and 80 °C) for different time periods (from less than 5 minutes to more than 60 days) using the same aging schedule illustrated in Figure 4.2.

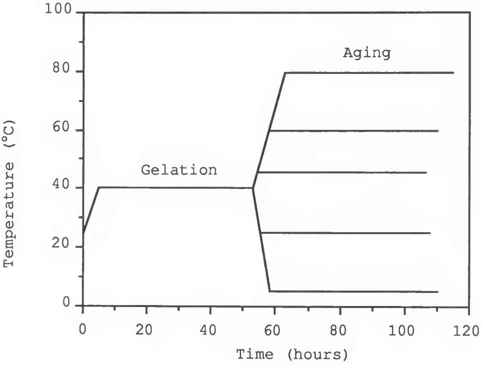

Figure 4.2 Schematic illustration of gelation and aging schedules for experiment A.

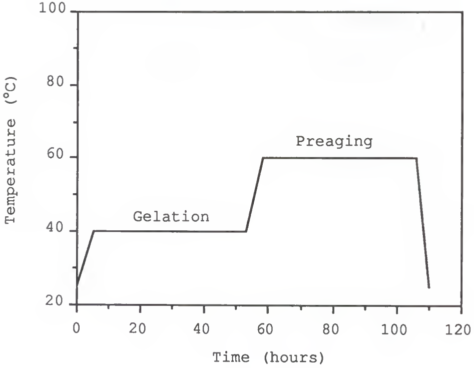

Figure 4.3 Schematic illustration of gelation and preaging schedules for experiment B.

NH_4OH was chosen as aging medium in our work. The reasons are as follows:

(1) It is less corrosive. Arrhenius [169] defined a base as a compound which, in aqueous solution, yields hydroxide ion (or a base, on the other hand, is defined as any substance that can accept a proton from any other substance), and the strength of a base is determined by the extent to which it is dissociated in solution to give hydroxide ions. Sodium hydroxide and potassium hydroxide, which, like all ionic compounds, are completely ionized in water solution, yields high concentrations of hydroxide ion and are, therefore, strong bases. They are placed with other ionic compounds in the category of strong electrolytes. In addition to the strong or ionic bases, there are some covalent compounds, of which ammonium hydroxide (NH_4OH) is the most typical example, which exhibit the characteristic properties of bases but conduct electricity only very poorly. Such compounds are called weak bases. NH_4OH is less strong than other ionic bases such as sodium hydroxide and potassium hydroxide. Many of the chemical properties of NH_4OH can be interpreted in terms of the assumption that the following equilibrium exists in the solutions:

$$NH_{3(aqueous)} + H_2O = NH_4OH_{(aqueous)} = NH_4{}^+{}_{(aqueous)} + OH^-{}_{(aqueous)} \qquad (4.1)$$

That the second step proceeds only slightly toward the right is shown by the fact that the value of the ionization constant

$$K_b = \frac{[NH^{4+}][OH^-]}{[NH_3]} \qquad (4.2)$$

is only 1.8 x 10 $^{-5}$.

It has also been found experimentally that the pre-aged gels with dimension of about 45 X 45 X 10 mm simply disappeared after treatment in 1 N NaOH solution for less than 2 days. However, no significant dimensional change of the gels treated by 4 N NH_4OH for more than 4 days was observed.

Comparing to HF, NH_4OH is much less hazardous, consequently, it can be handled more easily and safely.

(2) NH_4OH itself is pure so that no undesirable or harmful foreign ions, such as Na^+ and K^+ ions which would cause devitrification or crystallization problems, are introduced into the gel-silica. Since NH_4OH decomposes into NH_3 and H_2O at low temperature, no residue will remain inside the sample after proper heat-treatment.

Experiment A was the control experiment where aging was conducted in the standard pore liquor. Experiment B, aging in NH_4OH solutions, led to the discovery of a means to control the texture of gel-silica monoliths.

4.1.3 Drying

After aging treatment, the gel-silica samples, either from experiment A or experiment B, were dried in specially designed Teflon® (TEF) drying chambers, each with a pin-hole on its cover. The chambers initially filled with D.I. water were placed upside down in the oven. As the temperature increased the water was expelled out through the pin-holes by the expansion of the vapor gathered in the upper parts of the chambers. Finally there was no water left in the chambers and the samples gradually dried completely. The drying schedule is shown in Figure 4.4.

According to de Boer and Vleeskens [170,171] a silica dried at 120°C under atmospheric conditions has lost all physisorbed water and still contains all surface hydroxyls. Heating at higher temperatures partially depletes the surface of OH groups. The 120°C criterion is based on the following arguments:

(a) Below 110°C the residual "water" content depends upon the water vapor pressure of the air in which the silica is dried; at 115°C this influence becomes negligibly small.

(b) Silica samples dried at 120°C under atmospheric conditions have the same water content (as determined by heating at 1200°C) as when they are pre-dried at 105°C and afterwards kept over P_2O_5, or when they are pre-dried at

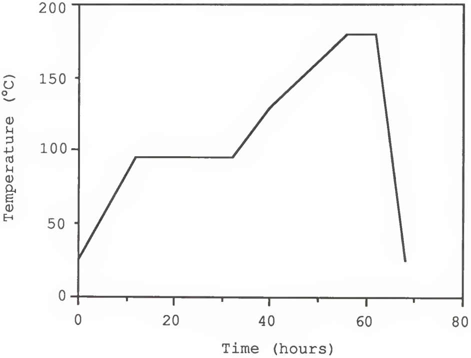

Figure 4.4 Schematic illustration of drying schedule for gel-silica samples.

105°C and then pumped off under high vacuum at room temperature.

However, this 120°C criterion has not been generally accepted in the literature. Lange [172] suggests that strongly physisorbed water, especially in very narrow micropores, requires drying temperatures approaching 180°C.

Experiments A and C had the same procedures before the drying step. In experiment C, the gel-silica samples were dried in an NH_4OH media (either solution or vapor) instead of D.I. water.

For convenience, the gel-silica samples obtained from experiments A, B and C are termed sample series A, B and C respectively.

4.1.4 Stabilization and Densification

Further stabilization and densification of gel-silica samples from all experiments were carried out at high temperatures in a box furnace in which the dried samples were placed in the quartz crucibles. The schedule is schematically shown in Figure 4.5.

In all the experiments, the linear contractions of the gel-silica samples were monitored during each processing step, especially the aging treatment step. The textural change and other property changes, including density,

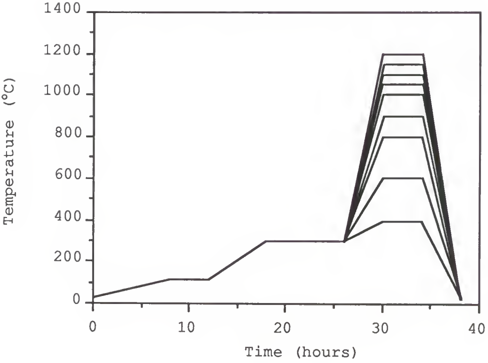

Figure 4.5 Schematic illustration of stabilization and densification schedules for gel-silica samples.

microhardness and UV transmission, of the samples were measured by the techniques summarized in the following section.

4.2 Texture Measurement

4.2.1 BET Theory

An understanding of the texture of a material can be achieved by the construction of an adsorption isotherm which is the result of measurement of the quantity of adsorbate on the surface of the material over a wide range of relative pressure at constant temperature.

In comparison with Langmuir theory [173], the BET theory developed by Brunauer, Emmett and Teller [174-176] is a more general theory which can be used to describe all types of adsorption isotherms. The BET theory assumes that the uppermost molecules in adsorbed stacks are in dynamic equilibrium with the gas or vapor and only the equilibrium between the vapor and the adsorbate in the first layer can be described by the Langmuir theory.

In spite of alternative equations to describe the isotherm, the BET equation has retained its utility for many years. Though subsequent proposed schemes are useful for certain situations, the BET equation is still widely used in the following final form [177]:

$$\frac{P}{V_a(P_o-P)} = \frac{1}{V_mC} + \frac{(C-1)P}{V_mCP_o} \qquad (4.3)$$

where V_a is the moles of gas adsorbed per gram of adsorbent when the gas pressure is P, V_m is the monolayer capacity of the surface, that is, the number of moles of gas per gram of adsorbent required to form a monomolecular layer, P_o is the saturation gas pressure at the temperature used, and C is a constant which is a function of the heat of adsorption and depends on the chemical nature of the surface. When $P/V_a(P_o-P)$ is plotted as ordinate versus P/P_o as abscissa a line is obtained with slope s and intercept, i, on the ordinate:

$$s = \frac{C-1}{V_mC} \qquad (4.4)$$

$$i = \frac{1}{V_mC} \qquad (4.5)$$

Thus, the volume of a monolayer V_m can be obtained by combining equations (4.4) and (4.5).

$$V_m = \frac{1}{s+i} \qquad (4.6)$$

From V_m, the specific surface area S_{BET} in square meters per gram is determined from the equation

$$S_{BET} = V_m\, a_m\, N \times 10^{-20} \qquad (4.7)$$

where a_m is the molecular cross-sectional area of one gas molecule in square angstroms which may vary on different surfaces, and N, the Avogadro constant, is 6.023×10^{23} molecules/mole.

The total pore volume can be derived from the amount of adsorbate vapor adsorbed at a relative pressure, P/Po, close to unity, by assuming that the pores are then filled with liquid adsorbate.

The average pore radius can be obtained from the pore volume and the specific surface area, by assuming cylindrical pore geometry. The pore size distribution is calculated using the method proposed by Barrett, Joyner and Halenda [178].

Because adsorption characteristics change with pore size [39], it is convenient to classify porosity by the terms micropores (radius < 20 Å), mesopores (radius from 20 to 2000 Å), and macropores (radius > 2000 Å). This terminology was proposed and later modified by Dubinin [178,179]

According to Brunauer et al. [176], all adsorption isotherms may be grouped into one of the five types shown in Figure 4.6.

The type I or Langmuir isotherm is concave to the P/Po axis and the amount of adsorbate approaches a limiting value as P/Po approaches 1. Type I physisorption isotherms are exhibited by microporous solids having relatively small external surfaces, for example, activated carbon and molecular sieve zeolites. The limiting uptake of adsorbate is governed by the accessible micropore volume rather than by the internal surface area.

The type II isotherm is the normal form of isotherm obtained with a nonporous or macroporous adsorbent. This type of isotherm represents unrestricted monolayer-multilayer adsorption. The starting point of the linear central section of the isotherm, is usually taken to indicate the relative pressure at which monolayer coverage is complete.

The type III isotherm is convex to the P/Po axis over its entire range. Type III isotherms are rarely encountered. However, a well-known example is the adsorption of water vapor on nonporous carbons. The absence of a distinct point B on a type III isotherm is caused by stronger adsorbate-adsorbate than adsorbate-adsorbent interactions.

The type IV isotherms are associated with capillary condensation in mesopores, indicated by the steep slope at

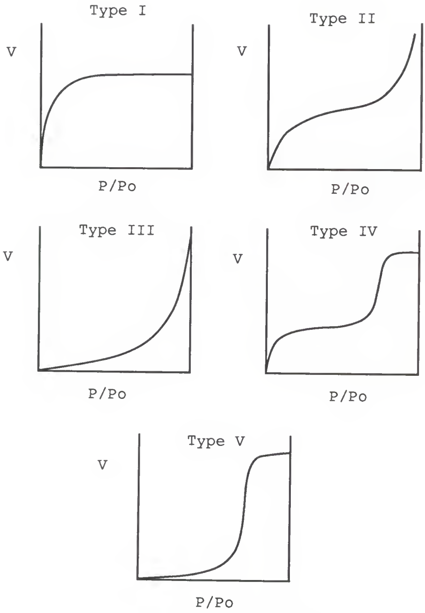

V: Volume of adsorbate

P/Po: Relative pressure

Figure 4.6 Five types of adsorption isotherms [176].

higher relative pressures. The initial part of the type IV isotherm follows the same path as the type II.

Type V isotherms are uncommon, corresponding to the type III, except that pores in the mesopore range (from 20 Å to 2000 Å) are present.

When the volume adsorbed (V) is plotted versus the relative pressure (P/P_O) for both adsorption and desorption processes a hysteresis loop is commonly formed.

De Boer [180] showed that in practical cases the shape of the hysteresis may lead to a more or less detailed picture of the shape of the pores present in a certain adsorbent. He has identified five types of hysteresis loops (Figure 4.7) and correlated them with various pore shapes among which three commonly denoted by the type A, B and E (Figure 4.8) have proved to be of great importance in the interpretation of sorption isotherms. Typically, type A hysteresis has two very steep branches and can be related in its simplest form to cylindrical pores open at both ends. A B-type hysteresis loop is characterized by a vertical adsorption branch near saturation and a steep desorption branch at intermediate relative pressures; it is associated with slit-shaped pores. An E-type hysteresis loop is intermediate between types A and B. While the desorption branch is steep, the adsorption branch is sloping. It has been attributed to "ink-bottle" pores (bottle shaped pores with narrow necks) [181].

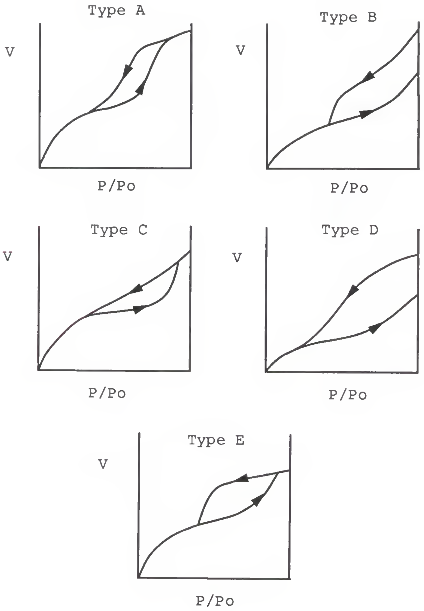

V: Volume of adsorbate

P/Po: Relative pressure

Figure 4.7 de Boer's five types of hysteresis loops [180].

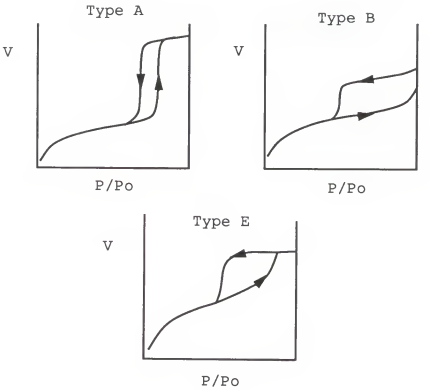

V: Volume of adsorbate

P/Po: Relative pressure

Figure 4.8 Three important types of hysteresis loops [84].

Despite the qualitative correlation between type of hysteresis and shape of pores, Broekhoff and Linsen [182] point out that there is no satisfactory quantitative theory of hysteresis behavior of adsorption isotherms.

Nitrogen is the most suitable adsorbate and is widely used for textural determinations since it exhibits intermediate values for the C constant (50-250) on most solid surfaces which makes it possible to calculate its cross-sectional area from its bulk liquid properties [183,184]. For the hexagonal close-packed nitrogen monolayer at 77 K, the molecular cross-sectional area, a_m, for nitrogen is 16.3 $Å^2$.

The BET theory and the nitrogen adsorption techniques have been widely used in the study of the texture of gel-silicas with well established applicability [84,185-190].

4.2.2 BET Equipment

The texture of gel-silica samples were measured using an automatic gas-adsorption equipment, the AUTOSORB-6 (Quantachrome, Inc.).

The AUTOSORB-6 operates by measuring the quantity of nitrogen adsorbed onto or desorbed from a solid surface at some equilibrium vapor pressure by the static volumetric method. The data is obtained point-by-point by admitting or removing a known quantity of nitrogen into or out of a sample cell containing the solid adsorbent maintained at a constant temperature below the critical temperature of nitrogen. As adsorption or desorption occurs the pressure in the sample cell changes until equilibrium is established. The quantity of nitrogen adsorbed or desorbed at the equilibrium pressure is the difference between the amount of nitrogen admitted or removed and the amount required to fill the space around the adsorbent (void space).

The AUTOSORB-6 has the capability of measuring adsorbed or desorbed volumes of nitrogen at relative pressures in the range of 0.01 to slightly under 1.0.

The volume-pressure data can be reduced by the AUTOSORB-6 into BET surface area (single and/or multipoint), Langmuir surface area, adsorption and/or desorption isotherms, pore size and surface area distributions, total pore volume and average pore radius.

It should be emphasized that since few bridging bonds are broken and reformed during solvent removal, the texture of the resulting porous xerogel (the standard glass preform) bears some relation to the structure at the gel point. Thus, the data from dried gel-silica samples can be used to explain the behavior of wet gels.

4.3. Property Characterization

4.3.1 Density

The true density of dried gel-silica samples was determined by a Quantachrome Micropycnometer which is an instrument specifically designed to measure the true volume of a small quantity of a solid sample via the application of the Archimedes principle of fluid displacement. The displaced fluid used in this instrument is helium, which can penetrate the finest of pores (approaching 1 Å) to insure maximum accuracy.

The micropycnometer determines the true density of the samples by measuring the pressure difference when a known quantity of helium under pressure is allowed to flow from a precisely known reference volume (V_R) into a sample cell containing the solid or powdered material [191].

Mercury pycnometry was utilized to measure the bulk density of dried gel-silica. After being dried at 180°C in the oven and cooled to room temperature, the sample was weighed and its bulk volume was determined by immersion in a pycnometry bottle in which mercury was used as the immersion liquid.

In our work, the bulk density of wet gels was also measured. Since wet gels were saturated with pore liquor, the pore liquid itself (with measured density of 0.945 g/cm^3) collected during the experiment was used as the immersion liquid instead of mercury.

4.3.2 Microhardness

The Vickers hardness number (VHN) is defined [192] as the load experienced by the material divided by the surface area of the indentation. The VHN is calculated using the following equation:

$$\mathrm{VHN} = (1.854\ P)/L^2 \qquad (4.8)$$

where P is the applied load in kilograms, and L is the average length of the diagonals of the indentation (mm).

The instrument used in our investigation was a semi-automatic Leco DM-400F Hardness Tester, incorporating an ACP-94 computing printer. A load P of 50 g, 100 g, 200 g and 300 g respectively but with a fixed loading time of 20 seconds was selected for different samples examined.

4.3.3. UV-VIS-NIR Spectra

The equipment used in this study was the Perkin-Elmer Lambda 9 UV-VIS-NIR Spectrophotometer which consists of a high performance double-beam, double-monochromator and a superior signal-to-noise energy optimized optical system throughout the entire 185-3200 nm wavelength range. The radiation sources change automatically during the operation of the instrument.

In order to minimize loss through geometric scattering, in most cases, 45 x 45 x 10 mm gel-silica samples with flat surfaces were used in the spectrophotometer.

4.3.4 pH Measurement

The pH of the aging medium before and after aging treatment was measured by an EA 920 Expandable IonAnalyzer (Orion Research).

4.3.5. Si Ion Concentration Measurement

The variation of concentration of Si ions in the solution during aging treatment was quantitatively analyzed by Inductively Coupled Plasma (IL Plasma 200) atomic emission spectrometry. The liquid samples were nebulized by a normal method and all the data including the location and the intensity of the emission lines in the conventional UV-visible region of the spectrum were processed and printed out by the IL PDS-1 Plasma Data System.

CHAPTER V
TEXTURAL AND PROPERTY CHANGES OF GEL-SILICA

5.1 Textural Changes

5.1.1 Surface Area, Pore Volume and Pore Radius

Based on the experiment from which the gel-silica monoliths were produced, the samples were grouped into three series: series A, series B and series C. Obviously, regular Type VI gel-silica belongs to series A.

Textural changes, mainly characterized by the surface area, the total pore volume and the average pore radius, of series A gel-silica sample with aging time and temperature were obtained by BET measurement. Results are shown in Figures 5.1-5.6, respectively.

In general, various aging parameters, including aging temperature and aging time, did not remarkably affect the gel texture. The so-called "one way change": the surface area decreases, the total pore volume remains constant and the average pore radius increases with increasing the aging time and aging temperature, which Iler proposed in his book "Chemistry of Silica" was not found.

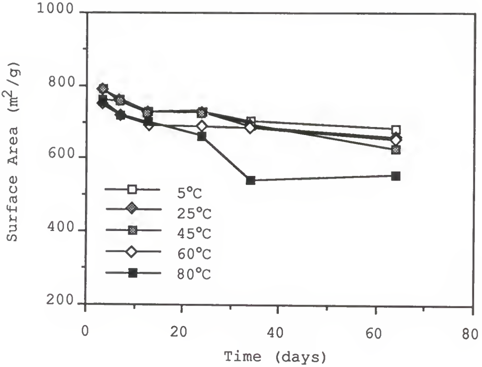

Figure 5.1 Variation of surface area of gel-silica samples aged in pore liquid at various temperatures as a function of time.

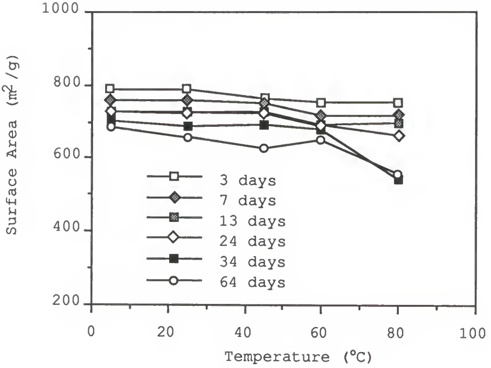

Figure 5.2 Variation of surface area of gel-silica samples aged in pore liquid for various times as a function of temperature.

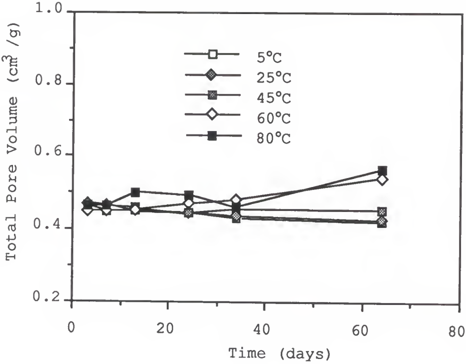

Figure 5.3 Variation of pore volume of gel-silica samples aged in pore liquid at various temperatures as a function of time.

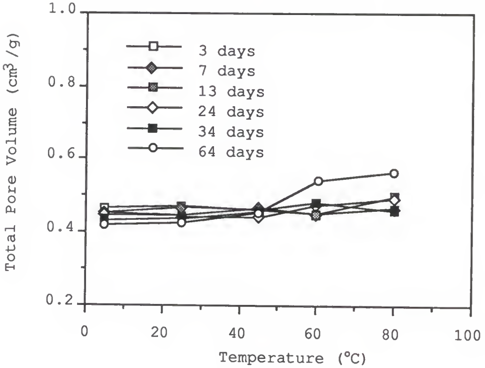

Figure 5.4 Variation of total pore volume of gel-silica samples aged in pore liquid for various times as a function of temperature.

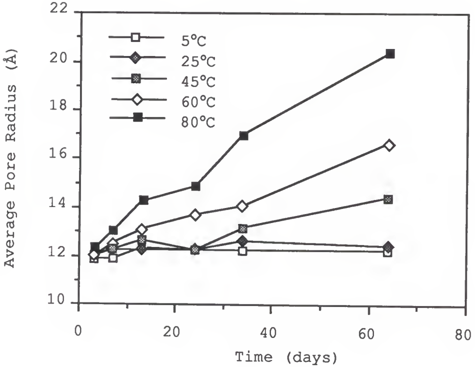

Figure 5.5 Variation of average pore radius of gel-silica samples aged in pore liquid at various temperatures as a function of time.

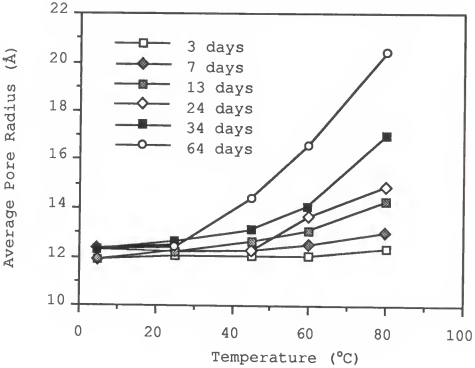

Figure 5.6 Variation of average pore radius of gel-silica samples aged in pore liquid for various times as a function of temperature.

During aging, the surface area and the total pore volume of series A gel-silica samples remained almost constant. Comparatively speaking, only the average pore radius slightly changed with the aging parameters.

As a general trend, the aging temperature has more profound effect than aging time on the texture of the series A gel-silica samples. Some textural changes occurred only when the aging temperature went to higher values.

It is interesting to point out that in Figure 5.7 there seems to be a linear relationship between the average pore radius of the gel-silica samples and the aging time at a fixed aging temperature. The straight lines shown in the figure were obtained by simple curve fitting which can be expressed by the following general equation:

$$R_{pore} = St + C_1 \qquad (5.1)$$

where R_{pore} is the average pore radius, t = aging time, S = slope which is closely related to the aging temperature and C_1 is a constant.

The slope S of the plot of average pore radius versus aging time changed with aging temperature in the following manner. When aging temperature was lower than 25°C, the slope was so low that the texture of the gel-silica samples remained unchanged with aging time. This has been proved by

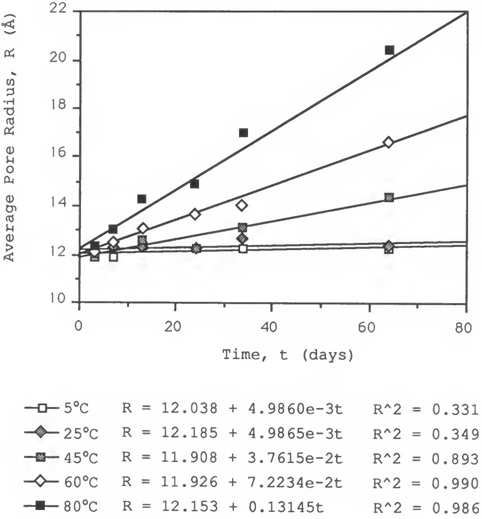

Figure 5.7 Variation of slope (S) of pore size vs time plots as a function of temperature.

the fact that the texture of gel-silica sample aged in its pore liquid at room temperature for as long as 227 days was almost the same as that of the sample aged under the same condition but only for 24 hours. For example, for both times the sample's surface area was 716.70 m^2/g, total pore volume was 0.40637 cm^3/g and the average pore radius was 11.34 Å. However, when aging temperature was increased above 45°C, the slope S increased and a significant change of the average pore radius with the aging time was observed.

The temperature dependence of the slope of the aging kinetics curve S can therefore be described as:

$$S = C_2 \exp(-E/kT) \qquad (5.2)$$

or

$$\mathrm{Log}S = C_3 - S'(1/T) \qquad (5.3)$$

where C_2 is constant, C_3 is equal to $\log C_2$, S' is equal to E/k, E is the activation energy which is related to the pore growth and k is Boltzmann's constant, i.e. 1.382×10^{-16} erg/K or 1.382×10^{-23} J/K.

By plotting log S versus 1/T, another straight line with slope S' could obtained (shown in Figure 5.8). The activation energy E was calculated from this plot. Since pore size is closely correlated with particle size in the gels [193], E can be considered as the activation energy of growth

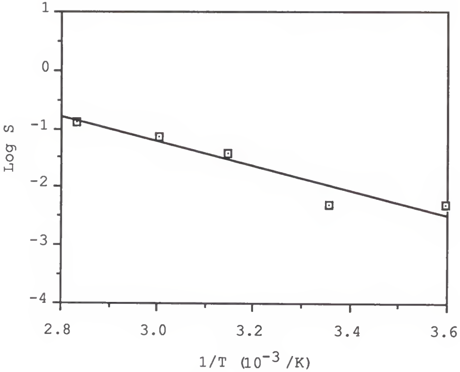

Log S = 5.0963 - 2.1046(1/T)
R^2 = 0.909

Figure 5.8 Log S vs. 1/T.

of gel particles and also as the activation energy of the proposed aging mechanisms. From Figure 5.1.1.8, S' equals 2.1046×10^3 and then E is equal to 2.91×10^{-20} J/K (17.53 kJ/mole·K). The significance of this value of E will be discussed later.

The maximum pore radius obtained through experiment A was around 20 Å, which is only twice as large as that of the regular Type VI gel-silica.

On the contrary, the texture of series B gel-silica samples changed tremendously during the aging treatment and Iler's "one way change" trend of textural change was observed.

Table 5.1 showed that, after being treated in 14 N NH_4OH solution at 60°C for 61 days, the surface area of dried gel-silica sample dropped from 750 to less than 200 m^2/g, the total pore volume expanded from 0.50 to around 1.15 cm^3/g, which means that the volume fraction of porosity expanded from 50% to 71%, and the average pore radius increased drastically from 14 Å to 130 Å, which is almost an order of magnitude change in mean size of pores in the monoliths.

Figures 5.9, 5.10 and 5.11 present the effect of aging treatment time on the texture of the NH_4OH treated series B gel-silica samples. With increasing aging treatment time, the surface area of the samples decreased and the total pore volume and the average pore radius increased. The texture of

Table 5.1
Textural change of gel-silica samples

Sample I.D.	Surface area (m^2/g)	Pore volume (cm^3/g)	Pore radius (Å)
A	749	0.56	14.8
B	175	1.15	131.0

Sample A: Gel-silica aged in the pore liquor at 60°C for 61 days.

Sample B: Gel-silica aged in a 14 N NH_4OH at 60°C for 61 days.

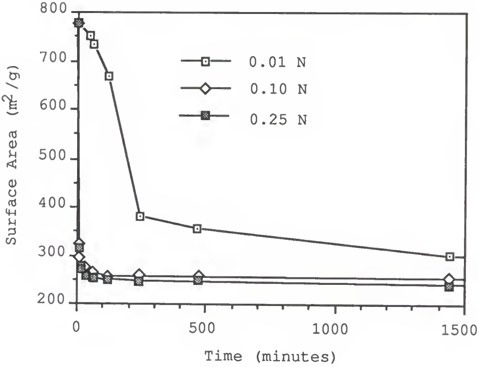

Figure 5.9 Time effect on surface area of gel-silica samples aged in NH4OH solution with various concentrations at 25°C.

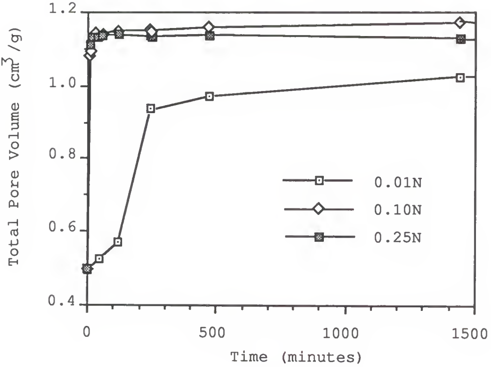

Figure 5.10 Time effect on total pore volume of gel-silica samples aged in NH4OH solution with various concentrations at 25°C.

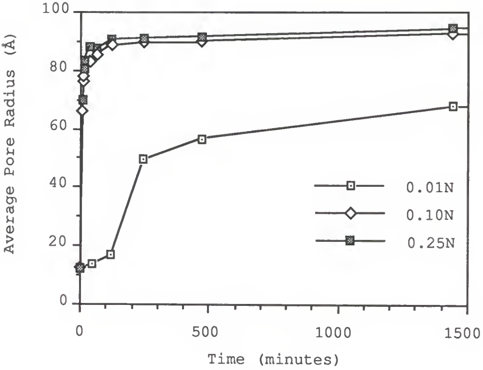

Figure 5.11 Time effect on average pore radius of gel-silica samples aged in NH4OH solution with various concentrations at 25°C.

all the samples changed sharply at the very early stage of the treatment. The detailed time dependence of the texture could be seen clearly in the dilute NH_4OH solution (e.g. 0.01 N). Table 5.2 reveals that drastic textural change for the gel-silica sample aged in a 0.01 N NH_4OH solution at 25°C occurred within 120 minutes. The length of this time span decreased with the increased NH_4OH concentration.

The variation of the surface area, the total pore volume and the average pore radius as a function of aging treatment temperature is demonstrated in Figures 5.12, 5.13 and 5.14 respectively. The aging treatment temperature seems to have little effect on the gel texture when aging in a NH_4OH solution.

Besides aging treatment time and temperature, another aging variable, i.e. the concentration of the aging medium NH_4OH, played the most important role during the aging treatment in the experiment B.

Figures 5.15, 5.16 and 5.17 show roughly the NH_4OH concentration dependence of the texture of the gel monoliths. The general trend is that the surface area of series B gel-silica samples decreased, the total pore volume increased and then slightly decreased, and the average pore radius increased with increasing NH_4OH concentration at a fixed treatment time (1 day). It has been found that the texture of the gel-silica samples was very sensitive to the NH_4OH

Table 5.2
Textural change as a function of aging time
for gel-silica samples
aged in a 0.01 N NH_4OH solution at 25°C

Time (minutes)	Surface area (m^2/g)	Pore volume (cm^3/g)	Pore radius (Å)
0	786	0.49	12.4
5	743	0.44	11.8
10	759	0.46	12.0
15	792	0.50	12.6
30	779	0.53	13.6
45	666	0.57	17.1
120	380	0.94	49.5
240	358	1.04	57.9
1440	302	1.02	67.7
5760	287	1.06	73.6

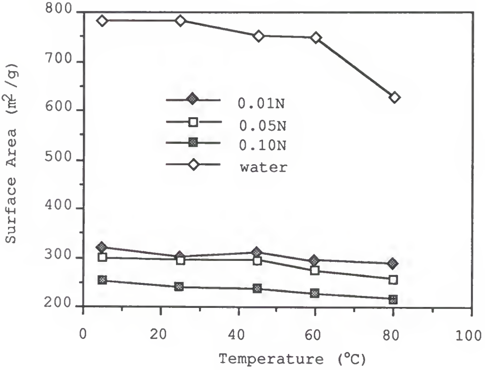

Figure 5.12 Temperature effect on the surface area of gel-silica samples aged in NH4OH solution with various concentrations for 1 day.

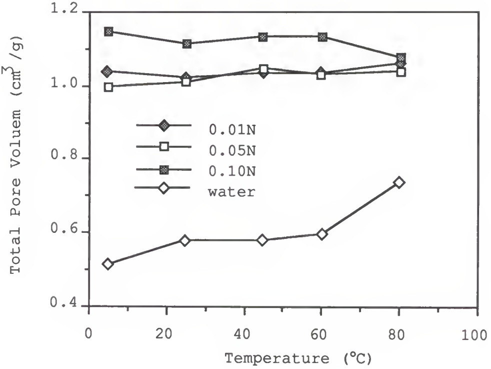

Figure 5.13 Temperature effect on the total pore volume of gel-silica samples aged in NH_4OH solution with various concentrations for 1 day.

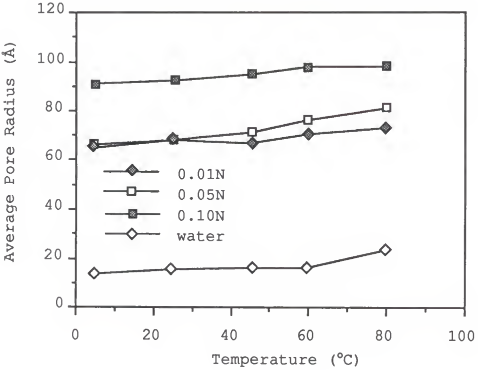

Figure 5.14 Temperature effect on the average pore radius of gel-silica samples aged in NH4OH solution with various concentrations for 1 day.

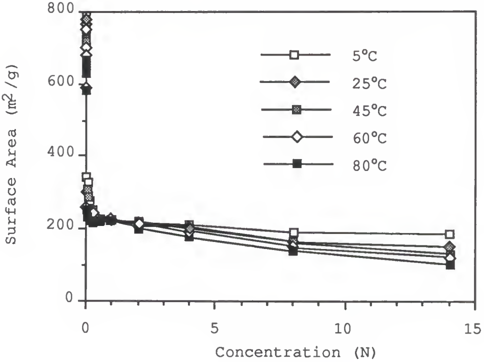

Figure 5.15 Concentration effect on surface area of gel-silica samples aged in NH4OH solution at different temperature for 1 day.

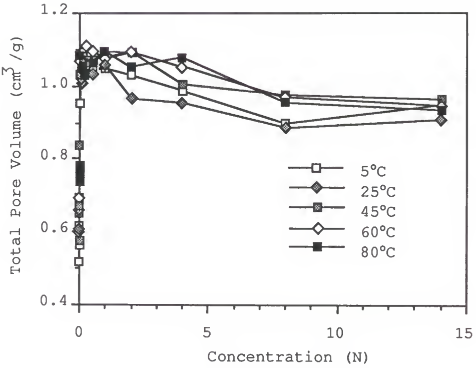

Figure 5.16 Concentration effect on total pore volume of gel-silica samples aged in NH4OH solution at different temperatures for 1 day.

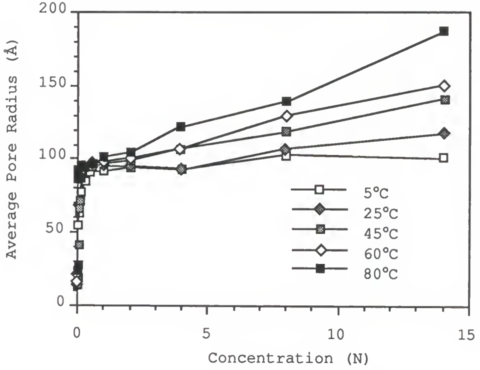

Figure 5.17 Concentration effect on average pore radius of gel-silica samples aged in NH4OH soluiton at various temperatures for 1 day.

concentration. All the figures demonstrate that the sharp textural change of the samples took place in a very dilute concentration range.

Figures 5.18, 5.19 and 5.20 provide the detailed information about the NH_4OH concentration effect on the texture of gel-silica samples. As shown in Table 5.3, the texture of the samples remained nearly unchanged until the NH_4OH concentration reached 0.01 N at which the surface area dropped from 678 m^2/g to 301 m^2/g, the total pore volume jumped from 0.65 cm^3/g to 1.02 cm^3/g, whereas at the same time the average pore radius increased from 19.1 Å to 67.7 Å. After that critical point no further significant textural changes with NH_4OH concentration were observed. The final values of the gel texture were found to be determined by the aging treatment temperature. In general, the higher the NH_4OH concentration and aging treatment temperature applied, the larger porosity of the gel-silica samples.

Even though NH_4OH is a weak base, high concentrations might damage the surface of the sample or even the bulk. It has been observed that improper treatment causes pitting and severe corrosion on the surface of gel-silica monoliths. In order to obtain monolithic gel-silica with relatively good optical or mechanical properties, use of dilute NH_4OH solutions, moderate treatment temperatures and longer treatment times are required.

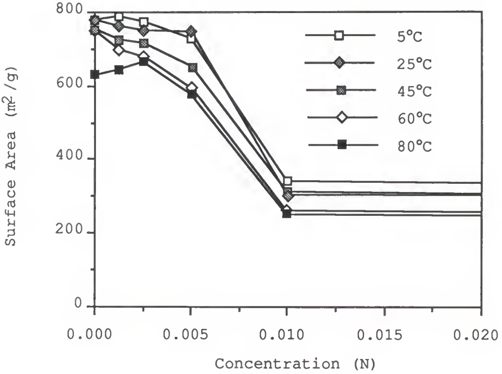

Figure 5.18 Concentration effect on surface area of gel-silica samples aged in dilute NH4OH solution at different temperature for 1 day.

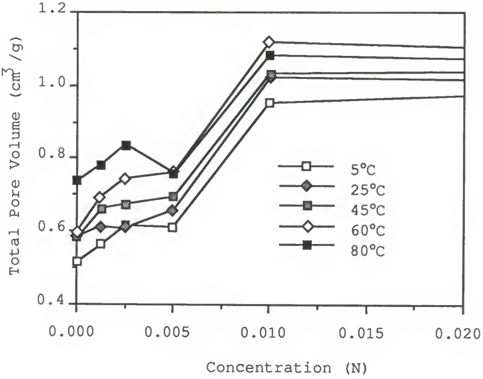

Figure 5.19 Concentration effect on total pore volume of gel-silica samples aged in dilute NH4OH solution at different temperatures for 1 day.

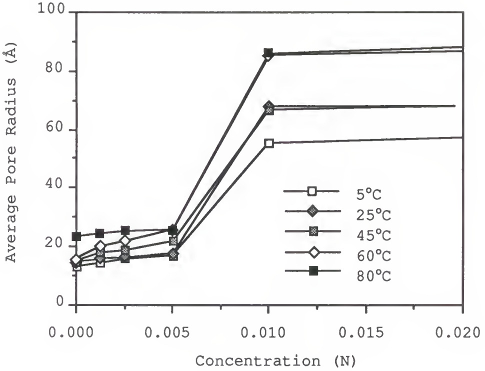

Figure 5.20 Concentration effect on average pore radius of gel-silica samples aged in dilute NH4OH soluiton at various temperatures for 1 day.

Table 5.3
Textural change as a function of NH_4OH concentration
for gel-silica samples aged
in NH_4OH solution at 25°C for 1 day

Concentration (N)	Surface area (m^2/g)	Pore volume (cm^3/g)	Pore radius (Å)
0	786	0.49	12.4
0.00125	784	0.61	15.6
0.00250	720	0.66	18.4
0.00500	678	0.65	19.1
0.01	302	1.02	67.7
0.05	296	1.01	68.2
0.10	252	1.17	92.6
0.25	222	1.03	92.7
1.00	219	1.05	95.9

Table 5.4 shows the textural change of series C gel-silica samples. During experiment C the medium in the drying chamber plays an important role in the evolution of the gel texture. Since series A and series C gel-silica samples were prepared from the same batch , gelled and aged under the same conditions, they should have the same texture if the drying variables were kept identical. In fact, as described earlier, the drying process, strictly speaking the medium (wither gaseous or liquid) in the the drying chamber, of the two series was different, Here, the series A samples were separately dried in an empty drying chamber, i.e. in an ambient atmosphere or we can say in the vapor of their own pore liquor. In contrast, gels from series C were dried in a drying chamber, also without D.I. water, but in the presence of series B samples which had been further aged in the NH_4OH solution for 4 days and saturated with ammonium hydroxide. Ammonium and hydroxide ions in aqueous solutions were in equilibrium with ammonia and water:

$$NH^{4+}{}_{(aqueous)} + OH^{-}{}_{(aqueous)} = NH_{3(aqueous)} + H_2O \qquad (5.4)$$

Thus during drying as the temperature increased, the NH_3 gas resulting from the decomposition of the NH_4OH solution in the pores of series B samples gradually filled the drying chamber and created a basic gaseous drying medium.

Table 5.4
The effect of atmosphere
in drying chamber on gel textures
(Experiment C)

Sample I.D.	Multi-point area (m^2/g)	Total pore volume (cm^3/g)	Average pore radius (Å)
A	716.70	0.406	11.34
B	151.15	1.021	135.13
C	271.35	1.117	82.33

Sample A	Gels aged in their own pore liquid at room temperature for 227 days, then dried at 180 °C.
Sample B	Gels aged in their own pore liquid at room temperature for 203 days, then aged in NH_4OH (assay 28-30%) for 4 days and finally dried at 180°C.
Sample C	Gels aged in their own pore liquid at room temperature for 207 days, then dried together with Sample B at 180 °C in the same drying chamber.

Ammonia has a strong tendency to dissolve in water; this is indicated by its high solubility in water (700 volume of ammonia gas to 1 volume liquid water at 20°C and 1 atm pressure). This addition undoubtedly occurs through hydrogen bonding; thus

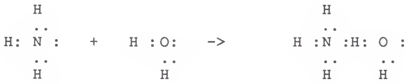

$$H{:}\overset{\overset{H}{\cdot\cdot}}{\underset{\underset{H}{\cdot\cdot}}{N}}{:} \quad + \quad H{:}\underset{\underset{H}{\cdot\cdot}}{O}{:} \quad \text{->} \quad H{:}\overset{\overset{H}{\cdot\cdot}}{\underset{\underset{H}{\cdot\cdot}}{N}}{:}H{:}\underset{\underset{H}{\cdot\cdot}}{O}{:} \qquad (5.5)$$

or

$$NH_{3(aqueous)} + H_2O = NH_4OH_{(aqueous)}$$
$$= NH^{4+}_{(aqueous)} + OH^{-}_{(aqueous)} \qquad (5.6)$$

As soon as the NH_3 vapor met the pore liquid on the surface of series C samples, the NH_4OH formed again and diffused into the gel through the pores and made the series C gel-silica samples undergo a process similar to the aging treatment in the NH_4OH media.

The series C gel-silica samples could also be produced in liquid media prepared by adding various amounts of NH_4OH into the D.I. water which was in the drying chamber. Similar results of textural change were observed. Compared with the texture of series B gel-silica samples, however, the texture of series C gels was difficult to predict and control, because the drying parameters had effects which introduced complexity into the experiment. Thus, in general, the results of experiment B were more favorable for use in controlling the texture of gel-silica monoliths.

5.1.2 Pore Shape and Pore Size Distribution

The specific surface area, the total pore volume and the average pore radius are still not sufficient to characterize a porous material. For a study of the texture of Type VI porous gel-silica, the shape and size distribution of the pores present in the material should also be known. The low temperature nitrogen adsorption BET technique also provides important information on this point.

An understanding of the porosity, including all the above information of a porous material, can be achieved by the construction of an adsorption isotherm. When the quantity of adsorbate on a surface is measured over a wide range of relative pressures at constant temperature, the result is an adsorption isotherm. The adsorption isotherm can be obtained point-by-point on the AUTOSORB-6 by admitting to the adsorbent successive known volumes of nitrogen and measuring the pressure. Similarly, a desorption isotherm can also be obtained by measuring the quantities of gas removed from the sample as the relative pressure is lowered which thereby forms the gas sorption hysteresis.

As mentioned in the preceding chapter, either adsorption isotherms or sorption hysteresis can be grouped into one of the five types shown in Figures 4.6, 4.7 and 4.8.

The gas sorption hysteresis for silica gels has been studied extensively [39,177,182,194,195]. Barrer et al. [196], investigated the shape of the isotherm and the hysteresis loop expected theoretically for different pore shapes, as calculated by means of Kelvin's equation:

$$RT\ln(Po/P) = \gamma V_L cos(\theta) \cdot (1/R_1+1/R_2) \qquad (5.7)$$

where P is the vapor pressure of the meniscus, Po is the saturation pressure of the bulk liquid, γ is the surface tension, V_L is the molar volume of the liquid phase, θ is the contact angle, and R_1 and R_2 are the two main radii of curvature of the meniscus. When it is assumed that the meniscus in the pore is hemispherical with two equal radii of curvature, the desorption pressure is thus given by:

$$RT\ln(Po/P) = 2\gamma V_L cos(\theta)/r \qquad (5.8)$$

where r is the radius of the capillary.

Following the reverse procedure, de Boer [197] showed that in practical cases the shape of the hysteresis loop may provide more or less detailed information about the shape of the pores present in a material.

It has been shown that the change in shape of the sorption hysteresis is not only indicative of a change in pore geometry but also in pore size distribution. For convenience, some rules are summarized as follows:

(1) The location of the hysteresis on the pressure axis is indicative of the average pore radius. As the average pore radius increases, the hysteresis is shifted to the right of the relative pressure axis. With very large pores, which are essentially infinite in size compared to a adsorbate molecule, pores are filled only at $p/p_o = 1.0$.

(2) The length of the hysteresis is indicative of the total pore volume. As the pore volume increases, the hysteresis increases in length.

(3) The width of the hysteresis is indicative of the relative size of the "neck" or other obstacles. A wider hysteresis indicates more difficulty in the desorption. A lower relative pressure is required for gas to be removed from the pores due to the narrower necks. If the pores are of uniform size, no hysteresis should be observed.

(4) The slope of the hysteresis is indicative of the pore size distribution. The steep slope indicates a narrow pore size distribution. If all the pores are the same size they would all fill at once when a certain vapor pressure is reached.

In experiment A, regardless of the length of aging or how high the aging temperature was, typical Type I adsorption isotherms were obtained. Type I isotherms are concave to the relative pressure (P/Po) axis. Also, Type E hysteresis loops, which are characterized by its steep desorption branch and sloping adsorption branch (curve (a) in Figure 5.21 for gel-silica sample aged in its pore liquor at 60°C for 61 days), were always observed. The results indicate that the series A gel-silica samples are microporous materials and the shape of the pores in the samples is ink-bottle-like. Since the width of the hysteresis loop was relatively large, the relative size of the necks of the "ink-bottle" were narrow.

In experiment B, for example, when gel-silica samples were aged in 1 N NH_4OH solution at 25°C, the adsorption isotherms changed shape from Type I to Type IV. The Type IV isotherms are featured by a steep slope at higher relative pressure. The change in isotherm type with aging treatment time occurred very quickly as shown in Figure 5.21, which symbolizes that most micropores (< 20 Å) were changed into micropores (20-2000 Å) during the treatment. Simultaneously,

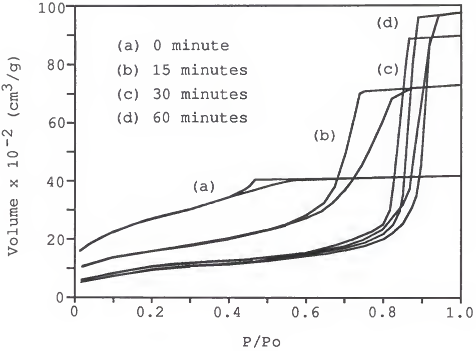

Figure 5.21 Variation of nitrogen sorption hysteresis as a function of time for gel-silica samples aged in a 1 N NH_4OH solution at 25°C.

the sorption hysteresis loop changed from Type E to Type A, which is characterized by two very steep branches. This change shows that the pores altered their shapes drastically from ink-bottle-like with narrow necks to cylindrical pores with both open ends. With increasing treatment time, the length of the hysteresis loop became larger indicating the total pore volume became larger; the width of hysteresis loop became smaller indicating that the relative size of the necks or other obstacles became smaller and the slope of the isotherm curves at high P/Po range became steeper indicating that the pore size distribution about the mean became narrower. All these changes ended within 60 minutes. Longer treatment times generated the same hysteresis loops which superimposed upon each other.

Pore shape changed with aging treatment time more slowly when more dilute concentrations of NH_4OH was used. Figure 5.22 shows the variation of nitrogen sorption hysteresis as a function of aging treatment time for gel-silica samples aged in a 0.01 N NH_4OH solution at 25°C. The shape of the hysteresis loop obtained after 120 minutes treatment looked just like that of curve (b) in Figure 5.21 which was generated after 15 minutes treatment in a 1 N NH_4OH solution at the same temperature.

The concentration dependence of pore shape is demonstrated in Figure 5.23. The shape of the pores

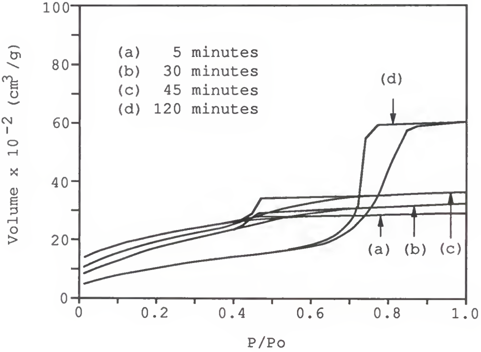

Figure 5.22 Variation of nitrogen sorption hysteresis as a function of time for gel-silica samples aged in a 0.01 N NH_4OH solution at 25°C.

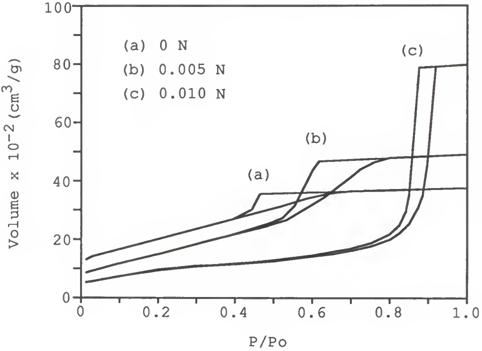

Figure 5.23 Variation of nitrogen sorption hysteresis as a function of NH4OH concentration for gel-silica samples aged in a NH4OH solution at 60°C for 1 day.

corresponding to the shape of the hysteresis loop changed with increasing NH_4OH concentration thereby following a similar trend. The pore shape changed from ink-bottle to a shape typical of cylindrical pores when the NH_4OH concentration reached 0.01 N at a fixed treatment temperature (60°C) for a fixed time (1 day). The shape of the hysteresis loop did not change significantly with the increased NH_4OH concentration which indicates that the pore shape of the gel-silica samples remained cylindrical.

The distribution of pore volume with respect to pore size is called a pore size distribution. A pore size distribution can be obtained either from an adsorption branch or from a desorption branch. The choice of using the adsorption or the desorption branch is determined by the most probable pore shape which may be inferred from the hysteresis loop. It is generally accepted [84] that although both adsorption and desorption branches are stable, the desorption isotherm is more appropriate than the adsorption isotherm for evaluating the pore size distribution of an adsorbent which has an ideal cylindrical shape of pores. The desorption branch of the isotherm, for the same volume of gas, exhibits a lower relative pressure, resulting in a lower free energy state. The adsorption branch is metastable relative to the desorption branch. Thus, the desorption isotherm is closer to true thermodynamic stability. However, in certain cases, for example, in samples exhibiting type E hysteresis, the adsorption branch has proved to be the thermodynamically stable one and the adsorption isotherm is recommended for determinations of pore size distribution.

The pore size distribution in sample series A is remarkably different from the pore size distribution in series B.

Figure 5.24 shows the variation of desorption pore size distribution as a function of aging time for gel-silica samples aged in a 1 N NH_4OH solution at 25°C. The mean pore radius increased with increasing the treatment time. In this figure, curve (a), which represents the series A gel-silica sample aged in the pore liquor at 60°C for 61 days, is asymmetric and broad. However, curves (b), (c) and (d) are symmetric and much narrower which should be related to the cylindrical pore shapes [198]. The change of pore size distribution also stopped after 60 minutes treatment. No further change was observed after 60 minutes aging.

The variation of pore distribution with aging treatment time in a dilute NH_4OH solution (0.01 N) is presented in Figure 5.25. The trend was similar to that shown in Figure 5.24 but the rate of change was slower. Although the significant change of pore size distribution of the gel-silica samples with aging treatment time in 0.01 N (dilute) NH_4OH solution occurred between 45 minutes to 120

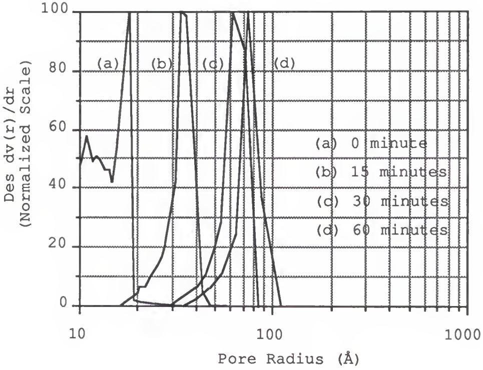

Figure 5.24 Variation of pore size distribution as a function of time for gel-silica samples aged in a 1 N NH_4OH solution at 25°C.

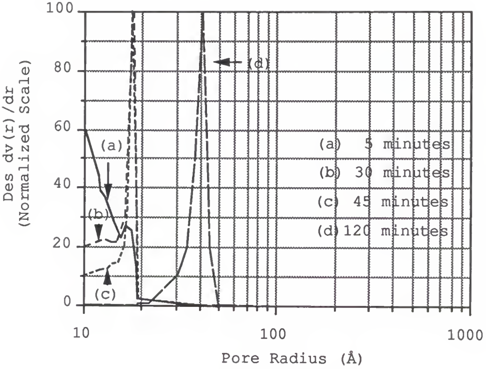

Figure 5.25 Variation of pore size distribution as a function of time for gel-silica samples aged in a 0.01 N NH_4OH solution at 25°C.

minutes, it did not stop there. After 120 minutes, the mean pore size continued to increase with increasing treatment time (see Table 5.2) which moved the distribution peak to the right.

It has been also found that the pore size distribution changed with NH_4OH concentration when the other parameters such as aging treatment temperature and time were fixed (Figure 5.26). As discussed earlier, NH_4OH concentration was the most effective parameter to control the texture. When the concentration reached 0.01 N, the substantial change of pore size distribution was completed.

The narrow pore size distributions resulting from these aging treatments should benefit subsequent steps of sol-gel processing. For example, the narrow distributions and larger pore sizes should greatly decrease the magnitude of capillary stresses induced during drying.

In summary, we have achieved control of the texture of gel-silica monoliths by varying the aging treatment temperature, aging treatment time and aging medium as well as the drying media. By controlling either aging parameters, mainly the aging medium and aging time (see Tables 5.2 and 5.3), or drying chamber environment (Table 5.4), the average pore radius of monolithic gel-silica samples can be varied from 12 Å to 148 Å or greater with very narrow pore size distributions around the mean. The volume fraction of

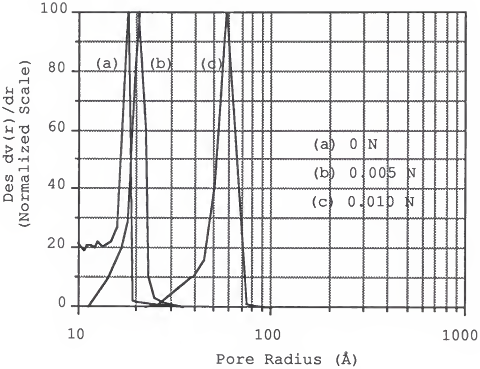

Figure 5.26 Variation of pore size distribution as a function of NH4OH concentration for gel-silica samples aged in NH4OH solution at 60°C for 1 day.

porosity can be varied from 52% to 74%. The shape of the pores can also be changed from ink-bottle-like with narrow necks to cylindrical pore open at both ends.

The above textural change greatly broaden the potential applications of Type-VI porous gel-silicas.

The large average pore radius with narrow size distribution and the large volume fraction of porosity will provide large accommodation for foreign molecules with different structures and various sizes. The cylindrical pores with open ends and less necks will favor the diffusion and impregnation processes required to make optical composites. The controllable surface area and surface chemistry will provide a large selection to match the chemical nature of impregnant phases.

5.2 Property Changes

5.2.1 Appearance and Dimension

Series A, B and C gel-silica monoliths with various dimensions (e.g. 45 x 45 x 10 mm and ϕ12 x 50 mm) and shapes including rods, disks, plates and slabs etc., were successfully obtained by the experimental procedures described in the preceding chapter. The series A gel-silica samples characterized by small average pore radius and small total pore volume were optically transparent and clear throughout the whole process. In contrast, the series B and C gel-silica samples were only slightly translucent or cloudy. Although the pore sizes of the sample series B and C were relatively larger than series A, obviously they are still not large enough to scatter the visible light except for a small amount of Rayleigh Scattering. Their translucent appearance is due to the larger pore volume rather than larger pore radius.

The general trend of linear dimensional change of gel-silica samples during aging in experiment A can be seen in Figures 5.27 and 5.28. The contraction of the wet gel resulting from syneresis increased rapidly with increasing aging temperature and then decreased its rate when the temperature became higher (>60°C) as shown in Figure 5.27. Figure 5.28 demonstrates the kinetics of contraction. The contraction increased with the increased aging time. However, when the time reached a critical point, the contraction of the sample eventually stopped.

The contraction behavior of series B gel-silica samples is shown in Figures 5.29 and 5.30. Actually, no contraction of the wet gel-silica samples was observed during aging treatment in experiment B. In contrast, the wet gel-silica samples swelled in the NH_4OH solution with the increase of aging treatment temperature as shown in Figure 5.29. Figure

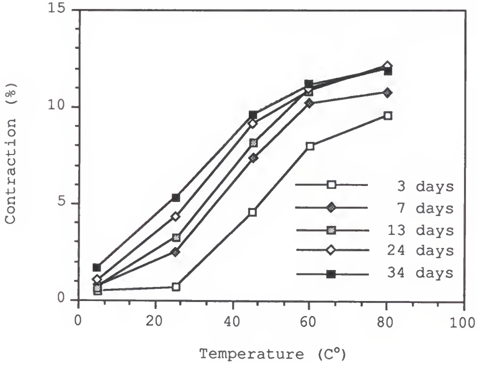

Figure 5.27 Variation of contraction as a function of aging temperature for wet gel-silica samples aged in their pore liquid for various times.

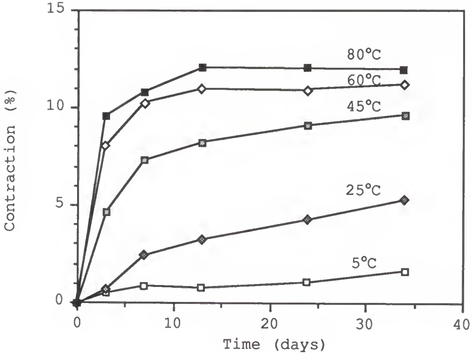

Figure 5.28 Variation of contraction as a function of aging time for wet gel-silica samples aged in their pore liquid at various temperatures.

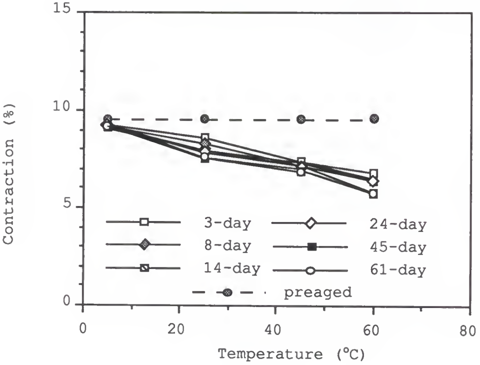

Figure 5.29 Variation of contraction as a function of aging temperature for wet gel-silica samples aged in a 14 N NH4OH solution for various times.

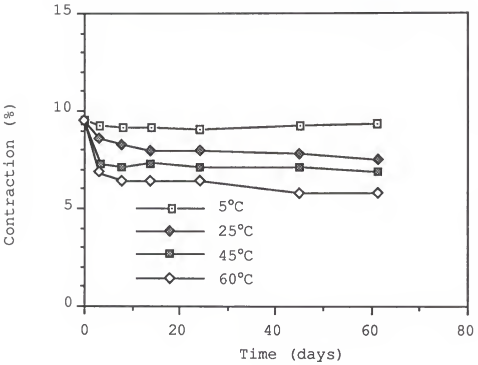

Figure 5.30 Variation of contraction as a function of aging time for wet gel-silica samples aged in a 14 N NH4OH solution at various temperatures.

5.30 indicates that the gel-silica samples dilated gradually with aging treatment time and finally reached a limit. The final dilation of the samples increased with the aging treatment temperature. The effect of aging temperature on the dilation is more profound than that of aging time. This is the first time the swelling phenomenon of gel-silica was observed. In most inorganic gels, syneresis is irreversible [93], and swelling of the gel has not been previously reported to the author's knowledge.

Comparing the dimensional changes of series A and series B gel-silica samples, it seems that between each set of figures, i.e. Figures 5.27 and 5.29, and Figures 5.28 and 5.30, there is a mirror through which the curves reflect each other. In other words, the changes in dimension of series A and B gel samples with aging temperature and aging time followed opposite ways.

5.2.2 Density

The true densities of both series A and series B gel-silica samples were measured using mercury pycnometry. Data collected from more than fifty samples aged at different temperatures (5, 25, 45, 60 and 80°C) for different times (3-64 days) yield an average true density of 2.19 g/cm^3 with a standard deviation of 0.068 g/cm^3 for series A gel-silica samples. The average true density of 2.12 g/cm^3 for series B gel-silica samples was obtained from the data collected from more than 20 samples aged in 14 N NH_4OH solution at different temperatures (5, 25, 45, 60 and 80°C) for different times (3-61 days). The standard deviation was only 0.020 g/cm^3.

In order to investigate the aging behavior more accurately, the bulk density of wet series A samples was measured using their pore liquor as immersion liquid. It has been observed that the bulk density of wet series A gel-silica samples increased greatly with both aging time and temperature. The effects of aging time and temperature on bulk density of the wet series A gel-silica samples shown in Figures 5.31 and 5.32 are very analogous to that on the contraction of the samples as shown in Figures 5.27 and 5.28. However, after drying, the effects of aging treatment temperature and time on bulk density of the dried samples were hardly detected. The bulk density of dried series A gel-silica samples remained almost constant (1.12 g/cm^3) regardless of how the aging parameter changed. This can be explained by the fact that the total pore volume of the dried series A gel-silica samples was nearly unchanged during aging, as shown in Figure 5.3. Since series A gel-silica samples are microporous materials in which the trapped water is difficult to remove, the measured densities are usually larger than the actual values. In practice, the bulk density

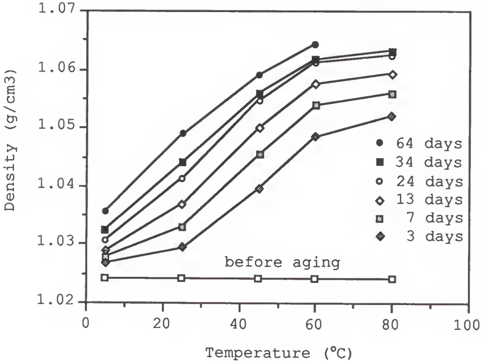

Figure 5.31 Variation of bulk density as a function of aging temperature for wet gel-silica samples aged in their pore liquor for various times.

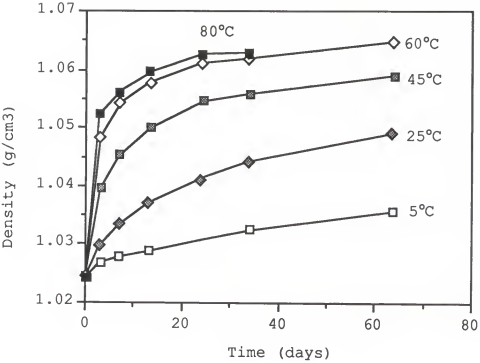

Figure 5.32 Variation of bulk density as a function of aging time for wet gel-silica samples aged in their pore liquor at various temperatures.

can be calculated directly from the BET data using Figure 5.33 by assuming the true density of the gels always remains constant (2.20 g/cm^3). This has been proved to be true in our work.

The bulk density of wet series B gel-silica samples, aged in 14 N NH_4OH solution at 45°C for longer than 3 days, was observed to fluctuate within a narrow range of 1.03 to 1.05 g/cm^3. The change in bulk density of the dried samples with aging time is shown in Figure 5.34. In concentrated NH_4OH solution, the rapid change in bulk density was believed to occur within a very short time period as other changes did. Therefore, after three days aging treatment, only the final value of the bulk density, around 0.65 g/cm^3, of the samples was observed which was no longer changed with aging time. This final value is very close to the calculated value of 0.67 g/cm^3 by using the total pore volume of 0.93 cm^3/g from the BET measurement and the relationship between the bulk density and the total pore volume shown in Figure 5.33.

5.2.3 Mechanical Strength

The microhardness (VHN, Vickers hardness number) of dried series A gel-silica samples was found not to change with aging parameters. The value of VHN remained around 40 regardless of the magnitude of aging temperature or length of

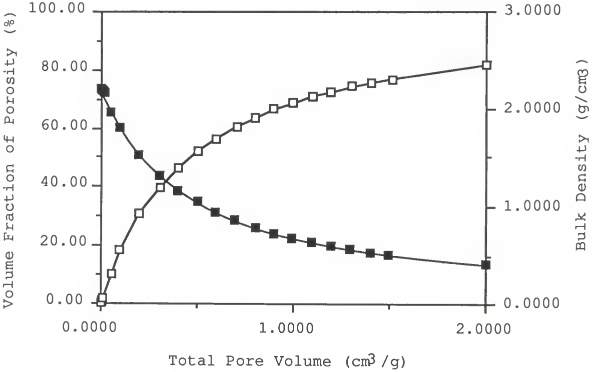

Figure 5.33 Theoretical relationship between volume fraction of porosity, bulk density and total pore volume of gel-silica samples. Assuming the true density of gel-silica is 2.20 g/cm3.

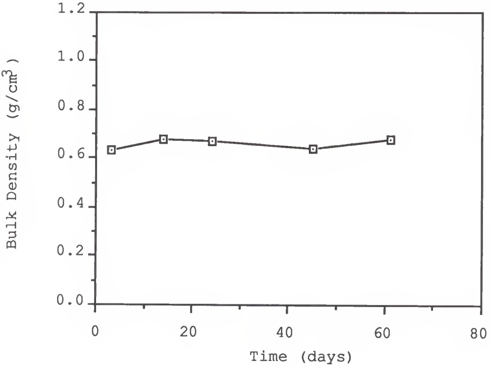

Figure 5.34 Variation of bulk density as a function of time for gel-silica samples aged in a 14 N NH_4OH solution at 45°C .

aging time. However, the microhardness of wet samples did change during aging.

The variation of microhardness as a function of aging time for wet gel-silica samples aged in the pore liquor (from experiment A) at different temperatures is shown in Figure 5.35. The standard deviations of the data were within 1.0. In order to make the curves distinguishable the error bares are not presented in the figure. The microhardness (VHN) increased with increase in aging time and the rate of increase became larger the higher the aging temperature. That means that the effect of aging time on the mechanical behavior of gels was strengthened by the aging temperature. The curve of gel-silica samples aged at 80°C shows a sharp change in its slope after 4 days. This is probably due to the loss of the liquid during the aging process. The actual value of VHN should be lower locating somewhere around the dashed line illustrated in the figure.

Since wet gel-silica samples became more rigid and elastic during aging in their own pore liquor, increasing the mechanical strength of gel-silica by this kind of aging treatment can still be considered as one of the most effective ways to solve the cracking problems during drying.

Use of high temperature aging is not always applicable to achieve high quality dried gels. The higher the aging temperature and the longer aging time used, the higher the

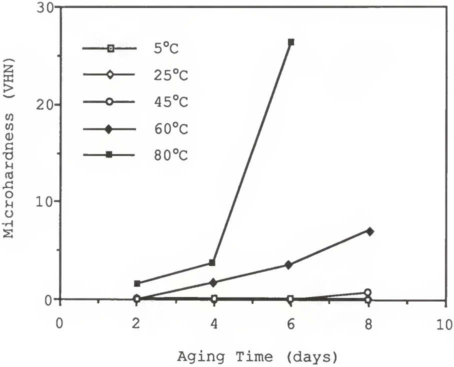

Figure 5.35 Variation of microhardness as a function of aging time for wet gel-silica samples aged in their pore liquor at different temperatures.

strength (including the microhardness) of the gel that was developed (Figure 5.35). However, at the same time, a larger contraction was also obtained (Figures 5.31 and 5.32). Consequently, the competition between these two factors will build considerable internal stresses in the gel which might break the gels during subsequent processing steps. Figure 5.36 shows that dried gels cracked severely when both high aging temperatures and long aging times were applied.

During aging treatment in experiment B, a contrary phenomenon was observed, i.e., the wet gel-silica samples always became more plastic. It was found that after extensive NH_4OH treatments, especially when an excess of concentrated NH_4OH (e.g. > 4 N) was employed, samples lost their rigidity and turned into very flexible paste-like materials which were even partially dissolved. Generally speaking, the microhardness (VHN) of the wet series B gel-silica samples was so low that it could not be measured by the available equipment. However, the strength of the gels was already high enough for the wet gels to undergo any subsequent process without failure. As long as proper parameters were optimized, wet gels with desired geometric dimension and shape as well as fairly good mechanical strength could be successfully produced using the NH_4OH aging treatment.

The strength of the dried series B samples was generally lower than that of the dried series A samples.

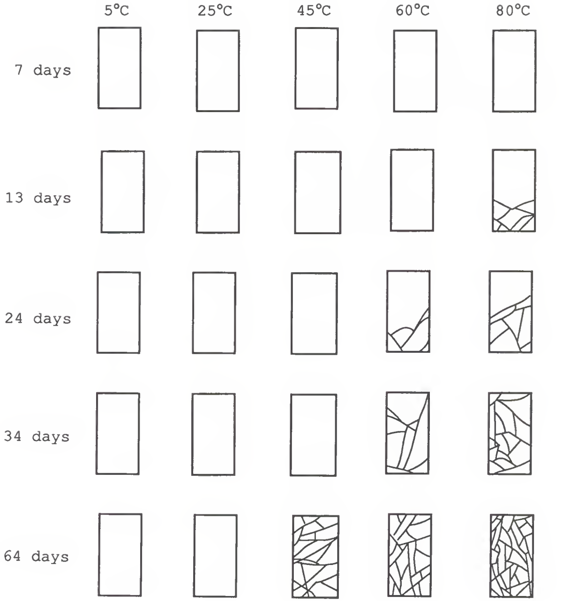

Figure 5.36 The appearance of gel-silica samples aged in their pore liquid at various temperatures for different periods of time after drying at 180°C. (Sample sizes are in arbitrary scales.)

Table 5.5 indicates that the dried strength of the samples aged in a 1 N NH_4OH solution at room temperature decreased sharply with the treatment time. The microhardness (VHN) dropped from 40.44 to 8.98 within only half an hour of aging. After 1 hour it decreased further to 7.88 and after 2 hours, 7.27, and remained almost unchanged even when the treatment time last as long as 15 days. The variation of microhardness (VHN) as a function of aging temperature is presented in Figure 5.37. Although the data were slightly scattered the VHN gradually decreased with the aging treatment temperature. The effect is especially large for the lower NH_4OH concentrations. The concentration of NH_4OH also plays an important role here. Figure 5.38 gives a general impression that the VHN of the samples dropped drastically with even low NH_4OH concentrations at first and then quickly reached a constant final value, determined by the treatment temperature. Figure 5.39 reveals the relationship between the VHN and the NH_4OH concentration in greater detail (for the same reason, the error bars are not presented in both figures). The mechanical property change of the samples occurred within a very narrow range (< 0.01 N) of NH_4OH concentration beyond which no further changes were observed.

In principle, gel-silica samples aged by a NH_4OH treatment were more difficult to dry due to the loss of

Table 5.5
Variation of microhardness as a function of aging time for gel-silica samples aged in a 1 N NH_4OH solution at 25°C then dried at 180°C

Aging treatment time	Microhardness (VHN)
0	40.44
30 minutes	8.98
60 minutes	7.88
120 minutes	7.27
15 days	7.74

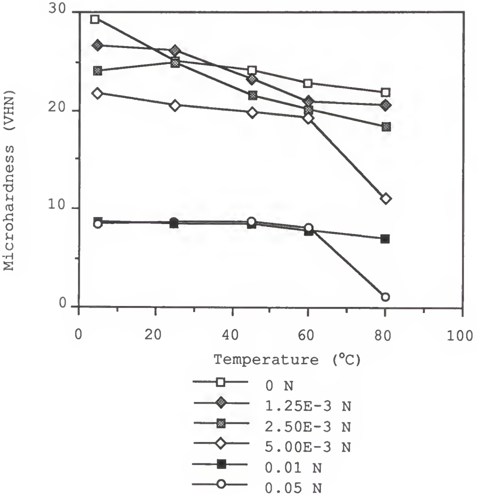

Figure 5.37 Variation of microhardness after drying at 180°C as a function of temperature for gel-silica samples aged in NH_4OH solution with various concentrations for 1 day.

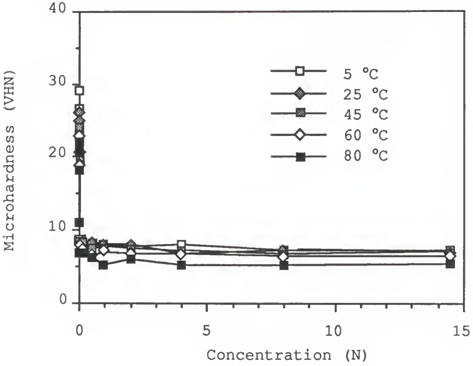

Figure 5.38 Variation of microhardness as a function of concentration of NH4OH for gel-silica samples aged in NH4OH solution at various temperatures for 1 day.

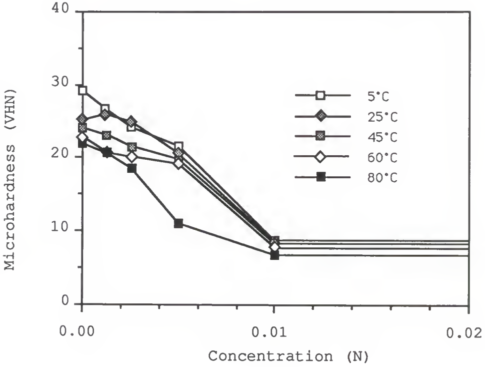

Figure 5.39 Variation of microhardness as a function of concentration of NH4OH for gel-silica samples aged in dilute NH4OH solution at various temperatures for 1 day.

mechanical strength during the treatment. Fortunately, once the gel-silica samples were dried, they could easily be stabilized at high temperature, e.g. 800 °C, which might be attributed to less further contraction during stabilization than the series A gel-silica (Table 5.6).

5.2.4 Densification Behavior

Densification is the last treatment process of gel-silicas. As already described, densification of a gel-silica network occurs between 1000-1700°C depending upon the radii of the pores and the surface area. Controlling the gel-glass transition is a difficult problem if one wants to obtain gel-silica monoliths with desired physical properties. It is essential to eliminate volatile species prior to pore closure and to eliminate density gradients due to nonuniform thermal or atmosphere gradients.

The driving force of densification is the reduction of specific surface area. Consequently, in the sol-gel processing of alcohol-derived gel-silicas it has been established that densification, including contraction behavior during the gel-to-glass conversion, depends greatly on the texture of the gels.

In our work, both series A and B gel-silica samples were densified using the schedules illustrated in Figure 4.5.

Table 5.6
Contraction of gel-silica samples after aging, drying and stabilization

	Contraction				
Sample series	After aging	After drying	B/w a & d	After stabilization	B/w d & s
A*	10.80%	50.01%	43.96%	55.25%	10.48%
B**	9.12%	41.65%	35.75%	43.25%	2.74%

* Gel aged in its own pore liquid at 60°C for 2 days then at 25°C for another 2 days.

** Gel aged in its own pore liquid at 60°C for 2 days and at 25°C for 2 days then treated in a 1 N NH_4OH for another 3 days.

The drying and stabilization schedules were kept identical.

Drying temperature: 180°C.
Stabilization temperature: 800°C.

During densification, neither gas flow nor an atmospheric chemical treatment was employed.

It is interesting to note that the densification behavior of series B gel-silica is quite different from that of series A gel-silica, including the regular small pore size Type VI gel-silica.

The densification of series A samples completely failed due to the serious foaming problem which usually started at 900°C. According to the Hench et al. [3], the regular gel-silica (12 Å average pore radius) which has a higher specific surface area (600-700 m^2/g) started to densify gradually above 600°C. The largest change in either bulk density or total pore volume of the gels occurred in the temperature range of 900-950°C. In order to obtain fully dense Type V gel-silica, chemical dehydration of the 12 Å pore size gels was required.

Figure 5.40 shows that the contraction of a typical series B gel-silica sample, with code number 0.25-1-25, which represents the sample was aged in 0.25 N NH_4OH for 1 day at 25°C, started densification at as high as 1000°C and ended at 1150°C.

It seems that full density was reached at 1150°C. After densification at 1200°C for 4 hours the final contraction of this series B gel-silica samples was 62.25%. Since the series B gel-silica samples shrank much less than the series A

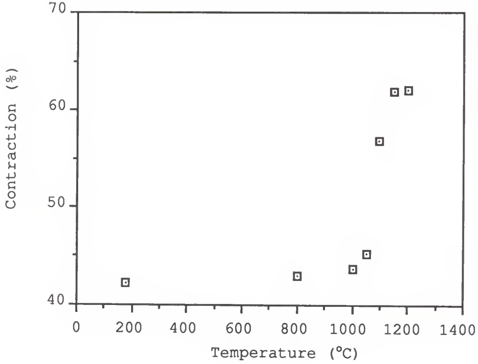

Figure 5.40 Contraction with densification temperature for gel-silica samples aged in a 0.25 N NH_4OH solution at 25°C for 1 day.

samples after drying, or even after stabilization (Table 5.6), the most significant contraction of series B samples occurred during densification. It is surprising that for 0.25-1-25 gel-silica samples with dimension as large as 45 x 45 x 10 mm, the yield of densification remained almost 100%, without cracking and foaming, and the total densification time was only about 38 hours, i.e. less than the 2 days often required to make Type V gel-silica. The resultant gel-silica samples had good optical properties which will be discussed later.

The possible reasons for the above phenomena are believed to rely on the gel texture. The texture of series A gel-silica was featured by its large surface area, small pore size and broad pore size distribution as discussed in preceding sections. Therefore, during densification, the large driving force resulting from the large surface area made the sintering process start at low temperature and proceed rapidly. Due to the broad pore size distribution, the pores were closed at different times. The smaller size pores usually collapsed first because of their higher "solubility" which blocked the path of the remaining volatile species to the outside atmosphere and consequently caused the foaming or bloating problems.

It is the textural features of the series B gel-silica samples, including a relatively low surface area and a large average pore radius with narrow pore size distribution, that helped the gels avoid foaming during densification. A low driving force due to low specific surface area allowed the sintering process to take place at a higher temperature with a relatively slower rate. The larger pore size makes it easier for the volatile species to diffuse out of the gels and allows more complete thermal dehydration to occur prior to pore closure. The narrow pore size distribution ensured that all of the pores inside the gels collapsed almost at the same time during the final stage of sintering and resulted in a foam-free structure.

The ease of densification might also be related to the good thermal shock resistivity of the series B gel-silica sample. The stabilized series B samples were rarely cracked or broken during grinding and polishing which often happened to the samples of series A.

Figure 5.41 demonstrates that the microhardness (VHN) of the samples changed with densification temperature in the same way that contraction did. The initial VHN of series B gel-silica samples was much lower than that of series A. However, VHN increased rapidly after 1100°C and finally reached a value of 630 at 1200°C which is almost as same as Vasconcelos reported for the densified 80 Å HF based gel-silica samples [96] and identical to the final density of densified series A samples as well.

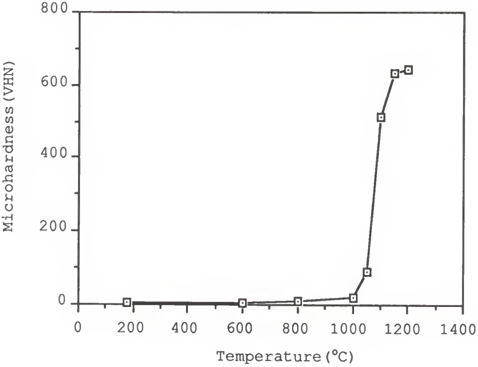

Figure 5.41 Variation of microhardness as a function of densification temperature for gel-silica samples aged in a 0.25 N NH_4OH solution at 25°C for 1 day.

It is very promising that the aging treatment can be used as an effective process to produce monolithic optical materials, such as lenses or preforms of fibers, requiring less or even no chemical dehydroxylation treatments which employ toxic gases, such as chlorine. Other procedures such as incremental heat-treatments or vacuum processing are also not required during densification of the NH_4OH aged gels.

The textural change of series B gel-silica as a function of densification temperature was also investigated. Figures 5.42, 5.43 and 5.44. show the variation of the surface area, the total pore volume and the average pore radius as a function of densification temperature for the 0.25-1-25 gel-silica samples, sometimes called 90 Å gel-silica samples based on their average pore radius. Compared with the textural change of series A gel-silica samples, e.g. the 12 Å gel-silica samples, with densification temperature shown in Figures 3.2 and 3.3, the following differences were found. The variation of the the texture of series A samples with densification temperature started at a lower temperature (around 600°C) than that of series B, then continued gradually and finally ended at 1200°C. However, the textural change of series B gel-silica samples were relatively stable over a broader temperature range. The surface area, the total pore volume and the average pore radius remained nearly constant until the densification

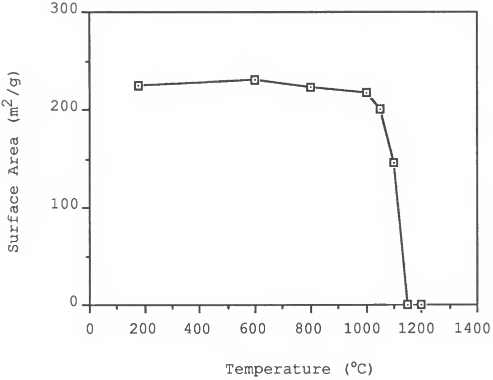

Figure 5.42 Variation of surface area of 90 Å average radius gel-silica samples as a function of processing temperature.

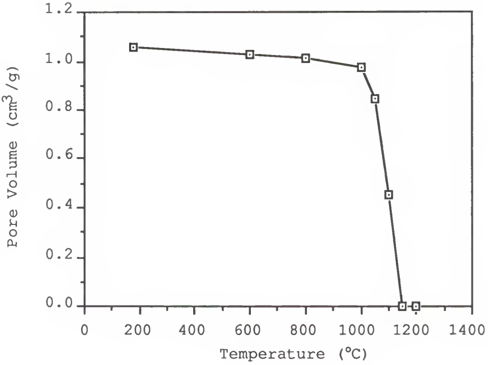

Figure 5.43 Variation of total pore volume of 90 Å average radius gel-silica samples as a function of processing temperature.

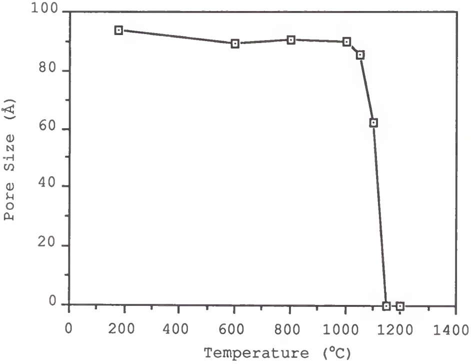

Figure 5.44 Variation of average pore radius of 90 Å gel-silica samples as a function of processing temperature.

temperature reached 1000°C then dropped drastically. The completion of densification was observed at 1150°C.

DeHoff [199] proposed that as in biology science function follows form; then in materials science, structure determines properties. Therefore, in order to study completely a material, two basic characteristics of the structure have to be defined:

1) The constitution of the structure, in terms of its chemical composition and components (e.g., its thermodynamic phases).

2) The geometry of the structure, which is described by two types of parameters: metric and topological parameters.

The metric properties of a structure include the change when the structure is stretched, distorted or twisted [199-208]. The topological properties include any property which is unchanged when the structure is stretched, distorted, or twisted without limit, so long as it is neither torn nor joined to itself during the deformation. Topological properties thus are closely related to the connectivity of a texture and are a measure of the "connectivity" of a structure. Topological properties are independent of details of shape and size and precisely because topology abstracts geometric properties without concern about metric detail they are valuable in characterizing complex structures.

Rhines [209] added to the metric parameters the topological concepts that provide complementary information about the sintering process [115,199,200,206]. In topological terms the densification process can be divided into three stages, according to the genus [209] (which is defined as the maximum number of non-self-reentrant closed curves that may be constructed on the surface without dividing it into two separate parts) [200]:

First stage: growth of weld necks while the genus remains constant.

Second stage: the genus decreases to zero as the pores become isolated.

Third stage: the genus remains constant at zero while the number of pores goes to zero.

The introduction of topological parameters to the structural characterization of gel-silica yields information that is not visible by considering metric parameters only. One important application of topological characterization is the characterization of an interconnected pore structure suitable for diffusion, doping, catalyst, and impregnation procedures. In those cases, knowledge about the volume or surface area of pores is not enough to characterize the structure, because one has to know the extent of interconnection of the structure.

Vasconcelos [96] proposed two topological models to describe the evolution of texture of alkoxide based gel-silicas: one based on tetrahedrally shaped pores, and one based on cylindrically shaped pores.

The first topological model developed assumes a prismatic geometry in which the pores are tetrahedra connected by triangular prisms. The second model uses a cylindrical geometry (Figure 5.45) in which all the volume and all the surface area is associated with the cylindrical branches of the texture. In this case a node represents the point where the branches meet and it has no volume associated to it. The cylindrical model assumes a constant number of nodes for the entire process, and the coordination number varies from 4 to 0. Correlating the volume fraction of pores (V_V), the surface area of pores per unit volume (S_V), one obtains a unique set of solutions that yield the average branch size (L), and the average pore diameter (D) to a particular geometry, the number of branches (B_V), number of nodes (N_V), the genus (G_V):

$$D = \frac{4V_V}{S_V} \qquad (5.9)$$

$$L = \frac{4(1-V_V)}{S_V} \qquad (5.10)$$

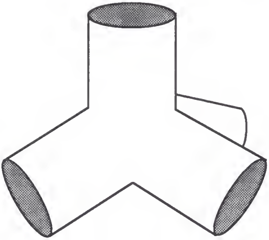

Figure 5.45 Cylindrical geometric model [96]

$$B_V = \frac{S_V{}^3}{16pV_V(1-V_V)} \qquad (5.11)$$

$$N_V = \frac{B_V{}^o}{2} \qquad (5.12)$$

where Bv^o corresponds to the number of branches of an arbitrary reference state.

$$G_V = B_V - N_V + 1 \qquad (5.12)$$

The topological concepts as mentioned above (for detail see ref.96) were applied to the 90 Å gel-silica samples using the cylindrical model, which is obviously more reasonable to be used in our work based upon the adsorption isotherm hysteresis discussed earlier. Since the number of nodes is assumed constant during the second stage of densification and genus is constant during the third stage of densification, the number of branches is a useful parameter for following the evolution of texture. The results, including the variation of surface area of pores per volume (Sv), the volume fraction of pores (Vv) and the number of branches (Bv) as a function of the processing temperature are shown in Figure 5.46, 5.47 and 5.48. The comparison of this work to Vasconcelos' [96] is presented in Figure 5.49.

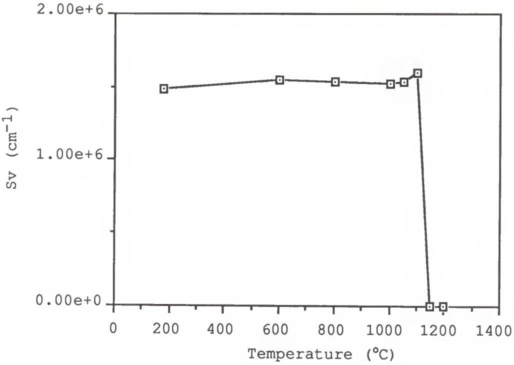

Figure 5.46 Variation of surface area per unit volume (Sv) as a function of processing temperature for 90 Å average pore radius gel-silica samples .

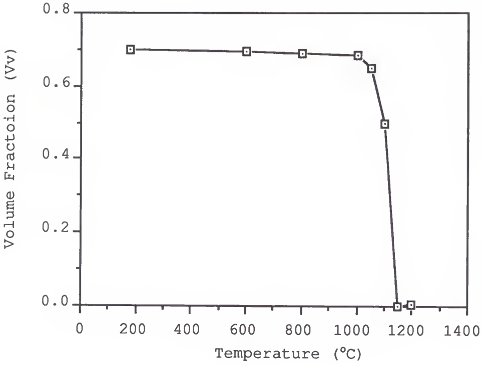

Figure 5.47 Variation of volume fraction of porosity (Vv) as a function of processing temperature for 90 Å average radius gel-silica samples .

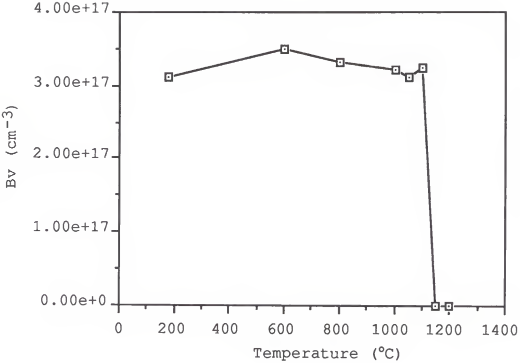

Figure 5.48 Variation of the number of branches (Bv) of 90 Å average radius gel-silica samples as a function of processing temperature.

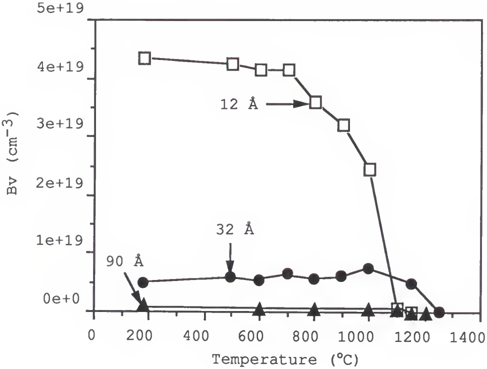

Figure 5.49 Variation of the number of branches (Bv) as a function of temperature for gel-silica samples with 12 Å, 32 Å and 90 Å average pore radius. 12 Å and 32 Å data from [96].

It has been shown that while B_v for the 12 Å pore radius structures deceases gradually after 600°C, B_v for the 90 Å pore radius structure remains roughly the same (in fact it increases slightly) over a much broader temperature range. The sharp change of the number of branches (Bv) of 90 Å average pore radius gel-silica samples started at 1100°C. When the sintering temperature reaches 1150°C, the Bv suddenly dropped from 10^{17} to 10^{11} per cm^3 indicating that the collapse of the structure occurs within a very narrow temperature range, here only 50 degrees. However, the densification behavior of 90 Å pore radius gel-silica samples seems different from that of the 32 Å pore radius gel-silica samples. Though the average pore size of the former is about three times as large as that of the later, the densification of 90 Å gel-silica samples completes at a lower temperature than that of the 32 Å samples. A possible explanation is a difference of pore size distribution. The pore size distribution of series B gel-silica samples is much narrower than those obtained by HF catalysis used in making the 32 Å gels. Material made by monodispersed particles is easier to be sintered as shown by Sacks and Sheu [210]. Thus gel-silica with monodispersed pores inside are easier to be densified.

The series B gel-silica samples were proven to have good connectivity of the pores. Since the second stage of the densification was not observed, or at least was not significant compared with the other two stages, the pores did not gradually become isolated with increasing densification temperature. When the temperature reached a critical point (say 1150°C) the first stage of sintering suddenly jumped to the third stage skipping the second stage.

In the relatively long first stage, the texture remained almost constant and the pores remained interconnected. However, the surface chemistry (silanols) changed with the densification temperature which ensures that gel-silica samples have the same texture but various surface chemistry states to meet different needs.

Thus, application of topological modeling to the densification of sol-gel-derived nanometer-scale structures reveals the same principles as determined for the sintering of micrometer to millimeter scale powder structures. As shown in the next section, the topological evolution of the gel structure can be related to physical properties and presents potentially useful information that is complementary to traditional metric parameters.

5.2.5 Optical Properties

The most troublesome impurity, "water", either free water within the ultraporous gel-silica structure (i.e., physical water), or hydroxyl groups associated with the gel-silica surface (i.e., chemical water) can be easily detected in a UV-VIS-NIR spectrophotometer by their characteristic vibrations absorption peaks, overtones and their combinations. Consequently, the optical properties of the porous gel-silica monoliths are usually evaluated by use of UV-VIS-NIR spectra. The vibration designation and the vibrational overtones and combinations of hydroxyl groups and their associated molecular water are presented in Table 5.7 and 5.8 [4] respectively.

The UV-VIS-NIR transmission spectra of series B gel-silica samples, 0.25-1-25, heat-treated at different temperatures of 180, 400, 600, 800, 1000, 1100, 1150 and 1200°C are shown in Figures 5.50-5.57. The textural change of the samples with densification temperature are listed in Table 5.59. Although the texture of series B gel-silica samples was remarkably different from the regular Type VI gel-silica, it has been found that their important absorption peaks and bands shown in the spectra were identical and were in good agreement with those discovered by previous researchers [85,211-217].

At first, all the major peaks at 938.95 nm ($3\nu_3$), 1237.85 nm ($[(2\nu_3+\nu_{OH})+(2\nu_2+\nu_{OH})]/2$, 1366.12 nm ($2\nu_2$), 1408.44 nm ($2\nu_3$), 1459.85 nm ($2\nu_4$), 1890.35 nm ($\nu_3+2\nu_{OH}$), and 2207.51 nm ($\nu_2+\nu_{OH}$) were observed in the spectra. In general, the

Table 5.7
Identification of molecular vibrations in gel-silica optical spectra

Identification	Type of vibration
v_{OH}	an out-of-plane bending vibration of silanol groups
v_1	stretching vibration of an isolated silanol group with no interaction with water molecules
v_2	stretching vibration of the adjacent silanol groups
v_3	stretching vibration of the adjacent silanol groups with hydrogen bonded water
v_4	stretching vibration of absorbed water

Table 5.8
Absorption peaks of the pore water and the surface hydroxyl groups of gel-silica monoliths

Wavelength (nm)	Identification	Observation command
2919.70	v_4	a broad peak on a broad band
2816.88	v_3	a tiny peak on a broad band
2732.24	v_2	a joint of two small peaks at 2768.90 nm and 2698.90 nm
2668.80	v_1	a very sharp symmetric peak
2262.48	v_4+v_{OH}	a broad band no peak
2207.51	v_2+v_{OH}	a high broad asymmetric peak
1890.35	v_3+2v_{OH}	a high broad asymmetric peak
1459.85	$2v_4$	a tiny peak on a broad band
1408.44	$2v_3$	a small peak on a broad band
1366.12	$2v_2$	a very sharp symmetric peak
1237.85	$[(2v_3+v_{OH})+(2v_2+v_{OH})]/2$	a small peak
1131.21	$2v_3+2v_{OH}$	a tiny peak
938.95	$3v_3$	a small peak
843.88	$3v_3+v_{OH}$	no peak observed
704.22	$4v_3$	a tiny peak

Source: [4]

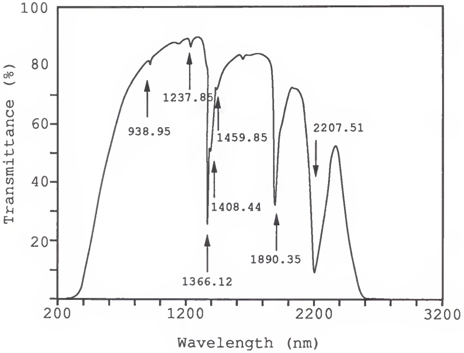

Figure 5.50 UV-VIS-NIR spectrum of 90 Å gel-silica samples dried at 180°C.

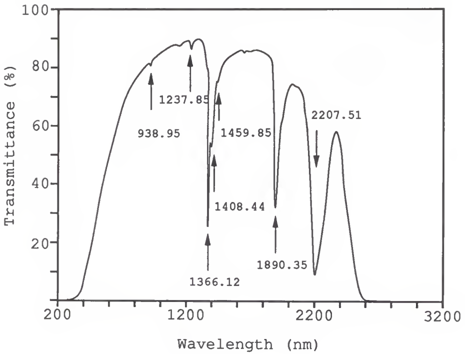

Figure 5.51 UV-VIS-NIR spectrum of 90 Å gel-silica samples heat-treated at 400°C.

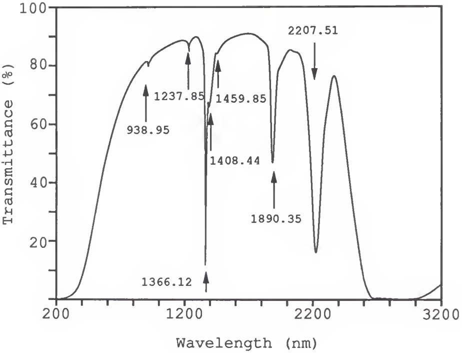

Figure 5.52 UV-VIS-NIR spectrum of 90 Å gel-silica samples heat-treated at 600°C.

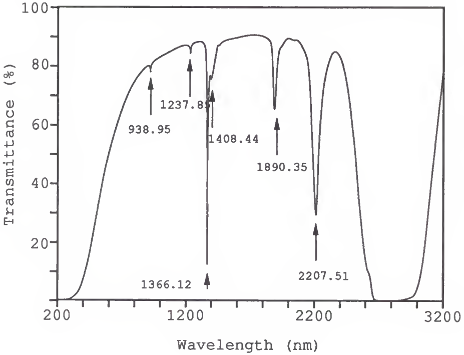

Figure 5.53 UV-VIS-NIR spectrum of 90 Å gel-silica samples heat treated at 800°C.

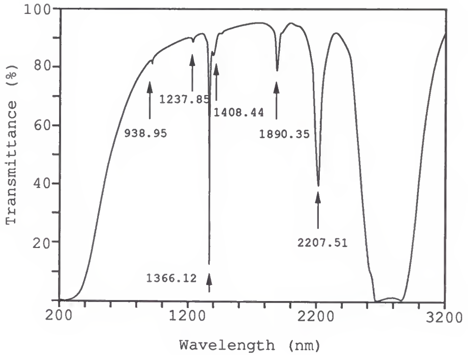

Figure 5.54 UV-VIS-NIR spectrum of 90 Å gel-silica samples heat-treated at 1000°C.

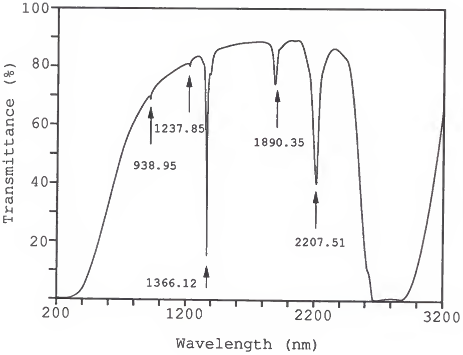

Figure 5.55 UV-VIS-NIR spectrum of 90 Å gel-silica samples heat-treated at 1100°C.

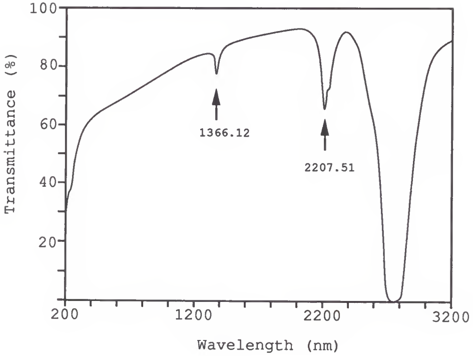

Figure 5.56 UV-VIS-NIR spectrum of 90 Å gel-silica samples heat-treated at 1150°C.

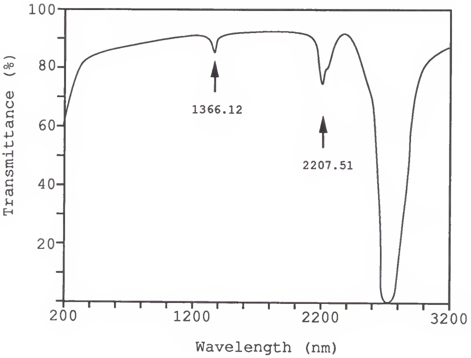

Figure 5.57 UV-VIS-NIR spectrum of 90 Å gel-silica samples heat-treated at 1200°C.

intensity of all absorption peaks gradually decreased as the temperature increased. The tiny peak at 1459.85 nm ($2\nu_4$) on a broad band disappeared after 600°C. After 1100°C, the small peak at 1408.44 nm ($2\nu_3$) disappeared. However, when the densification temperature reached 1150°C, a sudden change occurred. All the remaining peaks except those two at 1366.12 nm ($2\nu_2$) and 2207.51 nm ($\nu_2+\nu_{OH}$) (note: they both are related to ν_2) were vanished. At the same time, the UV cut-off (50% transmission) greatly shifted to the low wavelength side. With further increasing the densification temperature, the intensity of the peaks at at 1366.12 nm ($2\nu_2$) and 2207.51 nm ($\nu_2+\nu_{OH}$) decreased but still remained.

It should be noted that due to the resolution of the available equipment, the absorption peaks such as those at at 2207.52 nm, 2262.48 nm, 2668.80 nm, 2732.24 (ν_2), 2816.88 (ν_3), and 2919.70 nm (ν_4), can not be clearly identified. They form a broad absorption band in a region with wavelength longer than 2600 nm in the spectra. The width of the band decreased with the increased densification temperature.

Figure 5.58 shows that the optical property of the 0.25-1-25 gel-silica sample densified at 1200°C without any other special treatment is already identical to that of the commercial fused quartz cuvette.

Figure 5.59 demonstrates the effect of humidity in the environment on the UV-VIS-NIR spectra of the 90 Å porous

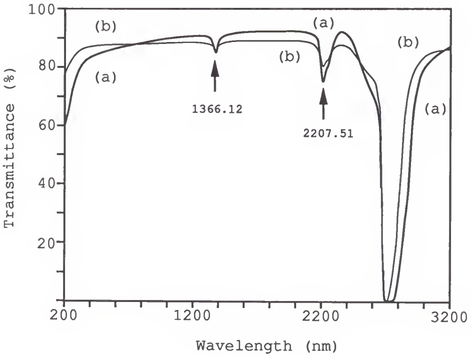

Figure 5.58 UV-VIS-NIR spectra of (a) 90 Å gel-silica samples heat-treated at 1200°C for 4 hours and (b) commercial fused quartz cuvette. (Note that the gel-silica sample was much thicker than the fused silica (Type III) cuvette.

gel-silica. The samples, after densification at 1000°C, were purposely exposed to ambient atmosphere for different time periods, such as 1 hour, 2 hours, 4 hours and 24 hours. All peaks except those at 1366.12 nm, 2207.51 nm increased their intensities with exposure time. The increase of 1408.44 nm, 1459.85 nm and 1890.35 nm peaks, which are related to v_3 and v_4, indicated that during the exposure time considerable amount of water was trapped in the samples and some of them were hydrogen bonded to the adjacent silanol groups.

The texture of 0.25-1-25 gel-silica samples heat treated at different temperatures is listed in Table 5.9. It has been proven that the textural change of gel-silica samples did not significantly affect the optical properties. The only variation observed for the samples with different textures is a shift of the UV-cutoff to higher wavelengths with larger average pore radius (Figure 5.60).

Good optical properties combined with interconnected porosities suitable for impregnation make it possible to use NH_4OH aging treated gel-silica monoliths as matrixes to produce high quality optical devices.

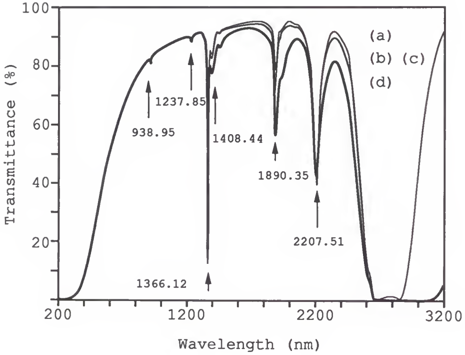

Figure 5.59 UV-VIS-NIR spectrum of 90 Å gel-silica samples heat-treated at 1000°C, then placed in open air for different times: (a) 0 hour, (b) 1 hour, (c) 2 hours and (d) 24 hours.

Table 5.9
Variation of texture
as a function of heat treatment temperature
for gel-silica samples aged in a 0.25 N NH_4OH solution
at 25°C for 24 hours

Sample ID	Heat treatment temperature (°C)	Surface area (m^2/g)	Pore volume (cm^3/g)	Pore radius (Å)
S-180	180	224	1.05	93.9
S-600	600	230	1.03	89.4
S-800	800	224	1.01	90.7
S-1000	1000	217	0.98	89.9
S-1050	1050	199	0.85	85.2
S-1100	1100	144	0.45	62.3
S-1150	1150	0.46	-	-
S-1200	1200	0.13	-	-

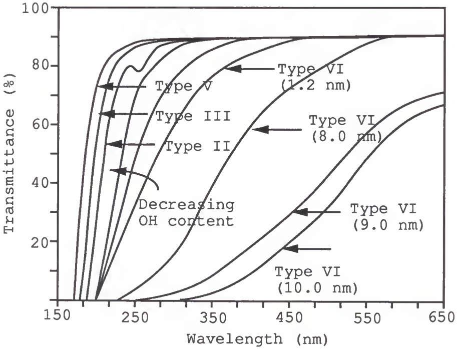

Figure 5.60 UV cutoffs for Types II and III optical silica, Type V fully dense optical silica, and Type VI porous optical matrices. Variation of UV cut-off with stabilization temperature and pore size of Type VI matrices is illustrated.

CHAPTER VI
POSSIBLE AGING MECHANISMS

6.1 Aging Mechanisms

So far aging has been proved very important in sol-gel processing. The aging step, depending upon the conditions under which it has been conducted, cannot only be used to increase the strength of gel-silica monoliths to avoid cracking during drying but also to control the texture of the gel-silicas to produce new types of porous materials.

As already discussed, in experiment A, the texture including the surface area, the total pore volume and the average pore radius of the gel-silica samples did not change significantly with the aging time and the aging temperature, while in experiment B, by varying aging parameters such as aging time, aging temperature and especially aging medium, the texture of gel-silica monoliths changed drastically. It has also been observed that other properties such as contraction, density and mechanical strength of series A and series B gel-silica monoliths changed in quite different ways.

All the results indicate that there must be at least two different mechanisms which govern the aging process independently or simultaneously.

Since the main difference between experiments A and B was the aging medium: pore liquor was used in experiment A and NH_4OH in experiment B, the difference in aging mechanisms should be closely related to the nature of the aging media. The pH is believed of the most importance.

Figure 6.1 shows the relationship between pH and the concentration of NH_4OH. In fact, the texture of the gel-silica samples changed in the same way the pH changed with NH_4OH concentration. So the concentration effect can also be referred as pH effect.

Figure 6.2 shows the variation of pH as a function of aging time for series B gel-silica samples after aging treatment. It can be seen that the pH of the pore liquor was less than 2 no matter how the aging temperature changed, represented by the starting points at 0 concentration in the Figure. The pH of most NH_4OH solutions, however, was in the range of 9 to 13 which was much higher than the pore liquor. Figure 6.3 shows that the sharp increase of the pH with NH_4OH concentration occurred in a very dilute concentration range. When the NH_4OH concentration reached 0.01 N, the rate of the change decreased and the pH finally approached a constant value (the slight decrease of this final value with the

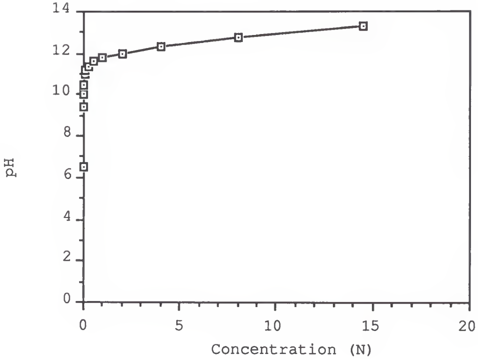

Figure 6.1 Variation of pH as a function of NH4OH concentration.

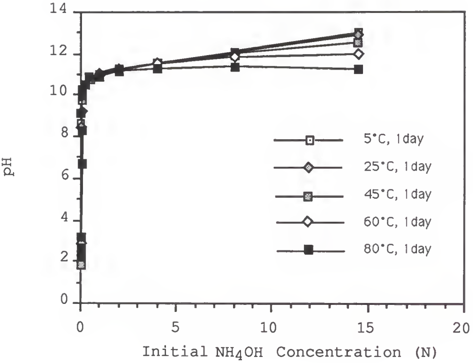

Figure 6.2 Variation of pH as a function of initial NH4OH concentration of the solution in which the gel-silica samples were aged for 1 day at different temperatures.

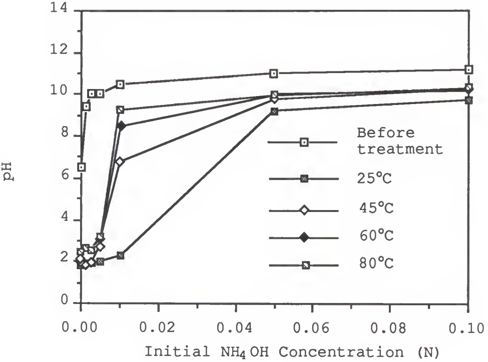

Figure 6.3 Variation of pH of the solution as a function of initial NH4OH concentration (dilute) before and after aging at different temperatures for 24 hours.

increased aging temperature shown in Figure 6.2 was probably due to the decomposition of NH_4OH and the evaporation of ammonia). This tend is in good agreement with the ways in which the NH_4OH concentration affected the texture and other properties of the gel-silica. Actually, the texture and properties of gel-silica were affected by the pH due to the influence of pH on to the solubility of the silica.

The solubility of either crystalline or amorphous silica and the effects of temperature, pH, electrolytes, impurity, particle size and the solvent has been extensively investigated and exhaustively reviewed by Iler [39]. The solubility of amorphous silica versus pH at different temperatures is shown in Figure 6.4.

Similar evidence of the importance of pH and temperature on silica solubility is also provided by our work. Figure 6.5 shows the variation of Si ion concentration in solution resulting from the ICP measurements as a function of aging treatment time when 10 x 10 x 40 mm gel-silica samples were treated in 50 ml 0.10 N and 0.25 N NH_4OH respectively. Figure 6.6 reveals the aging temperature effect. The concentration of Si ion changed rapidly during the early stage of the treatment (shown more clearly in Table 6.1) then gradually approached a final value. The amount of Si in solution at the end which was an indication of the equilibrium between dissolution and reprecipitation of silica

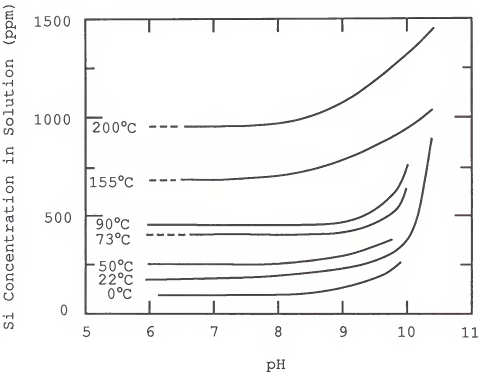

Figure 6.4 Solubility of amorphous silica versus pH at different temperatures. From Iler [39].

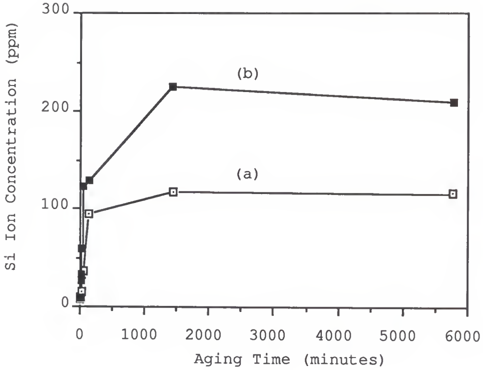

Figure 6.5 Variation of Si concentration in solution as a function of aging time for gel-silica samples aged at 25°C in (a) 0.10 N and (b) 0.25 N NH_4OH.

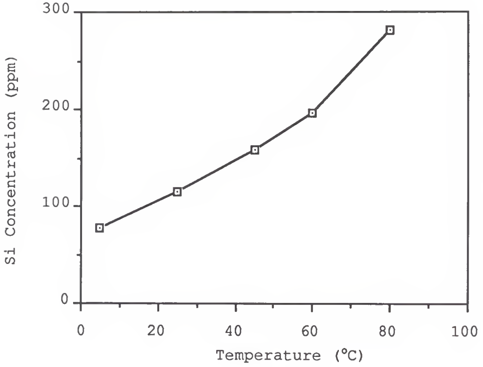

Figure 6.6 Variation of Si concentration in solution as a function of aging temperature for gel-silica samples aged in a 0.10 N NH_4OH for 4 days.

Table 6.1
Variation of Si ion concentration
in the solution as a function of aging time
for gel-silica samples aged in NH_4OH solution at 25°C

	Si concentration (ppm)	
Treatment time (minutes)	in 0.01 N	in 0.25 N
5	8.1	9.8
10	8.8	26.7
15	14.6	32.4
30	31.9	56.3
60	35.4	122.5
120	93.4	128.9
1440	116.2	222.8
5760	115.0	211.7

and was obviously determined by the concentration of NH_4OH and the aging temperature.

Alexander, Broge, and Iler [218] proposed that the aging mechanism of silica is Ostwald ripening which is the process of growth of large particles at the expense of smaller ones due to the diminishing surface energy. They believed that once the liquid-solid interfaces are created, further structural changes which occur during aging can be attributed primarily to surface energy effects. The silica from a gel structure of smaller radius dissolves and deposits on the larger or thicker region of the surface. It is also well known that surfaces exhibiting positive radii of curvature dissolve more readily than surfaces exhibiting negative radii of curvature. Therefore, as the dissolution increases (e.g. by increasing temperature or pH), dissolution and redeposition result in neck formation (Figure 6.7). In most cases, the terms of Ostwald ripening and neck formation (necking) are used interchangeably and they are considered the same mechanism of aging. These concepts appear to be always true for aqueous silicates or particulate gel-silicas. As mentioned, aging governed by this mechanism results in a one-way process: loss of specific area and an increase in pore size which has been well described by Iler [39].

Recently, some investigators [88] have argued that the aging mechanism of polymeric gel-silicas may be different

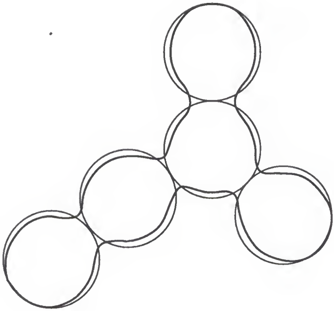

Figure 6.7 Dissolution and reprecipitation causes growth of necks between particles. [39]

from that of colloidal silica [219]. In contrast to aqueous systems, in most alkoxide derived gel-silica, condensation begins before hydrolysis is complete and continues long after the gelation point [219]. Since the solubility of silica in alcohols is much less than in water, especially when the pH is lower, there can be comparatively little rearrangement or "ripening" to more highly compacted states. Hence, condensation is a possible mechanism of aging. Unfortunately, the available data on aging of alkoxide based gels is extremely limited and therefore the understanding of the aging mechanism for alcohol gel-silica system is still lacking.

6.2 Models for Aging Process

Since silica does not dissolve at low pH, especially in the presence of alcohol, the acidic pore liquor has little effect on the texture of wet gels. In experiment A, the general trend of textural change due to an Ostwald ripening mechanism was not observed. Thus we proposed that in experiment A the condensation reaction dominated the entire aging process. Owing to the insolubility of silica under the conditions of the experiment, the gel texture could not undergo rearrangement.

For experiment B, however, the aging mechanism was relatively complicated. Though the so-called one-way process in textural change was observed, it could not simply propose that the aging mechanism was more than just Ostwald ripening. It is well established that the presence of H_3O^+ in the solution increases the rate of the hydrolysis reaction whereas OH^- ions increase the condensation reaction [92]. Since the pH increased drastically at the very early stage of aging the texture and other properties of the wet gel were established at that period of time by a condensation reaction. Ostwald ripening or neck formation and growth predominated in the later stage of the aging process and played secondarily important roles.

In order to describe these mechanisms more clearly, two models, model A and model B, indicative of the aging processes in experiments A and B are schematically illustrated in Figures 6.8 and 6.9,respectively.

In principle, the gel texture is determined by the relative rates of the hydrolysis and condensation reactions. As already mentioned, the simultaneous occurrence of hydrolysis and condensation reactions in the sol result in polymeric structures. It has been proved [92] that chain structures are more likely to be formed than ring structures during the polycondensation reaction, especially in the early stages of hydrolysis and condensation. Since the sol is acid

Experiment A

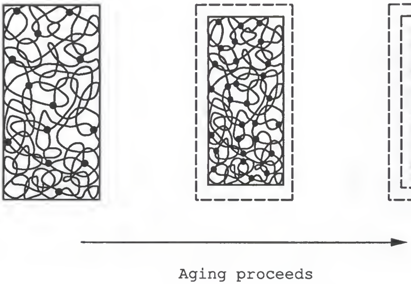

Figure 6.8 Proposed model of textural evolution during aging for gel-silica aged in the pore liquor.

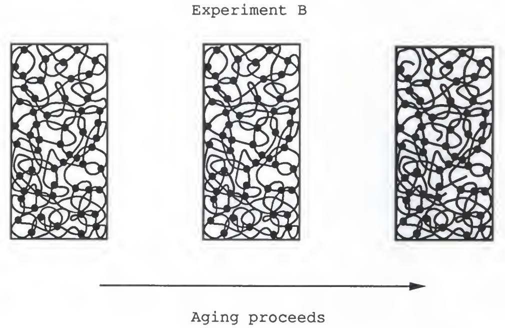

Figure 6.9 Proposed model of textural evolution during aging for gel-silica aged in an NH4OH solution.

catalyzed, the rate of hydrolysis is much faster than the rate of condensation. Thus we propose that the polymeric structure is a coil-like structure in which coils, or polymeric clusters, are formed by linear chains through entanglement.

In the sol, when two hydrolyzed monomers encounter each other, the condensation reaction may occur between the functional groups (OH or OR, aqueous condensation or alcohol condensation respectively) to form a dimer. When two dimers or one dimer and one monomer meet each other, a higher level member chain is formed. Afterwards the situation becomes more complicated. When one end of a chain reacts with another end of itself, a ring forms. Moreover, if there is no steric effect the condensation reaction may take place between any pair of the functional groups wherever they are located resulting in branching and crosslinking of the chains. Consequently, nodes are generated and the three dimensional gel network is formed. During aging, the condensation reaction continues and so does the formation of the nodes.

6.2.1 Model A

Model A (Figure 6.8) shows that the number of nodes increases and the network contracts as aging proceeds. Since the rate of the condensation reaction is low, the changes are relatively slow. There is no coarsening of the chains due to the insolubility of SiO_2 in the low pH pore liquor solution, particularly in the presence of alcohol.

Therefore, in experiment A, the condensation reaction mechanism is responsible for contraction (syneresis) and progressive strengthening and stiffening of the gel.

Contraction (syneresis) in series A gel-silicas is generally attributed to formation of new bonds through condensation reactions. It is easy to imagine that a siloxane bridging bond between two neighboring silicon atoms, Si-O-Si, takes up less space than the two silanol, SiOH, groups from which it was formed. Therefore, the solid phase will contract as a result of condensation (Figure 6.10 a). Greater shrinkage could result from "diffusion" or flexure of the chains of solid phase (Figure 6.10 b). If a local movement of a chain brings surfaces close enough to form a bond, the deformation will be irreversible; this process will continue to cause a net contraction as long as the solid phase remains flexible and elastically compliant. This reaction-driven mechanism might be accomplished by the tendency to reduce the huge solid-liquid interfacial area of the gel [119].

The stiffness and strength of the gel-silica samples increase gradually with the condensation reaction and node formation. The gels become more rigid during aging. However, for most of the time the wet gels are relatively flexible

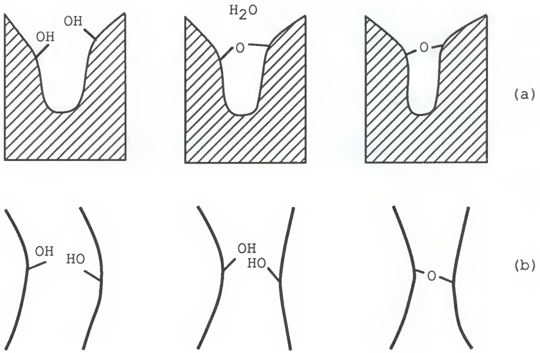

Figure 6.10 Schematic illustration of bond formation resulting in shrinkage of the gels
(a) Shrinkage results from condensation between neighboring groups on a surface as the strain in the new bond relaxes.
(b) Movement of flexible chains may permit new bonds to form that prevent the chain from returning to their original position; this permits extensive shrinkages as long as the network remains flexible [93].

because of the slow condensation reaction rate. The rigidity (indicated by the microhardness data, Figure 5.35) of the samples due to the formation of new chemical bonding between silica chains and rings increases with temperature and time of aging. The stiffer and stronger the gel network becomes, the better it can withstand the capillary pressures of drying and removal of pore liquor.

It is very interesting to note that the condensation reaction mechanism for experiment A is supported by the following fact: the activation energy of 17.53 kJ/mole·K obtained from the rate of pore growth at various temperatures during aging in experiment A (see Chapter V and Figures 5.7 and 5.8 for details) is similar to the value of 25 KJ/mole·K obtained by Ponomareva et al. [156] and close to the value of 19 kJ/mole·K suggested by Brinker [93] for a condensation reaction driven process.

6.2.2. Model B

Model B (Figure 6.9) proposes that right after replacing the mother pore liquor with NH_4OH, the pH of the gel rapidly increases from 2 to higher than 9 (Figure 6.2) which greatly promotes the condensation reaction rate. The effect is that a condensation reaction occurs suddenly at all the sites where the functional groups encounter a neighbor.

As a result, a large number of nodes forms which pin and freeze the entire structure of the gels. As aging proceeds, the number of nodes remains almost constant. However, the chains (back bones) become thicker and coarser due to the dissolution and reprecipitation of silica. No contraction of the wet gel is observed during this process. In contrast, if the rate of dissolution is higher than that of reprecipitation (see the results of ICP measurement, Figure 6.5), some nodes may in fact be disintegrated, some bonds may be broken and dangling ends may be formed which cause the dilation of the gel network, as shown in Figures 5.29 and 5.30.

Since the texture of the wet gel thus produced is looser, the mechanical strength of the gel is weaker as shown in Figures 5.37, 5.38 and 5.39.

The strengthening of the gel by dissolution-reprecipitation which has been reported in aqueous systems [39] was not observed in experiment B. That means the dissolution-reprecipitation process does not always strengthen the gel, though the growth of necks adds to the strength and stiffness of the network. On the contrary, the dissolution always destroys the chemical bonding and reprecipitation only builds up van der Waal's bonding. This work shows that sometimes the changes during aging weaken the gel structure especially when the equilibrium between the dissolution and precipitation reactions (or processes) has not been reached.

In NH_4OH solutions in which the silica is soluble, dissolution and reprecipitation processes cause coarsening.

As already shown in Figure 6.7, the particles have positive radii of curvature ($r>0$), so they are more soluble than a flat plate of the same material. Also the smaller the particle, the greater its solubility. Therefore, smaller particles dissolve and the solute precipitates onto larger particles. Crevices and necks between particles have negative radii ($r<0$), so their solubility is especially low and dissolved material accumulates there. The result of dissolution- reprecipitation is to reduce the net curvature of the solid phase. Thus small particles disappear and small pores are filled in so the interfacial area decreases, the average pore size increases and the pore shape changes. Note that this does not produce shrinkage, because the center of the particles do not move toward one another. This model is consistent with the results shown in Figures 5.29 and 5.30.

6.3. Molecular Orbital Calculations

Recently, molecular orbital calculations have been introduced into the field of sol-gel processing to yield conceptual ideas of molecular structures and to predict experimental results [220-228].

Materials are made up of large numbers of atoms with a corresponding large number of electrons. These atoms are bound together by the interaction of electrostatic forces. The type of bond, its strength, and physical orientation depends on the interaction of the electrons of the bound atoms. The calculation of molecular orbitals (MO's) gives us insight into the nature of chemical bonds between atoms in a solid. Since the extreme complexity of large molecules makes it difficult to calculate the MO's exactly, nearly all computer programs make some simplifying assumptions in order to make computations easier.

In our work, Huckel molecular orbital (HMO) calculations, which is one of the simplest methods, were performed to model the process of condensation reaction during aging using an HMO program on a personal computer. There are two primary steps in the calculations. First, the Hamiltonian or energy matrix must be generated. The matrix is an energy set for each of the n electrons in the molecule. Nothing can be done until this is defined [229].

H_n = Kinetic energy + Potential energy + Interactions (6.1)

The Hamiltonian operator will yield the energy eigenvalues according to the Schrodinger equation:

$$H_n \Psi = E_n \Psi \qquad (6.2)$$

Once the Hamiltonian is formed, then the second phase of the problem is to diagonalize it by an appropriate transformation matrix. The diagonalization operator or transformation matrix makes all the nondiagonal elements of H_n equal to zero. The resulting diagonalized matrix represents the energy eigenvalue matrix, E_n.

The transformation matrix T represents the eigenvector matrix ψ of the molecule. T is also the square root of the probability of finding an electron in a specific molecular orbital for a specific atom and is related to the eigenvector matrix through a delta (Δ) operator:

$$T = \Delta\ \psi \qquad (6.3)$$

where Δ represents the nonorthogonality of the molecular orbitals under study.

Finally,

$$T = |\psi^* \psi|^{1/2} \qquad (6.4)$$

which is the square root of the probability distribution of the electrons. The following simplifying assumptions are made for the Huckel molecular orbital theory (HMO):

1. The πMOs are the only orbitals considered in the calculations. All other electrons in the molecule are neglected.

2. It is assumed that -11.26 ev of energy is required to remove an electron from a p_z orbital of carbon. This is called α_i in the standard HMO theory. This energy eigenfunction becomes the diagonal of the Hamiltonian.

3. The bond energy of the pi bond is -2.5 ev. This HMO model neglects all other bond energies (differential overlaps) between nonneighboring orbitals. This energy is defined as β_{ij} in the standard HMO theory. These energy values form the nondiagonal elements.

4. Atoms other than carbon (such as oxygen and silicon) pi-bonded to carbon are called heteroatoms. Energy required to remove the p_z heteroatom elections is assumed to be a linear function of carbon.

$$\alpha_i = h_i(-11.26\ )\mathrm{eV} \qquad (6.5)$$

and the bond energy

$$\beta_{ij} = k_{ij}(-2.5)\mathrm{eV} \qquad (6.6)$$

where *h* and *k* are called the heteroatom parameters.

Typical values for the heteroatom are determined from experimental bond strengths. The values are arrived at empirically and only conceptually represent the bond energy or binding energy of the electrons.

The values for the heteroatom parameters, *k* and *h*, listed in Table 6.2 are obtained either from the other sources directly, or from the empirical calculation through the bond energy and the ionization energy of elements shown as follows.

The bond energies we are interested are listed in Table 6.3. They depend closely on the environment of the given bond---the portion of the molecule close to the bond. For example, the energy required to dissociate one H atom from an H_2O molecule, that is, to break one O-H bond, is about 502 kJ/mol. The value showed here, 428 kJ/mol, is the average for breaking both O-H bonds in water. Other values in the table are also average values, but they are generally adequate for making comparisons [231].

Table 6.2
Heteroatom parameters

Bond (*ij*)	*k*-Parameter	Atom (*i*)	*h*-Parameter
Si-O	1.4 [229]	H	1.30 [230]
O-H	1.285 *	O	1.00 [229]
(O-)H···O	0.060 *	Si	0.80 [229]
N-H	1.169 *	N	1.50 [229]
(N-)H···N	0.054 *	C	1.00 [229]
N-O	0.690 *		
C-O	0.80 [229]		

Source: [229]

* The result of calculation.

Figure 6.11 shows the UV-VIS-NIR spectrum of deionized (D.I.) water in which a sharp absorption (UV cut-off) can be seen at 190 nm. Since $E=h\nu$ (where h is the Planck constant and ν is the frequency), the gap energy of pure water is equal to 6.526 ev. The *k*-parameter of 1.285 is finally obtained. By using different *k*-parameters to do the HMO calculation of water molecule repeatedly to make the calculated gap energy of water molecule approach this empirical value.

The energy of the hydrogen bond shown in Table 6.3 is 20.90 kJ/mol, only about one twentieth of the average O-H bond strength which is 428 kJ/mol. The *k*-parameter of hydrogen bond of 0.06 can then be calculated from the following arithmetic relationship: 1.285 x (20.90/428).

Using the *k*-parameters of both O-H and hydrogen bonds to conduct the HMO calculation of the water molecule:

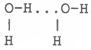

$$\underset{\substack{|\\ \mathrm{H}}}{\mathrm{O}}\text{-}\mathrm{H}\cdots\underset{\substack{|\\ \mathrm{H}}}{\mathrm{O}}\text{-}\mathrm{H}$$

The resultant gap energy of 6.535 ev is very close to the experimental value.

The preliminary results obtained from HMO calculations using these heteroatom parameters, k and h, show that:

(1) In general, a hydrolysis reaction takes place spontaneously, however, condensation reactions require energy (need a driving force) to take place as shown in Tables 6.4

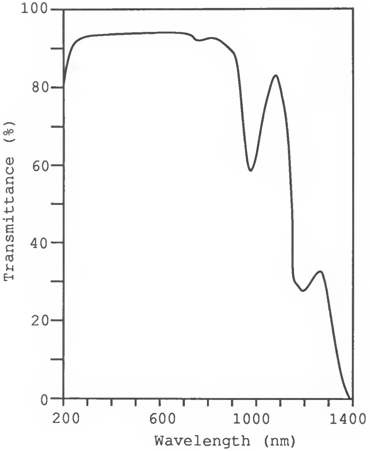

Figure 6.11 UV spectrum of D.I. water (in quartz cuvette).

Table 6.3
Some representative bond energies and *k*-parameters

Bond type	Bond strength	*k*-parameter
O-H	428 kJ/mol [231]	1.285
Hydrogen bond O-H···O	20.90 kJ/mol [232] (5 kcal/mol)	0.060
N-H	389 kJ/mol [233]	1.169
Hydrogen bond N-H···N	18 kJ/mol [169] (formed by NH_3)	0.054
C-O	326 kJ/mol [234] 359 kJ/mol [230]	0.979 1.078
N-O	230 kJ/mol [234]	0.690
Si-O	466 kJ/mol [230]	1.400

Table 6.4
Results of Huckel molecular orbital calculation for hydrolysis reactions

Chemical species	Huckel molecular energy (ev)
$Si(OCH_3)_4$	-345.9162
$Si(OCH_3)_3OH$	-297.0436
$Si(OCH_3)_2(OH)_2$	-248.0262
$Si(OCH_3)(OH)_3$	-199.6225
$Si(OH)_4$	-150.4725
CH_3OH	-100.0385
H_2O	-50.2298
$Si(OCH_3)_4 + H_2O$	-396.1460
$Si(OCH_3)_3OH + CH_3OH$	-397.0821
$Si(OCH_3)_3OH + H_2O$	-347.2734
$Si(OCH_3)_2(OH)_2 + CH_3OH$	-348.0647
$Si(OCH_3)_2(OH)_2 + H_2O$	-298.2560
$Si(OCH_3)(OH)_3 + H_2O$	-249.8523
$Si(OH)_4 + CH_3OH$	-250.5110

and 6.5. For example, the Huckel molecular energy of $Si(OR)_4$ + nH_2O is always higher than that of $Si(OR)_{4-n}(OH)_n$ + nROH, whereas the molecular energy of $Si(OH)_4$ is lower than $(HO)_3Si-O-Si(OH)_3$.

(2) The chain structure is more likely than the ring structure to be formed through a condensation reaction. This result supports the models proposed in the previous section. One of the typical examples shown in Table 6.5 is that the trisiloxane ring has a much higher Huckel molecular energy than the three-member chain.

(3) During a condensation reaction there exists an intermediate (pentacoordinated) state of silicon. This can be proved by the reaction steps proposed in Figure 6.12-6.15.

Step 1 as shown in Figure 6.12 illustrates a portion of a gel surface formed at gelation. Experimental evidence shows that a gel surface was covered by a substantial fraction of trisiloxane silicate rings, known as a D_2 ring in Raman Spectroscopy [235]. During aging two such rings can approach close enough to undergo a condensation reaction between neighboring silanol species.

Figure 6.13 indicates that during step 2, the pentacoordinated intermediate state is formed between the two trisiloxane silicate rings.

Table 6.5
Results of Huckel molecular orbital calculation for condensation reactions

Species	Huckel molecular energy
$Si(OH)_4$	-150.4725 ev.
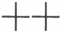	-249.8769 ev
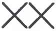	-196.8040 ev.
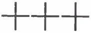	-349.0830 ev.
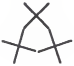	-297.6991 ev.
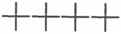	-445.6620 ev.
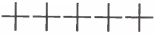	-547.3388 ev.
$2Si(OH)_4$	-300.9450 ev.
$(HO)_3Si-O-Si(OH)_3 + H_2O$	-300.1067 ev.

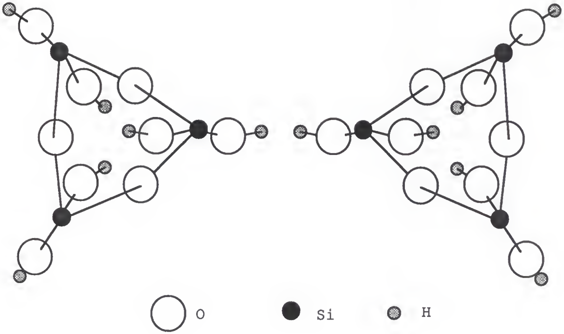

Figure 6.12 Schematic illustration of step 1: two trisiloxane rings encounter each other.

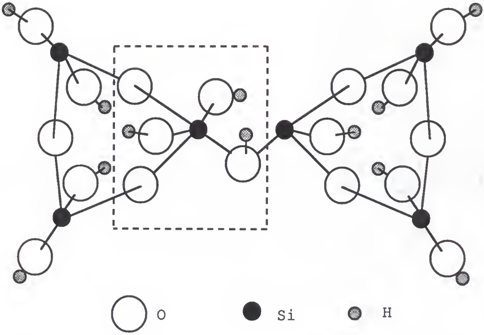

Figure 6.13 Schematic illustration of step 2: the formation of pentacoordinated intermediate state.

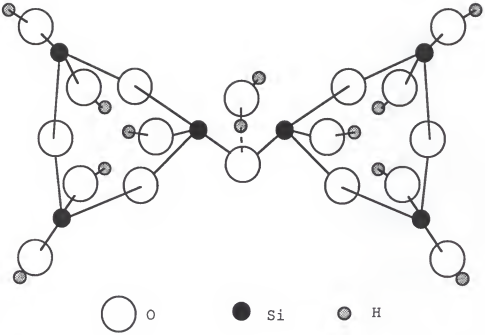

Figure 6.14 Schematic illustration of step 3: the formation of hydrogen-bonded water.

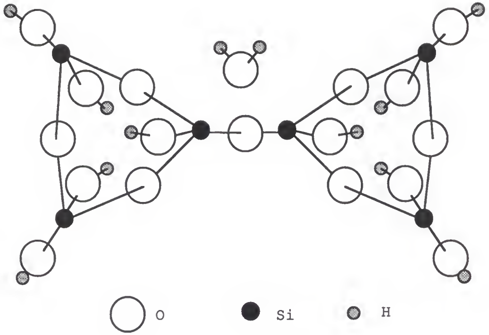

Figure 6.15 Schematic illustration of step 4: the formation of siloxane, Si-O-Si, bond and removal of water.

Figure 6.14 shows step 3 is the formation of hydrogen bonded water, the reaction product of the condensation reaction.

During step 4 as demonstrated in Figure 6.15, the Si-O-Si siloxane bond is formed and the water molecule was removed.

The comparison of the Huckel energies for the various reaction steps is presented in Figure 6.16. It has been found that $E_{step1} > E_{step2}$, so the pentacoordinated intermediate state was more stable. During the condensation reaction, step 3 had the lowest Huckel molecular energy than any other steps. This indicates that the water molecule as a product of condensation reaction was more likely to be bonded to the gel network. $E_{step4} > E_{step3}$ indicates that there was an energy barrier to be overcome for the removal of the water molecule from the structure which is consistent with the drying process.

Though Huckel molecular orbital calculations do not take bond lengths and bond angles into account and is less accurate than other MO methods, it is still a useful and convenient tool to provide valuable complementary information about the chemical processes.

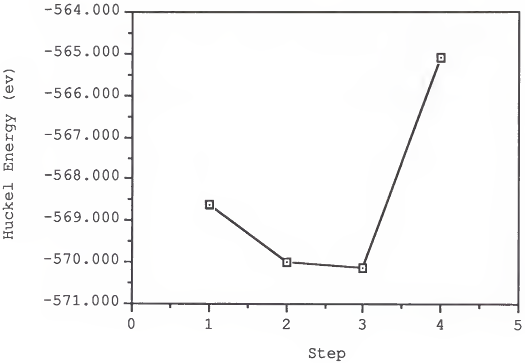

Figure 6.16 Variation of Huckel molecular energy as a function of reaction steps.

CHAPTER VII
APPLICATIONS OF GEL-SILICA TREATED BY NH_4OH

7.1 Solid State Dye Laser

As mentioned in the first chapter, gel-silica, especially type VI porous gel-silica, has many potential applications. A solid state dye laser made by using a series B porous gel-silica matrix impregnated with 4PyPO-MePTS laser dye will be discussed here as a typical example.

According to the lasing species, lasers can be divided into four groups: solid state lasers, gaseous lasers, liquid state lasers and semiconductor lasers, as shown in Table 7.1.

Liquid lasing species (organic dyes) are attractive for use in lasers because they offer tunability, which means they can produce an tunable output extending from the near UV to the near IR [9]. This wide range of accessible wavelengths is in contrast to tunable lasers based on transition elements, such as chromium III, doped in crystals which operate only in the near IR [236,237]. Recently, dye lasers have become important tools for spectroscopy, photochemistry, and laser isotope separation [238].

Since solid state dye lasers have many potential advantages over their liquid dye counterparts, listed in

Table 7.1
Different types of laser
(Light Amplification by Stimulated Emission of Radiation)

Solid State	Crystalline	Ruby (0.6943 mm)	Single-crystalline
		Nd-doped YAG (1.064 mm)	Polycrystalline
		Nd-doped Y_2O_3	Polycrystalline
	Glass	Nd^{3+} Yb^{3+}, Er^{3+} (1.54 mm), Ho^{3+} and Tm^{3+}	
	Ceramics	Nd doped optical ceramics	
Gaseous state		He-Ne (0.6328 mm)	
		Ar (0.4880 mm)	
		CO (5 mm)	
		CO_2 (10.6mm)	
		N_2 (0.3371 mm)	
Liquid state		Organic dye solutions (0.3 - 1.0 mm)	
Semiconductor		GaAs (0.840 mm)	

Table 7.2, incorporation of laser dyes in a solid matrix has been intensively studied for many years with the goal of obtaining a lightweight, portable solid state system which is inexpensive to fabricate, is reliable, and is safe to handle [9]. Several groups have pioneered the growing interest in solid state dye lasers including Reisfeld, Avnir and colleagues in Israel [239-242], Mackenzie [243] and Dunn [244] and co-workers at UCLA; King [245,246] and colleagues at the University of Manchester, U.K., Prasad and Karasz at SUNY at Buffalo and University of Massachusetts [247] and Nogues and co-worker at the University of Florida and Geltech, Inc [248]. Their developments involve: photostable solid state tunable lasers in the visible, infrared solid-state lasers and other tunable solid state lasers.

Key criteria in selecting a material suitable for a dye laser host include the following: The host must have good optical, mechanical and thermal properties to withstand the severe operating conditions of practical lasers. Desirable properties include hardness, chemical inertness, absence of internal strain and refractive index variation, resistance to radiation-induced color centers, and ease of fabrication. Also, the dyes within the host must maintain sharp fluorescent lines, strong absorption bands, have a reasonably high quantum efficiency for the fluorescent transition of interest, and a reasonable lifetime in order for the laser to

Table 7.2
Advantages of solid state dye lasers

Advantage	Consequence
1) Eliminate fluid pumping and flow system	Compactness, ease of handling, less expensive
2) Isolation of dye molecules by pore walls	Minimizes dimerization and aggregation
3) Increase thermal stability	Operate at high power
4) Isolate dye molecules	Inhibits destructive photo processes
5) Steric hindrance of dye molecules by porous silica matrix	Reduces rotational modes that cause non-radiative loss
6) Easy substitution of laser rods with different dyes	Wide selection of wavelength throughout UV, visible and NIR
7) High thermal conductivity	High pumping thresholds than liquids

Source: [9]

achieve desirable operational performance. Solid-state host materials used to be broadly grouped into crystalline solids, glasses [249-251] and polymers [243] which generally show the above characteristics.

The introduction of organic dyes into sol-gel glasses was started in 1983 [239,240]. The use of sol-gel chemical processing has made it possible to develop solid-state dye lasers which have two or more phases, and thereby possess unique lasing properties [3,92]. For example, porous Type VI gel-silica matrices offer as potential advantages their high doping concentrations, homogeneity, high optical quality, and higher thermal conductivity and better thermal shock resistance compared with lower silica or non-silicate glasses.

In this study solid-state dye lasers made by aging treated porous gel-silica matrices with an organic laser dye were successfully developed and their lasing properties were characterized. The effects of the texture of the gel-silica matrices as well as the concentration of dye solution and the impregnation temperature on lasing characteristics of the hybrid optical composites were investigated.

7.2 Experimental Procedures

There are two alternative pathways for making solid state dye lasers via the sol-gel route; method I termed sol processing and method II adsorption or impregnation processing [9]. In brief, the main difference between those two methods is: in method I, the optical organic molecules are mixed with organic precursor during the sol preparation step; while in method II, the optical organic phase is diffused or impregnated into the porous silica matrix after the stabilization stage. For a detailed discussion of those two methods see Ref.9. Both process options have advantages and disadvantages. The primary advantage of method I is its simplicity but the mechanical and chemical behavior of a composite made in this manner is restricted by the temperature limitation of drying imposed by the thermal stability of the optical polymer. The primary advantages of optical composites made by method II is that the textual properties such as the volume fraction of porosity, the average pore radius and the pore size distribution can be tailored for specific applications (for example, accommodating molecules with different sizes and achieving different doping concentrations etc.). Also, the chemical nature of the pore network, largely controlled by the surface area, the silanol concentration, and the absorbed water layers can be varied during stabilization and optimized for a particular organic impregnate. Furthermore, method II circumvents the thermal stability limitation on processing.

This study focused on method II which is practically a two part process. During the first part of the process, optically transparent gel-silica matrices with a wide range of volume fraction of interconnected porosity and average pore radius (up to 14 nm) were prepared by using various aging treatments (see chapter IV). The rectangular gel-silica specimens of size 6 x 6 x 10 mm were then chemically stabilized at 800°C for 4 hours (Figure 1.2 step 6). Both ends of the specimens were cast parallel to each other and were polished to 600 grit after stabilization, if necessary. Other surfaces of the rectangular matrices were not polished and were kept in an as-cast condition. In the second part of the process, steps 7 and 8, stabilized gel-silica with controlled textures were soaked in the solution at different temperatures (25°C and 45°C) for 24 hours. The laser dye was diffused or impregnated into the porous matrix where it was chemically or physically absorbed within the pore network.

The laser dye, used in our work, developed by Lee and Robb [238] was 4-{2-(5-phenyl-oxazolyl)}-1-methyl pyridinium ρ-toluenesulfonat (4PyPO-MePTS). This is one of the most photostable dyes. Its structure is shown in Figure 7.1. The dye is water soluble which is a major advantage in the

5-Phenyl-2-(4-pyridyl)oxazole, methyl tosylate salt, 99%

[1-Methyl-4-(5-phynel-2-oxazolyl)pyridinium
ρ-toluenesulfonate]

4PyPO-MePTS

$C_{22}H_{20}N_2SO_4$

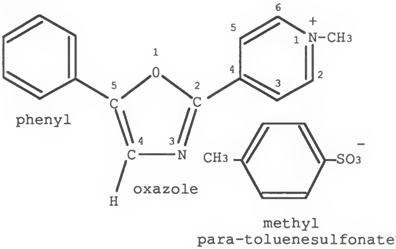

F.W. 408.48

m.p. 221-222°

Cat. # 23,749-3, Aldrich Chemical Co. Inc.,
Milwaukee, Wisconsin

Figure 7.1 4PyPO-MePTS laser dye.

processing of the composite. Dye solutions with different concentrations were prepared at room temperature by simply dissolving the dye in D.I. water. The solution has exceptionally high photostability, as discussed by Lee and Robb [238].

The laser action was tested as follows: the impregnated specimens were pumped for lasing in a single cavity using a nitrogen gas laser with its output at 337.1 nm in the ultraviolet in a transverse configuration where the rectangular nitrogen laser beam was focused to a line within the specimen. The maximum average power of the system was 50 mW, the maximum energy per pulse, 2.5 μJ, and the pulse duration, 800 ps. Laser dye solutions with different concentrations were tested. The testing system has an amplifier to increase the signal output. All the specimens, including dye solutions, were pumped by the nitrogen beam spilt from the primary laser source in an oscillation stage without any amplification and an additional amplifier stage to increase the population density of the signal. The output of the dye laser was monitored. The wavelength, selected through a grating system, was measured and the amplification factor, e.g. the peak ratio, was calculated.

7.3 Results and Discussion

7.3.1 Texture Effects

The type VI porous gel-silica monolithic optical matrices with a wide range of volume fraction (up to 74%) of interconnected porosity and average pore radius (up to 14 nm) were prepared by using the NH_4OH aging treatments of experiment B. The high transmittance of the type VI gel-silica matrix over a wide spectral region combined with good mechanical and thermal properties (see Chapter V), make this an ideal host material for the impregnated laser dye. After impregnation, the optical properties of the sample, became even better as shown in Figure 7.2. The major feature of the transmittance spectra from 200 to 1300 nm for the 4PyPO-MePTS water solution and for the dye impregnated gel-silica specimens is an absorption at the region between 200 and 400 nm due to the presence of the dye molecules. Therefore, it is possible to use a nitrogen laser at 337.1 nm as the primary source for pumping.

Almost all gel-silica specimens impregnated with 4PyPO-MePTS laser dye showed lasing action. However, the lasing characteristics of the solid state dye laser depended greatly upon the texture of the matrices. The general trend is that the larger the average pore size and the total volume

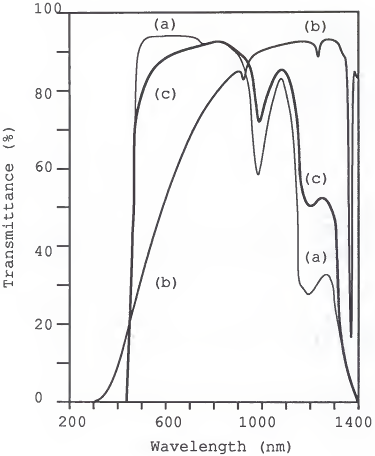

Figure 7.2 UV spectra for (a) 6 x10^{-3} M 4PyPO-MePTS dye solution; (b) porous gel-silica matrix (100Å) and (c) gel-silica matrix (100 Å) impregnated with 6 x 10^{-3} M 4PyPO-MePTS dye solution.

fraction of porosity of the matrix, the higher the total output energy and the more intense was the lasing peak emitted by the solid-state dye laser device. The gel-silica matrix with average pore radius of 100 Å (texture characterized in Table 7.3) soaked in 3 x 10^{-3} M 4PyPO-MePTS dye solution at room temperature for 24 hours had a total output of 4.8 μJ and a gain of 12. This result was 1.5 and 6-10 times as high as that of 12 Å average pore radius gel-silica dye laser specimens (Table 7.4).

It is apparent that the matrix which has a larger volume fraction of porosity can accommodate more organic dye molecules in its structure. For example, gel-silica samples with pore of 12 Å average pore radius has a volume fraction of porosity of 52%. Therefore, the theoretically maximum amount of organic dye solution which can be incorporated will not exceed 52%. In fact, much less than that amount of dye solution can be doped into the gel-silica matrix if special procedures are not followed. However, in our work, about 64% 4PyPO-MePTS dye solution was determined to be impregnated into the 100 Å average pore radius gel-silica matrix which has a volume fraction of 72% porosity. Previous chapters have shown that not only the volume fraction of porosity and the average pore radius, but also the pore shape and the pore size distribution of gel-silica matrices change with various aging treatments. The gel-silica specimens used in this work

Table 7.3
Texture of gel-silica aged in a 0.5 N NH_4OH solution at 25°C for 4 days

Surface area (m^2/g)	223
Total pore volume (cm^3/g)	1.12
Average pore radius (Å)	100.8

Theoretically:	Volume fraction of porosity > 70 %
Experimentally:	About 64 % volume was occupied by the dye solution.

Table 7.4
Texture effects on lasing characteristics of 4PyPO-MePTS impregnated (at 25°C) gel-silica specimens

Sample	Wavelength (nm)	$I_{w/o\ amp.}$ (μJ)	$I_{w/\ amp.}$ (μJ)	$I_{w/}/I_{w/o}$
Dye-dye	510	1.91	52.9	27.70
12 Å	510	1.49	1.82	1.22
12 Å	510	0.89	1.80	2.02
100 Å	510	< 0.4	4.80	12.00

I : Total output energy.
$I_{w/amp.}$: Total output with amplification.
$I_{w/o\ amp.}$: Total output without amplification.
$I_{w/}/I_{w/o}$: Gain or amplification factor.

with a larger pore size usually have a narrower pore size distribution and a more cylindrical pore shape. The combination of large pore size, large volume fraction of porosity, narrow pore size distribution and cylindrical pore shape all favor higher gain and total output of composite dye laser.

7.3.2 Dye Concentration Effects

Because of the superior thermo-optical properties and the excellent safety factors associated with water, researchers have expressed the need for high efficiency water soluble lasing dyes that can produce a continuously tunable output extending from the near UV to the near IR [238]. 4PyPO-MePTS is considered as one of the most photochemically stable blue-green lasing dyes in pure water for dye lasers to achieve high repetition rates and high outputs/pulse at high pumping energy.

Figures 7.3-7.6. show the change in UV-VIS-NIR transmission spectrum of 4PyPO-MePTS dye solution as a function of concentration of the dye.

A transmission peak at 300 nm appeared when the dye concentration is decreased to 1.0 x 10^{-3} M, as shown in Figure 7.4. The intensity of this peak increased with the decreased concentration of the dye. When the concentration

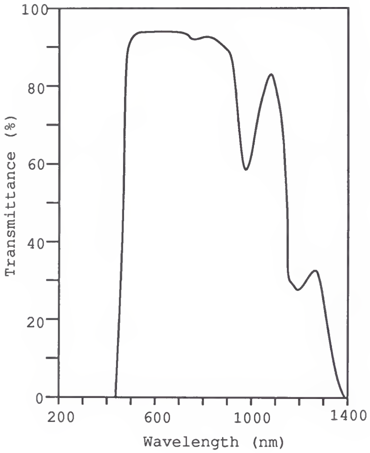

Figure 7.3 UV spectrum of 1 x 10^{-2} M 4PyPO-MePTS dye solution (in quartz cuvette).

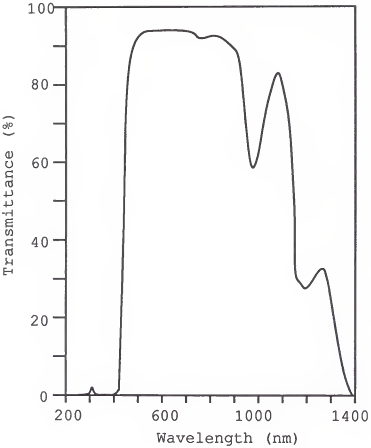

Figure 7.4 UV spectrum of 1 x 10^{-3} M 4PyPO-MePTS dye solution (in quartz cuvette).

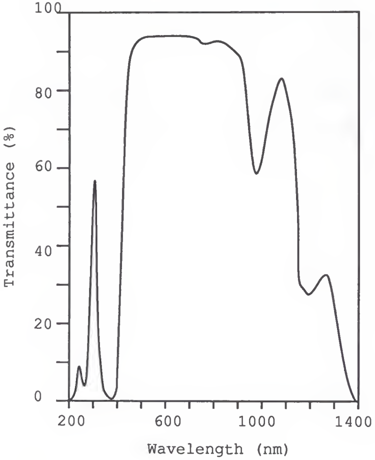

Figure 7.5 UV spectrum of 1.875×10^{-4} M 4PyPO-MePTS dye solution (in quartz cuvette).

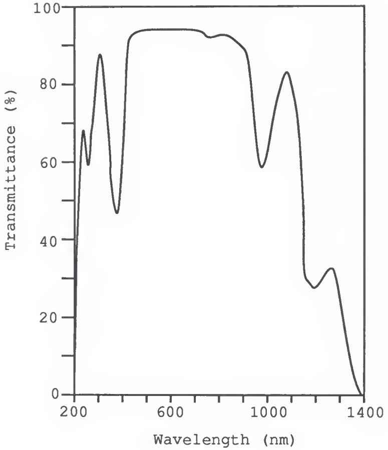

Figure 7.6 UV spectrum of 1.1718 x 10^{-5} M 4PyPO-MePTS dye solution (in quartz cuvette).

reached 1 x 10^{-4} M, another transmission peak at 240 nm is observed (Figure 7.5) combining with the former peak to form a transmission band. The intensity of the whole band sharply increases with further decrease of the dye concentration and finally the absorption in the region of 200-400 nm no longer exists (Figure 7.6). Obviously, the dye solutions with concentration lower than 1.0 x 10^{-3} M are not good candidates for solid state dye lasers.

The spectra of dye solution with concentrations higher than 1.5 x 10^{-3} M (from 1.5 x 10^{-3} to 1 x 10^{-2} M) are almost identical (they all have absorptions in the region of 200-400 nm) except their ultraviolet cutoffs and absorption edges slightly shift to longer wavelengths from 420 nm to 440 nm, with increasing dye concentration. However, organic dyes in aqueous solution have a tendency to form dimers and higher molecular weight (MW) aggregates which have different lasing characteristic from the monomer. The equilibrium between monomers and dimers shifts to the dimers with increasing dye concentration. Dimers result in self-quenching of the laser dyes. Therefore, dye solutions with higher concentrations of dyes are not suitable either. Consequently, for this study, dye solutions with three different concentrations: 1.5 x 10^{-3} M, 3.0 x 10^{-3} M and 6.0 x 10^{-3} M were selected to investigate dye concentration effects when adsorbed in the optical matrices.

4PyPO-MePTS is very water soluble and after dissolving in D.I. water the dye results in an optically transparent solution even at room temperature. Even though no significant difference in the transmittance spectra of dye solution was observed due to aggregation or formation of dimers and higher MW aggregates, the lasing properties of the laser dye solutions were found to depend on the concentrations of the dyes. A solution with higher concentration had relatively poorer lasing properties than solutions of lower concentration. The change of total energy output with dye concentration, which was detected with a photodiode and includes both lasing and fluorescence energies emitted by the specimens, is shown in Figure 7.7. The total output energy is substantially less for the 6.0 x 10^{-3} M dye solution than for the 1.5 x 10^{-3} M solution. The concentration dependence of the peak ratio, which is the ratio of intensity of lasing peak to that of the fluorescence peak, is shown in Figure 7.8. Larger dye concentrations decreased the ratio. The figures also show that the maximum output energy and the maximum peak ratio seem not to be achieved at the same wavelength. Since the gel-silica matrices prepared by experiment B have a volume fraction of porosity in the range of 52% to 74%, the composite laser made with a gel-silica matrix and a 3.0 x 10^{-3} M dye solution hopefully achieves the same lasing characteristics as a 1.5 x 10^{-3} M dye solution.

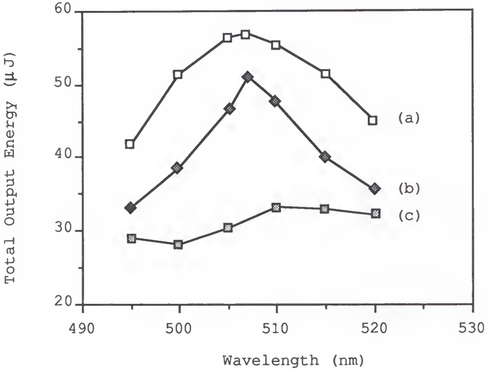

Figure 7.7 Variation of total output energy as a function of concentration of dye solution: (a) 1.5 x 10^{-3} M (b) 3.0 x 10^{-3} M and (c) 6.0 x 10^{-3} M.

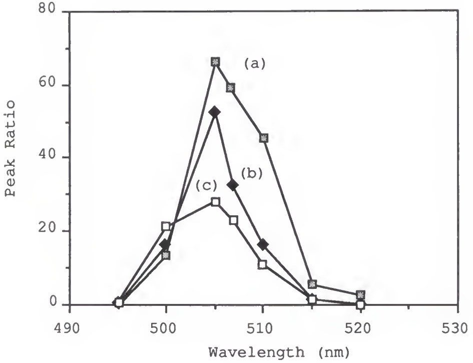

Figure 7.8 Variation of peak ratio as a function of concentration of dye solution: (a) 1.5 x 10^{-3} M, (b) 3.0 x 10^{-3} M and (c) 6.0 x 10^{-3} M.

Considering both results of total energy output and peak ratio a dye concentration of 3 x 10^{-3} M was finally selected as the preferable concentration in this work.

7.3.3 Impregnation Temperature Effects

The comparison of Table 7.4 with Table 7.5 clearly shows that the impregnation temperature also played an important role in the lasing characteristics of a solid-state dye laser made with a gel-silica matrix and a 4PyPO-MePTS dye solution. When the impregnation temperature was raised from 25°C to 45°C, keeping the duration of impregnation constant, the dye laser specimens made with gel-silica matrices of 90 Å average pore radius and 3 x 10^{-3} M 4PyPO-MePTS dye solution repeatedly showed one fifth the total output energy and almost the same peak ratio as the dye solution itself. The maximum output energy of 9.49 μJ with a gain of 23.58 for 90 Å average pore radius samples is shown in Table 7.6. This is 5 and 10 times as high as those for a 12 Å average pore radius specimen in which the dye solution was impregnated at 25°C. It should be pointed out that each data point here is the average of 100 pulses. After more than 2,000 pulses of pumping the total output and peak ratio still remained constant which indicates that the composite dye specimen has good photostability.

Table 7.5
Texture effects on lasing characteristics of 4PyPO-MePTS impregnated (at 45°C) gel-silica specimens

Sample	Wavelength (nm)	$I_{w/o\ amp.}$ (μJ)	$I_{w/\ amp.}$ (μJ)	$I_{w/}/I_{w/o}$
12 Å	500	< 0.4	3.71	9.28
	505	< 0.4	3.91	9.78
	510	< 0.4	3.25	8.13
30 Å	500	0.72	5.23	7.26
	505	0.79	7.34	9.29
	510	0.74	6.99	9.45
90 Å	500	<0.4	6.31	15.78
	505	<0.4	8.36	20.90
	510	<0.4	8.43	21.08

I : Total output energy.
$I_{w/amp.}$: Total output with amplification.
$I_{w/o\ amp.}$: Total output without amplification.
$I_{w/}/I_{w/o}$: Gain or amplification factor.

Table 7.6
Lasing characteristics of 4PyPO-MePTS
impregnated (at 45°C) 90 Å gel-silica specimen

Sample ID	Wavelength (nm)	$I_{w/o}$ amp. (μJ)	$I_{w/}$ amp. (μJ)	$I_{w/}/I_{w/o}$
Dye-dye	510	2.60	48.0	18.46
		2.34	48.7	20.81
		2.07	49.3	23.82
		1.97	50.6	25.59
		1.91	52.9	27.70
	(Average)	2.18	49.9	22.89
90 Å	510	< 0.4	5.69	14.23
		< 0.4	6.38	15.95
		< 0.4	7.06	17.65
		< 0.4	7.60	19.00
		< 0.4	8.07	20.18
		< 0.4	8.44	21.10
		< 0.4	8.51	21.28
		< 0.4	7.17	17.93
		< 0.4	7.95	19.88
		< 0.4	9.02	22.55
		< 0.4	9.12	22.80
		< 0.4	9.36	23.40
		< 0.4	9.49	23.73
		< 0.4	9.35	23.38
		< 0.4	9.43	23.58
		< 0.4	9.37	23.43
		< 0.4	9.27	23.18
		< 0.4	9.23	23.08
		< 0.4	9.07	22.68
		< 0.4	8.99	22.48
	(Average)	< 0.4	8.43	21.08

I : Total output energy.
$I_{w/amp.}$: Total output with amplification.
$I_{w/o\ amp.}$: Total output without amplification.
$I_{w/}/I_{w/o}$: Gain or amplification factor.

The extent of chemical interaction between the optical organic phase and the silica network is strongly influenced by the stabilization treatment which controls the silanol concentration on the surface of the pores [235,252]. Figure 7.9 illustrates the pore geometry, silanol concentrations, adsorbed and bound water layers, and sorbed organic molecules that are possible using method II processing of optical composites. Thickness of the bound-water layer varies from 0.7 to 1.2 nm as the pore radius increases from 1.2 to 7.5 nm [24]. Therefore, the impregnation temperature is more significant for the smaller pore size gels than for the larger ones. In a small pore size (<2.0 nm) gel-silica matrix, the bound water layer on the pore surface as well as the ink-bottle neck of the pores hinders the movement of molecules of second phase. It has been reported that a 12 Å gel-silica matrix has great hindering effects on both percolation and diffusion processes of inorganic ions, such as Cr^{+++} etc. [253], as well as organic molecules [254]. When 12 Å average pore radius gel-silica was used as a dye matrix, not only the diffusion of dye solution molecules into the matrix was difficult, but also the percolation process takes considerably longer to complete. Air is more likely to be trapped inside the small pore samples resulting in negative effects on the lasing characteristics. An increase of the impregnation temperature accelerates the percolation and

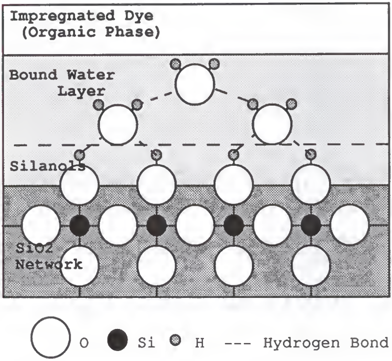

Figure 7.9 Schematic illustration of surface structure.

diffusion processes which prevail over the hindering effects of the pores.

7.4 Conclusion

The solid state dye laser composites made by impregnating Type VI gel-silica matrices with controlled textures with a dilute 4PyPO-MePTS laser dye solution show good lasing action. Porosity of the gel-silica matrix plays an important role in determining the lasing characteristics. A larger pore size, a larger volume fraction of porosity, a narrower pore size distribution, and a more cylindrical pore shape of the gel-silica matrices all provide a higher gain and total energy output of the laser.

These findings indicate that controlled aging will play more and more important roles in the sol-gel processing of optical matrices. The applications of type VI gel-silica will be broadened by the availability of a range of controllable textures obtained by varying the aging treatment.

A method of preparing a solid-state dye laser has been developed. The concentration of dye solutions and the impregnation temperature also affect the lasing characteristics; optimization of both factors have to be carefully conducted to achieve reliable and reproducible laser characteristics.

CHAPTER VIII
SUMMARY AND CONCLUSIONS

In recent years, sol-gel processing has made it possible to produce with high reliability two new types of silica glasses: Type V fully dense gel-silica and type VI optically transparent ultraporous gel-silica. By comparison, the new types of silica glasses made via the sol-gel route show advantages over traditional Types I and II fused quartz and Types III and IV synthetic fused silica glasses with respect to both processing and physical properties, especially optical properties. Due to their unique controllable textures, Type VI gel-silica has many potential applications. However, some of the applications have been limited by the relatively narrow range of the textures previously available. This study has eliminated the restriction.

A general introduction to sol-gel processing including its history, advantages, applications and processing steps was made in Chapter II which is essential to develop an effective way to produce Type VI gel-silica with a wider range of controllable textures. At the same time, two main categories of gel-silica: aqueous gels and alcohol gels were described and compared. It has been shown that the alcohol gel-silica system is different from the aqueous gel-silica system in almost all aspects of processing except the chemical composition. Alcohol gel-silica has more potential applications but is less understood than its aqueous competitor.

Our main purposes were then determined: (1) to develop an effective method of producing a new generation of Type VI gel-silicas with a wider range of controllable textures than previously available, (2) to extend the applications of Type VI gel-silicas, and (3) to investigate the effects of processing parameters on the texture and other properties of alcohol gel-silicas and extend the knowledge about the aging of gel-silica monoliths.

Different ways to change and control the texture of gel-silica were reviewed in Chapter III. The texture of gel-silica is formed and developed during gelation, aging, and drying. Textures can be controlled by changing the parameters of all those processing steps such as catalyst, R ratio, temperature and time etc., basically by controlling the relative rates of hydrolysis and condensation reactions.

The concepts of aging of gel structures and the main changes during the aging process for both aqueous and alcohol gel-silicas were discussed. Compared with other methods, controlling the texture by varying aging treatment was believed to be more convenient and the most effective.

In Chapter IV, three experimental procedures were designed. In experiment A, alkoxide-derived silica gel monoliths were aged in the mother liquor. In experiment B, the silica gel monoliths were aged in NH_4OH solutions with various concentrations. In experiment C silica gel monoliths were first aged in the mother liquor and then dried in an NH_4OH atmosphere. Our attention was focused on the former two experiments: experiment A and experiment B.

In Chapter V, the texture and properties of gel-silica samples derived from experiment A and B were considerably different. The effects of time, temperature and pH on the texture and other physical properties were investigated. In experiment A, the texture of gel-silica changed only slightly with aging time and temperature. By comparison, the aging temperature showed more of a profound effect on the textural change. The maximum average pore radius of gel-silica samples in experiment A was only 20 Å. The pore shape of the samples, obtained by nitrogen sorption hysteresis analysis, remained like ink-bottle type pores (bottle shaped pores with narrow necks) throughout the aging history and no essential change of pore shape was observed in the experiment.

In experiment B, the texture changed significantly with treatment time, temperature and concentration of the aging medium, an NH_4OH solution. The concentration of NH_4OH played the most important role in changing the texture. The surface area decreased, the total pore volume increased, and the average pore radius increased generally with increased aging time, temperature and pH. These results for the alcohol gels are similar to the behavior described by Iler for aqueous gel-silica. It is very important to note that the pore shape of all the samples aged in NH_4OH solutions were changed from "ink-bottle" to cylindrical pores.

The pore size distribution about the mean of series B gel-silica samples was much narrower than that of series A gel-silica samples.

The properties of gel-silica samples derived from those two experiments were also quite different. The wet gels contracted gradually with aging time and temperature in experiment A and finally reached a limit due to the competition between syneresis and the stiffness of the gel-silica. In contrast, in experiment B, the wet gels dilated rather than contracted. The final limit reached was determined by the competition between dissolution and reprecipitation of silica within the network.

The change of bulk density of gel-silica samples showed a similar trend. In experiment A, the bulk density of wet gels measured by the pore liquid immersion method increased with the increased aging time and temperature due to the syneresis. The bulk density of dried series A gels did not change significantly with the aging parameters. In contrast, the bulk density of dried gels derived from experiment B decreased with the increased aging treatment time, temperature and the concentration of NH_4OH.

The microhardness of both wet and dried gels derived from experiment A were measured. Microhardness increased with increasing aging time as well as aging temperature indicating that the gels were strengthened effectively by the aging treatment. However, these results did not mean that a longer aging time and a higher aging temperature were always good for the production of monolithic gel-silica. The increases of contraction and the stiffness resulted in high residual internal stresses which usually caused severe cracking problems. Though the microhardness decreased with aging treatment time, temperature, and the concentration of NH_4OH solution in experiment B, the gels still maintained sufficient mechanical strength to prevent cracking. High reliability was observed.

UV-VIS-NIR spectra showed that gel-silica samples produced by both experiment A and experiment B had good optical properties. In spite of the large pore size and large total pore volume of series B gel-silica, the only difference was a slight shift of UV cutoff to the longer wavelengths as pore size increased.

It should be emphasized that densification behavior of the gels derived by those two different experiments differed from each other. The densification behavior of dried gels made from experiment B was greatly improved by the aging treatment. The dried gel monoliths could easily be densified without foaming or cracking even in an open air furnace within a very short time period. In contrast, it is almost impossible for gels made from experiment A to be densified under the same condition. Besides the measured metric properties, the calculated topological properties showed that the pores of the series B gel-silica samples remained interconnected over a relatively wide temperature range during densification. When the temperature reached a critical point, all the pores collapsed at the same time mainly due to the narrow pore size distribution about the mean.

Possible aging mechanisms were proposed in Chapter VI. So far, the large differences in both texture and properties between the two gel-silica series indicated that there must be different mechanisms governing the aging processes in the experiments. We proposed two models which illustrate that the aging stage in experiment A was dominated by the condensation reaction. In experiment B aging was governed by some other mechanisms including Ostwald ripening. Since SiO_2 is almost insoluble, it is impossible for dissolution and reprecipitation processes to take place in low pH solutions, especially in the presence of alcohol. During aging in experiment A, the condensation reaction continued and controlled the aging process. However, in experiment B, as soon as the gels were taken out of the pore liquid and immersed into the NH_4OH solution the suddenly increased pH promoted the condensation reactions. The entire structure of the gel was frozen at the very beginning of the aging stage. The following processes occurring in the system should be dissolution and reprecipitation which was proved by the ICP measurements. The dissolution process degrades the network weakening the structure and causing dilation. The reprecipitation process coarsened the network and strengthened the gel structure. The final texture of the gel-silicas was probably determined by the equilibrium between those two processes.

Huckel molecular orbital (HMO) calculations provided complementary information about the pathway of condensation reactions and the structural evolution of the gels. The results show that there was a pentacoordinated intermediate state existing in the condensation reactions. According to the Huckel molecular energy calculation, chain structures were more likely to be formed than the ring structures during aging which is consistent with the results by other MO calculations using AM1, etc. [92].

Chapter VII demonstrated an important application of monolithic gel-silica samples. The solid state dye laser composites made by porous monolithic gel-silica matrices impregnated with 4PyPO-MePTS laser dye solutions showed good lasing characteristics. The texture of the gel-silica matrix played an important role in the performance of the composites. The gel-silica monoliths can also be tailored as host materials for other optical devices.

Thus we conclude that:

(1) The texture of gel-silica can effectively be controlled by aging. By varying aging parameters, the pore radius of the resultant gel-silica can be altered from 1.2 nm to 14.8 nm with very narrow distributions of the pore size. The volume fraction of porosity can be extended from 50% to as high as 74%. The pore shape can also be changed from wide voids of differing diameters with narrow necks to pores with smooth cylindrical cross sections.

(2) The application of Type VI gel-silica has been extended. Gel-silica with wider range of controllable texture and other unique properties, including good optical, mechanical and thermal properties has more practical applications than ordinary Type VI gel-silica with limited ranges of volume fraction and size of pores.

(3) The importance of the aging stage in sol-gel processing has been extended: it is not only a useful tool to increase the wet gel strength avoiding cracking problems during drying, but also a powerful method to control the texture of gel-silica monoliths. The proposed different aging

mechanisms and interrelated models provide a new basis for further understanding the science of aging.

REFERENCES

[1] W.D. Kingery, H.K. Bowen and D.R. Uhlmann, Introduction to Ceramics, Second Edition, Wiley, New York, 5 (1976).

[2] N.P. Bansal and R.H. Doremus, Handbook of Glass Properties, Academic Press, 8 (1986).

[3] L.L. Hench, S.H. Wang and J.L. Nogues, Multifunctional Materials, R.L. Gunshor, ed., SPIE, V.878, Bellingham, WA, 76 (1988).

[4] S.H. Wang, Sol-Gel Derived Silica Optics, Ph.D. Dissertation, University of Florida, Gainesville, FL (1988).

[5] M. Grayson, ed., Encyclopedia of Glass, Ceramics, Clay and Cement, Wiley, New York (1985)

[6] R.H. Doremus, Glass Science, Wiley, New York, 121 (1973).

[7] S.H. Wang, C. Campbell, and L.L. Hench, in Ultrastructure Processing of Advanced Ceramics, J.D. Mackenzie and D.R. Ulrich, eds., Wiley, New York, 145 (1988).

[8] S. Wallace and L.L. Hench, in Science of Ceramic Chemical Processing, L.L. Hench and D.R. Ulrich, eds., Wiley, New York, 148 (1986).

[9] L.L. Hench, G. Orcel and J.L. Nogues, in Better Ceramics Through Chemistry II, Vol. 73, C.J. Brinker, D.E. Clark and D.R. Ulrich, eds., Materials Research Society, Pittsburgh, PA, 35 (1986).

[10] L.L. Hench, in Ceramic Transactions, Vol. 19, M.D. Sacks, ed., Am. Ceram. Soc., Westerville, OH, 265 (1991).

[11] L.L. Hench, J.K. West, B.F. Zhu and R. Ochoa, Proceedings of SPIE meeting, San Diego, CA, July 11-13 (1990) (in press).

[12] J.D. Mackenzie, J. Non-Cryst. Solids, 48 (1982) 1.

[13] L.L. Hench, in Ultrastructure Processing of Ceramics, Glasses and Composites, L.L.Hench and D.R. Ulrich, eds., Wiley, New York, 3 (1984).

[14] S. Sakka, in Treatise on Materials Science and Technology Volume 22, Glass III, Mikmoru Tomozawa and R.H. Doremus, eds., Academic Press, New York, 129 (1982).

[15] I. Artaki, M. Bradley, T. Zerda, J. Jonas, G. Orcel and L.L. Hench, in Science of Ceramic Chemical Processing, L.L. Hench and D.R. Ulrich, eds., Wiley, New York, 73 (1986).

[16] K.A. Andrianov, Organic Silicon Compounds, State Scientific Publishing House for Chemical Literature, Moscow, (1955), translation 59-11239 U.S. Dept. of Commerce, Washington, DC.

[17] M. Ebelmen, Ann. Chim. Phys. 15 (1845) 319.

[18] M. Ebelmen, Comptes Rend de L'Acd des Sciences, 25 (1847) 854.

[19] D.C. Bradley, R.C. Mehrotra, and D.P. Gaur, Metal Alkoxides, Academic Press, New York (1978).

[20] T. Graham, J. Chem. Soc., 17 (1864) 318.

[21] W.Z. Ostwald, Z. Phys. Chem., 27 (1897) 365.

[22] L. Rayleigh, Philos. Mag., 38 (1919) 738.

[23] D.J. Lloyd, in Colloid Chemistry, J. Alexander, ed., Chemical Catalog Co., New York, 767 (1926).

[24] H.N. Holmes, in Colloid Chemistry, J. Alexander, ed., Chemical Catalog Co., New York, 796 (1926).

[25] K.H. Stern, Bibliography of Liesegang Rings, National Bureau of Standards Miscellaneous Publication No. 292, (1967).

[26] H.K. Heinisch, Crystal Growth in Gels, Pennsylvania State University Press, State College, PA, (1970).

[27] W. Geffcken and E. Berger, German Patent No.736,411, May (1939).

[28] H. Schroeder, Phys. Thin Films, 5 (1969) 87.

[29] H. Schroeder, Opt. Acta. 9 (1962) 249.

[30] H. Dislich, Angewandt Chemie, Int. Ed. Engl., 10, No. 6 (1971) 363.

[31] C.B. Hurd, Chem. Rev., 22 (1938) 403.

[32] S.S. Kistler, J. Phys. Chem., 36 (1932) 52.

[33] R.H. Ewell and H. Insley, J. Res. NBS, 15 (1935) 173.

[34] R.M. Barrer and L. Hinds, Nature, 166 (1950) 562.

[35] R. Roy, J. Am. Ceram. Soc., 53 (1969) 344.

[36] R. Roy, J. Am. Ceram. Soc., 39, No. 4 (1956) 145.

[37] D.M. Roy and R. Roy, Am. Mineral, 39 (1954) 957.

[38] G.J. McCarthy R. Roy and J.M. McKay, J. Am. Ceram. Soc., 54 (1971) 637.

[39] R.K. Iler, The Chemistry of Silica, Wiley, New York (1979).

[40] W. Stober, A. Fink and E. Bohn, J. Colloid Interface Sci., 26 (1968) 62.

[41] R.M. Dell, in Reactivity of Solids, J.S. Anderson, M.W. Roberts, and F.S. Stone, eds., Chapman and Hall, New York, 553 (1972).

[42] J.L. Woodhead, Silicates Ind., 37 (1972) 191.

[43] L. Levene and I.M. Thomas, U.S. Patent No. 3,640,093, February (1972).

[44] K. Kamiya, S. Sakka and T. Tatemichi, J. Mater. Sci., 15 (1980) 1765.

[45] E.M. Rabinovich, D.W. Johnson, J.B. Mac Chesney, and E.M. Vogel, J. Non-Cryst. Solids, 47 (1982) 435.

[46] E.M. Rabinovich, D.W. Johnson, J.B. Mac Chesney, and E.M. Vogel, J. Am. Ceram. Soc., 66 (1983) 683.

[47] D.W. Johnson, E.M. Rabinovich, J.B. Mac Chesney and E.M. Vogel, J. Am. Ceram. Soc., 66 (1983) 688.

[48] L.R. McCreight, H.E. Rauch and W.H. Stutton, Ceramic Fibers and Fibrous Composite Materials, Academic Press, New York (1965).

[49] L.E. Seufer, U.S. Patent No. 3,808,015, April (1974).

[50] K. Miyahara and N. Nakayama, U.S. Patent No. 4,159,205 (1979).

[51] M. Leitheiser and H.G. Snowman, U.S. Patent No. 145,383 (1980).

[52] E. Wainer, German Patent No. 1,249,832, April (1968).

[53] H.G. Snowman, U.S. Patent No. 3,795,524, March (1974).

[54] S. Horikuri, K. Tsuji, Y. Abe, A. Fukui and E. Ichiki, Japanese Patent No. 49-108325, October (1974).

[55] J.D. Mackenzie, in Ultrastructure Processing of Ceramics, Glasses and Composites, L.L. Hench and D.R. Ulrich, eds., Wiley, New York, 15 (1984).

[56] J. Wenzel, in Glass...Current Issue, A.F. Write and A.F. Dupuy, eds., Martinus Nijhojj, Dordrecht, Netherlands, 224 (1985).

[57] H. Dislich and P. Hinz, J. Non-Cryst. Solids, 48 (1982) 11.

[58] N.J. Arfsten, R. Kaufmann and H. Dislich, in Ultrastructure Processing of Ceramics, Glasses and Composites, L.L. Hench and D.R. Ulrich, eds., Wiley, New York, 189 (1984).

[59] H. Dislich, J. Non-Cryst. Solids, 73 (1985) 599.

[60] S.S. Kistler, Nature, 127 (1931) 742.

[61] J. Fricke, ed., Aerogels: Springer Proceedings in Physics, Vol. 6, Springer-Verlag, Heidelberg (1986).

[62] J. Phalippou, M. Prassas, J. Zarzycki, J. Non-Cryst. Solids 48 (1982) 17.

[63] M. Prassas, J. Phalippou, J. Zarzycki, Int. Conf. Glasses, 13th, Hamburg, Germany (1985).

[64] B.E. Yoldas, Bull. Am. Ceram. Soc. 54 (1975) 286.

[65] L.L. Hench, D.R. Ulrich, eds., Ultrastructure Processing of Ceramics Glasses and Composites, Wiley: New York, (1984).

[66] L.L. Hench, D.R. Ulrich, eds., Science of Ceramic Chemical Processing, Wiley: New York, (1986).

[67] J.D. Mackenzie, D.R. Ulrich, Eds. Ultrastructure Processing of Advanced Ceramics, Wiley: New York, (1988).

[68] D.R. Uhlmann, M. Weinberg, D.R. Ulrich, eds., Ultrastructure Processing IV, Wiley: New York, (1989).

[69] C.J. Brinker, D.E. Clark, and D.R. Ulrich, eds., Better Ceramics Through Chemistry, Elsevier: New York, (1984), Vol.32.

[70] C.J. Brinker, D.E. Clark, and D.R. Ulrich, eds., Better Ceramics Through Chemistry II, Vol. 73, Materials Research Society: Pittsburgh, PA (1986).

[71] C.J. Brinker, D.E. Clark, D.R. Ulrich, eds., Better Ceramics Through Chemistry III, Vol. 121, Materials Research Society: Pittsburgh, PA (1988).

[72] J. Zarzycki, ed., Glasses and Ceramics From Gels. J. Non-Cryst. Solids 1-3 (1986) 1-436.

[73] L.C. Klein, Sol-Gel Technology for Thin Films, Fibers Preforms, Electronics and Specialty Shapes, Noyes Publications: Park Ridge, NJ (1988).

[74] J. Zarzycki, J. Non-Cryst. Solids, 48 (1982) 105.

[75] J. Phalippou, T. Woignier and J. Zarzycki, in Ultrastructure Processing of Ceramics, Glasses and Composites, L.L. Hench and D.R. Ulrich, eds., Wiley, New York, 70 (1984).

[76] L.J. White, Ind. Engng. Chem. Ind. Edn, 51 (1959) 232.

[77] R.A. Assink and B.D. Kay, in Better Ceramics Through Chemistry, C.J. Brinker, D.E. Clark, and D.R. Ulrich, eds., Elsevier North-Holland, New York, 301 (1984).

[78] K.D. Keefer, in Science of Ceramic Chemical Processing, L.L. Hench and D.R. Ulrich, eds., Wiley, New York, 131 (1986).

[79] D.W. Schaefer and K.D. Keefer, in Better Ceramics Through Chemistry, C.J. Brinker, D.E. Clark, and D.R. Ulrich, eds., Elsevier North-Holland, New York, 1 (1984).

[80] A.V. Kiselev, Kolloidn. Zh., 2 (1936) 17.

[81] P.C. Carmen, Trans, Faraday Soc., 36 (1940) 964.

[82] A.V. Kiselev, Trans, Faraday Soc., 52 (1971) 14

[83] D. Barby, in Characterization of Powder Surfaces, G.D. Parfitt and K.S.W. Sing, eds., Academic Press, New York, 353 (1976).

[84] C. Okkerse, in Physical and Chemical Aspects of Adsorbents and Catalysts, B.G. Linsen, ed., Academic Press, New York, 214 (1970).

[85] M.L. Hair, Infrared Spectroscopy in Surface Chemistry, Dekker, New York, 79 (1967).

[86] H.P. Boehm, Angew. Chem., 5 (1966) 533.

[87] H.P. Boehm, Adv. Catal., 16 (1966) 226.

[88] C.J. Brinker, E.P. Roth, D.R. Tallant and G.W. Scherer, in Science of Ceramic Chemical Processing, L.L. Hench and D.R. Ulrich, eds., Wiley, New York, 37 (1986).

[89] C.J. Brinker, W.D. Drotning, and G.W. Scherer, in Better Ceramics Through Chemistry, C.J. Brinker, D.E. Clark, and D.R. Ulrich, eds., Elsevier North-Holland, New York (1984).

[90] G.W. Scherer and J.C. Luong, J. Non-Cryst. Solids, 63 (1984) 163.

[91] M.D. Sacks and T.Y. Tseng, J. Am. Ceram. Soc. 67 (1984) 532.

[92] L.L. Hench and J.K. West, Chem. Reviews, 90 (1990) 33.

[93] C.J. Brinker and G.W. Scherer, Sol-Gel Science, Academic Press, New York (1990).

[94] C.J. Brinker and G.W. Scherer, J. Non-Cryst. Solids, 70 (1985) 301.

[95] E.J.A. Pope and J.D. Mackenzie, J. Non-Cryst. Solids, 87 (1986) 185.

[96] W.L. Vasconcelos, Topological Evolution and Properties of Sol-Gel Silica Monoliths, Ph.D. Dissertation, University of Florida, Gainesville, FL (1989).

[97] R.K. Iler, in Science of Ceramic Chemical Processing, L.L. Hench and D.R. Ulrich, eds., Wiley, New York, 3 (1986).

[98] J.L. Nogues, C. Balaban, M.V. Moreshead and R.S. Sheu, in Advanced Ceramics, W.P.E. Longo, S.N. Monteiro and J.D. Filho, eds., Florida-Brazil Institute, Rio de Janeiro, 51 (1989)

[99] T. Tanaka, Sci. Amer., 244 (1981) 124.

[100] G. Orcel and L.L. Hench, in Science of Ceramic Chemical Processing, L.L. Hench and D.R. Ulrich eds., Wiley, New York, 224 (1986).

[101] S.A. Khan, E.M. Rabinovich, R.K. Prudhomme, M.J. Sammon and N.J. Kopylor, in Better Ceramics Through Chemistry III, Vol. 121, C.J. Brinker, D,E. Clark and D.R. Ulrich, eds., Materials Research Society, Pittsburgh, PA, 73 (1988).

[102] P.J. Flory, in High Molecular Weight Organic Compounds, (Frontiers in Chemistry), R.E. Burk and O. Grummitt, eds., Vol. VI, Interscience Publishers, New York, 211 (1949).

[103] P.J. Flory, Fundamental Principles of Condensation Polymerization, Chemical Reviews, 39 (1946) 137.

[104] G.W. Scherer, J. Non-Cryst. Solids, 73 (1985) 661.

[105] G.W. Scherer, in Better Ceramics Through Chemistry III, Vol. 121, C.J. Brinker, D.E. Clark and D.R. Ulrich, eds., Materials Research Society, Pittsburgh, PA, 179 (1988).

[106] J. Zarzycki, in Glass...Current Issues, A.F. Wright and J. Dupuy, eds., Martinus Nijhoff Publishers, Boston, 203 (1985).

[107] G.F. Wang, Thermal Stability of the Porous Gel-Silica, M.S. Thesis, University of Florida, Gainesville, FL (1988).

[108] T.K. Sherwood, Ind. Eng. Chem., 21 (1929) 12.

[109] T.K. Sherwood, Ind. Eng. Chem., 22 (1930) 132.

[110] T.K. Sherwood, Ind. Eng. Chem., 21 (1929) 976.

[111] R.B. Keey, Drying Principles and Practice, Pergamon Press, New York (1972).

[112] A.S. Mujumdar, ed., Advances in Drying, Hemisphere, New York, Vol. 1 (1980).

[113] A.S. Mujumdar, ed., Advances in Drying, Hemisphere, New York, Vol. 2 (1983).

[114] F. Moore, Trans. Brit. Ceram. Soc., 60 (1961) 517.

[115] S. Whitaker, Adv. Heat Transfer, 13 (1977) 119.

[116] A.R. Cooper, in Science of Ceramic Processing Before Firing, G. Onoda and L.L. Hench, eds., Wiley, New York 261 (1978).

[117] R.W. Ford, Ceramics Drying, Pergamon, New York (1988).

[118] G.W. Scherer, J. Non-Cryst. Solids, 100 (1988) 77.

[119] G.W. Scherer, J. Non-Cryst. Solids, 87 (1986) 199.

[120] G.W. Scherer, J. Non-Cryst. Solids, 91 (1987) 83.

[121] G.W. Scherer, J. Non-Cryst. Solids, 91 (1987) 101.

[122] G.W. Scherer, J. Non-Cryst. Solids, 92 (1987) 122.

[123] G.W. Scherer, J. Non-Cryst. Solids, 89 (1987) 217.

[124] T. Kawaguchi, J. Jura, N. Taneda, H. Hishikura and Y.J. Kokubu, J. Non-Cryst. Solids, 82 (1986) 50.

[125] R.K. Dwivedi, J. Mater. Sci. Lett., 5 (1986) 373.

[126] J. Zarzycki, in Science of Ceramic Chemical Processing, L.L. Hench and D.R. Ulrich, eds., Wiley, New York, 21 (1986).

[127] M.J.R. Wilson, Drying Kinetics of Pure Silica Xerogels, M.S. Thesis, University of Florida, Gainesville, FL (1989).

[128] M.J.R. Wilson and L.L. Hench, Proceedings of 4th International Conference on Ultrastructure Processing of Ceramics, Glasses, and Composites, Tucson, AZ, (1989).

[129] S. Liu and L.L. Hench, in Chemical Processing of Advanced Material, L.L. Hench and J.K. West, eds., Wiley, New York (in press).

[130] C.J. Brinker, G.W. Scherer and E.P. Roth, J. Non-Cryst. Solids, 72 (1985) 345.

[131] G.W. Scherer, C.J. Brinker and E.P. Roth, J. Non-Cryst. Solids, 72 (1985) 369.

[132] F. Orgaz-orgaz, J. Non-Cryst. Solids, 100 (1988) 115.

[133] T. Tseng and J. Yu, J. Mater. Sci., 21 (1986) 3615.

[134] I. Matsuyama, K. Susa, S. Satoh, and T. Suganuma, Ceramic Bull., 63 (1984) 1408.

[135] P.F. James, J. Non-Cryst. Solids, 100 (1988) 93.

[136] L.L. Hench and S.H. Wang, Phase transformations, 24-26 (1990) 785.

[137] B.E. Yoldas, J. Non-Cryst. Solids, 63 (1984) 145.

[138] M. Yamane and S. Okano, J. Japan Ceram. Soc., 87 (1979) 434.

[139] M.G. Voronkov, V.P. Mileshkevich, and Y.A. Yuzhelevski, The Siloxane Bond, Consultants Bureau, New York (1978).

[140] R. Aelion, A. Loebel, and F. Eirich, J. Am. Chem. Soc., 72 (1950) 5705-5712.

[141] R. Aelion, A. Loebel, and F. Eirich, Recueil Travaux Chimiques, 69 (1950) 61.

[142] H. Schmidt, A. Kaiser, M. Rudolph, and A. Lentz, in Science of Ceramic Chemical Processing, L.L. Hench and D.R. Ulrich, eds., Wiley, New York, 87 (1986).

[143] M. Prassas and L.L. Hench, in Ultrastructure Processing of Ceramics, Glasses and Composites, L.L. Hench and D.R. Ulrich, eds., Wiley, New York, 100 (1984).

[144] E. Elias, Pore Size Effects on the Thermal Stability of Sol-Gel Derived Silica Monoliths, M.S. Thesis, University of Florida, Gainesville, FL (1989).

[145] R.J.P. Corriu and J.C. Young, in The Chemistry of Organic Silicon Compounds, S. Patai and Z. Rappoport, eds., Wiley, New York, 1241 (1989).

[146] K.A. Andrianov, Metal Organic Polymers, Wiley, New York (1965).

[147] R.J.P. Corriu, D. LeClercq, A. Vioux, M. Pauthe, and J. Phalippou in Ultrastructure Processing of Advanced Ceramics, J.D. Mackenzie and D.R. Ulrich, eds., Wiley, New York, 113 (1988).

[148] J. Zarzycki, M. Prassas and J. Phalippou, J. Mater. Sci., 17 (1982) 3371.

[149] W. Vasconcelos, R.T. DeHoff and L.L. Hench, in Proceedings of the 4th International Conference on Ultrastructure Processing of Ceramics, Glasses and Composites, Tucson, AZ (1989).

[150] L.W. Kels, N.J. Effinger and S.M. Melpolder, J. Non-Cryst. Solids, 83 (1986) 365.

[151] T.W. Zerda, I. Artaki and J.J. Jonas, J. Non-Cryst. Solids, 81 (1986) 365.

[152] B.E. Yoldas, J. Mater. Sci., 21 (1986) 1087.

[153] Z.Z. Vysotskii and D.N. Strazhesko, in Adsorption and Absorbents, No. 1, D.N. Strazhesko, ed., Wiley, New York, 55 (1973).

[154] Y.P. Klimentova, L.F. Kiricheko and Z.Z. Vysotaskii, Ukr. Khim. Zh. 26 (1970) 49 (Eng. Trasl.).

[155] E.G. Acker, J. Colloid Interface Sci., 32 (1970) 41.

[156] T.P. Ponomareva, S.I. Kontorovich, M.I. Chekanov and E.D. Shchukin, Koll. Zh. 46 (1984) 118 (Eng. Trasl.).

[157] G.W. Scherer, S.A. Pardenek and R.M. Swiatek, J. Non-Cryst. Solids, 107 (1988) 14.

[158] S.A. Pardenek, J.W. Flemming and L.C. Klein, in Ultrastructure Processing of Advanced Ceramics, J.D. Mackenzie and D.R. Ulrich, eds., Wiley, New York, 379 (1988).

[159] J. Dumas, J.F. Quinson, C. Bovier, S. Baza and J. Serughetti, J. Non-Cryst. Solids, 82 (1986) 220.

[160] J.K. West, R. Nickles and G. LaTorre, in Better Ceramics Through Chemistry III, Vol. 121, C.J. Brinker, D.E. Clark and D.R. Ulrich, eds., Mat. Res. Soc., Pittsburgh, PA, 219 (1988).

[161] D.N. Strazhesko, ed., Adsorption and Adsorbents, Vol. 1, Wiley, New York (1973).

[162] R.Y. Sheifain, O.P. Stas, and I.E. Neimark, Kolloidn. Zh., 27 (6), 916 (1965). (Chem. Abstr. 64,4309c)

[163] C.J.G. van der Grift, J.W. Geus, H. Barten, R.G.I. Leferink, J.C. van Miltenburg, and A.T. den Ouden, in Characterization of Porous Solids, Elsevier, Amsterdam, 619 (1988).

[164] C. Okkerse and J. H. de Boer, in Reactivity of Solids, J. H. de Boer, ed., Elsvier, Amsterdam, 240 (1960).

[165] B.S. Girgis, Z. Phys. Chem., Frankfurt, 83 (1973) 75.

[166] E.E. Jenkins and A.B. Schwatz (Mobil Oil Corp.), Ger. 1,266,742, (1968) (Chem. Abstr. 69,61810k)

[167] I.E. Neimark and I.B. Slinyakova, Kolloidn. Zh., 18 (1956) 219.

[168] C.J. Brinker and G.W. Scherer, in Ultrastructure Processing of Ceramics, Glasses and Composites, Wiley, New York, 43 (1984).

[169] H.H. Sisler, R.D. Dresdner and W.T. Mooney Jr., Chemistry, A Systematic Approach, Oxford University Press, New York (1980).

[170] J.H. de Boer and J.M. Vleeskens, Koninkl. ned. Akad. Wet., Proc., B60 (1957) 23, 45, 54.

[171] J.H. de Boer and J.M. Vleeskens, Koninkl. ned. Akad. Wet., Proc., B61 (1958) 2, 85.

[172] K.R. Lange J. Colloid Sci., 20 (1965) 231.

[173] I. Langmuir, J. Amer. Chem. Soc., 40 (1918) 1368.

[174] S. Brunauer, The Adsorption of Gases and Vapors, Physical Adsorption, Vol. 1, Princeton University Press, Princeton, NJ (1945).

[175] S. Brunauer and P.H. Emmett, J. Am. Chem. Soc., 57 (1935) 1754.

[176] S. Brunauer, P.H. Emmett, and E. Teller, J. Am. Chem. Soc., 60 (1938) 309.

[177] S. Lowell and J.E. Schields, Powder Surface Area and Porosity, 2nd ed., Champion and Hall, London (1984).

[178] E.P. Barrett, L.G. Joyner and P.P. Halenda, J. Amer. Chem. Soc., 73 (1951) 373-380

[179] M.M. Dubinin, J. Colloid Interface Sci., 23 (1967) 487.

[180] A.V. Kiselev and Y.A. Eltekov, World Congress on Surface Activity, Vol. II, Butterworths, London, (1957) 228.

[181] S. Lowell, J.E. Shields, G. Charalambous and J. Manzione, J. Colloid Interface Sci., 86 (1982) 191.

[182] J.H. deBoer, in The Structure and Properties of Porous Materials, D.H. Everett and F.S. Stone, eds. Butterworths, London, 68 (1958).

[183] V.W. McBain, J. Amer. Chem. Soc., 57 (1935) 699.

[184] J.C.P. Broekhoff and B.G. Linden, in Physical and Chemical Aspects of Adsorbents and Catalysts, B.G. Linsen, ed., Academic Press, London, 1 (1970).

[185] W.B. Spencer Jr., Determination of the Porous Properties of Some Silica Gels, M.S. Thesis, University of Pittsburgh, Pittsburgh, PA (1950).

[186] B.F. Roberts, Proc. 145th National Meeting of the Amer. Chem. Soc., New York (September, 1963).

[187] S. Brunauer, R.Sh. Mikhail, and E.E. Bodor, J. Colloid and Interface Sci., 24 (1967) 451.

[188] R.Sh. Mikhail, S. Brunauer, and E.E. Bodor, J. Colloid and Interface Sci., 26 (1968) 54.

[189] W. Cao, R. Gerhardt, and J.B. Watchman Jr., J. Am. Ceram. Soc., 71 (1988) 1108.

[190] S.P. Mukherjee, J.F. Cordaro, and J.C. Debsikdar, Adv. Ceram. Mater., 3 (1988) 463.

[191] Micropycnometer Operators Manual, Quantachrome Corp., Syosset, New York, (1984).

[192] G.E. Deiter, Mechanical Metallurgy, 3rd ed., McGraw-Hill, New York, (1986).

[193] J.D.F. Ramsay and B.O. Booth, J. Chem. Soc., Faraday Trans., 79 (1983) 173.

[194] S. Brunauer, L.S. Deming, W.S. Deming, E. Teller, J. Amer. Chem. Soc., 62 (1940) 1723.

[195] B.G. Linsen, ed., Physical and Chemical Aspects of Adsorbents and Catalysts, Academic Press, London (1970).

[196] R.M. Barrer, N. McKenzie, and J.S.S. Reay, J. Colloid Sci., 11 (1956) 479.

[197] J.H. de Boer, Angew. Chem., 70 (1958) 383.

[198] A. Wheeler, Catalysis, 2 (1955) 105.

[199] R.T. DeHoff, in Encyclopedia of Materials Science and Engineering, M.B. Bever, ed., Pergamon, Oxford, UK (1986) 4633.

[200] R.T. DeHoff, in Quantitative Microscopy, R.T. DeHoff and F.N. Rhines, eds., (McGraw-Hill, New York (1968) 291.

[201] D.J. Struik, Lectures on Classical Differential Geometry, Addison-Wesley, Cambridge, UK (1950).

[202] J.W. Cahn, Trans AIME, 239 (1967) 611.

[203] R.T. DeHoff, Trans. AIME, 239 (1967) 617.

[204] J.E. Hilliard, in Quantitative Microscopy, R.T. DeHoff and F.N. Rhines, eds. McGraw-Hill, New York, 45 (1968).

[205] E.E. Underwood, in Quantitative Microscopy, R.T. DeHoff and F.N. Rhines, eds., McGraw-Hill, New York, 77 (1968).

[206] F.N. Rhines, R.T. DeHoff and J. Kronsbein, A Topological Study of the Sintering Process, Final Report for the U.S. Atomic Energy, Commission, University of Florida, Gainesville, FL (1969).

[207] E.E. Underwood, Quantitative Stereology, Addision-Wesley, Reading, MA (1970).

[208] F.N. Rhines, Microstructology, Riederer-Verlag, Stuttgart (1986).

[209] F.N. Rhines, Plansee Pro., 3rd Seminar, Reutte, Tyrol, Austria (1958) 58.

[210] M.D. Sacks and R.S. Sheu, In Science of Ceramic Chemical Processing, L.L. Hench and D.R. Ulrich, eds., Wiley, New York, 102 (1986).

[211] H.A. Benesi and A.C. Jones, J. Phys. Chem., 63 (1957) 179-182.

[212] J.H. Anderson Jr. and K.A. Wickersheim, Surface Science, 2 (1964) 252.

[213] J.B. Peri, J. Phys. Chem., 70 (1966) 2937.

[214] N.W. Cant and L.H. Little, Canadian Journal of Chemistry, 42 (1964) 802.

[215] N.W. Cant and L.H. Little, Canadian Journal of Chemistry, 43 (1965) 1252.

[216] M.L. Hair and I.D. Chapman, J. Amer. Ceram. Soc., 49 (1966) 651.

[217] T.H. Elmer, I.D. Chapman and M.E. Nordberg, J. Phys. Chem., 66 (1962) 1517.

[218] G.B. Alexander, E.C. Broge and R.K. Iler, U.S. Patent 2,765,242 (Du Pont), (1956).

[219] E.M. Rabinovich, J. Non-Cryst. Solids, 71 (1985) 187.

[220] L.P. Davis and L.W. Burggraf, in Science of Ceramic Chemical Processing, L.L. Hench and D.R. Ulrich, eds., Wiley, New York, 400 (1986).

[221] L.P. Davis and L.W. Burggraf, in Ultra Structure Processing of Advanced Ceramics, J.D. Mackenzie and D.R. Ulrich, eds., Wiley, New York, 367 (1988).

[222] L.W. Burggraf and L.P. Davis, In Better Ceramics Through Chemistry II, Vol.73, C.J. Brinker, D.E. Clark and D.R. Ulrich, eds., Materials Research Society: Pittsburgh, PA, 529 (1986).

[223] J.J.P. Stewart, Quantum Chemistry Program Exchange, Program 455, Department of Chemistry, Indiana University, Bloomington, IN.

[224] M.J.S. Dewar, W.J. Theil, Am. Chem. Soc. 99 (1977) 4899.

[225] M.J.S. Dewar, E. Healy, Organometallics, 1 (1982) 1705.

[226] L.W. Burggraf, L.P. Davis and M.S. Gordon, in Proceedings of the 4th Ultrastructure Processing of Ceramics, Glasses and Composites, Tucson, AZ (1989).

[227] J.K. West and S. Wallace, in Mat. Res. Soc. Symp. Proc., Vol. 180, Materials Research Society, Pittsburgh, PA 255 (1990).

[228] J.K. West and S. Wallace, in Ceramic Transactions, Vol. 19, M.D. Sacks, ed., Am. Ceram. Soc., Westerville, OH, 183 (1991).

[229] L.L. Hench and J.K. West, Principles of Electronic Ceramics, Wiley, New York, 1990.

[230] A.G. Sharpe, Inorganic Chemistry, Longman, New York, 79 (1986).

[231] P.W. Atkins, Physical Chemistry, 3rd Ed., Freeman, New York, 821 (1986).

[232] T.W.G. Solomons, Organic Chemistry, 2nd Ed., Wiley, New York, 78 (1980).

[233] R.H. Petrucci, General Chemistry, Principles and Modern Applications, Third Edition, MaCmillan Publishing, New York, 215 (1982).

[234] T. Moeller, J.C. Bailar, J. Kleinberg, C.O. Guss, M.E. Castellion and C. Metz, Chemistry, with Inorganic Qualitative Analysis, 2nd Ed., Academic Press, New York, 264 (1984).

[235] S. Wallace, Porous Silica Gel Monoliths: Structural Evolution and Interactions with Water, Ph.D. Dissertation, University of Florida, Gainesville, FL (1991).

[236] R. Reisfeld, Mater. Sci. Eng. 71 (1985) 375.

[237] R. Reisfeld and C.K. Jorgensen, Structure and Bonding, 69 (1988) 63.

[238] L.A. Lee and R.A. Robb, IEEE J. Quantum Electronics, QE-16, 7 (1980) 777.

[239] D. Avnir, D. Levy and R. Reisfeld, J. Phys. Chem. 88 (1984) 5956.

[240] D. Avnir, V. R. Kaufman and R. Reisfeld, J. Non-Cryst. Solids, 74 (1985) 395.

[241] R. Reisfeld, J. Non-Cryst. Solids, 121 (1990) 254.

[242] R. Reisfeld, Sol-gel Optics, SPIE International Symposium on Optical & Optoelectronic Applied Science & Technology. San Diego, CA, July 8-13 (1990).

[243] E.J.A. Pope and J.D. Mackenzie, Incorporation of Organic Dyes in Polymer/Oxide Composites, MRS Bulletin, March 17/May 15, 29 (1987).

[244] B. Dunn, J.D. Mackenzie, J.I. Zink, O.M. Stafsudd, Solid-State Tunable Lasers Based on Dye-Doped Sol-Gel Materials, SPIE Sol-Gel Optics Conf., San Diego, July (1990).

[245] T.A. King, SPIE High Power Solid State Laser Conf., Vol. 1277 TheHague, the Netherlands (1990).

[246] A.J. Berry and T.A. King, Characterization of Doped Sol-Gel Derived Silica Hosts for Use in Tunable Glass Lasers, J. Phys. D: Appl. Phys. 22 (1989) 1419, Printed in the UK.

[247] P.N. Prasad, F.E. Karasz, Y. Pang and C.J. Wung, U.S. Patent Appl. #312132.

[248] J.L. Nogues, S. Majewski, J.K. Walker, M. Bowen, R. Wojcik and W.V. Moreshead, J. Am. Ceram. Soc., 71 (1988) 1159.

[249] W. Koecher, Solid-State Laser Engineering, Springer Series in Optical Sciences, Springer-Verlag, Berlin (1988).

[250] R. Reisfeld, J. Phys. (Paris) Colloque, 48 C7 (1987) 423.

[251] M. Eyal, R. Gvishi and R. Reisfeld, J. Phys. (Paris) Colloque, 48 C7 (1987) 471.

[252] V. Ya. Davydov, A.V. Kiselev and L.T. Zhuravler, Trans. Faraday Soc. 60 (1964) 2254.

[253] J. Kunetz and L.L. Hench, in Chemical Processing of Advanced Material, L.L. Hench and J.K. West, eds., Wiley, New York (in press).

[254] L. Nikiel and T. W. Zerda, Adsorption of Pyridine on Silica Gels, submitted to J. Phys. Chem. (in press).

BIOGRAPHICAL SKETCH

Shuyuan Liu was born May 9, 1945, in Shanghai, China. He attended high school in Shanghai. He received a Bachelor of Science degree in materials science and engineering in 1967 and a Master of Science degree in materials science and engineering in 1982 from the East China Institute of Chemical Technology. In 1987, he entered the University of Florida to pursue a Doctor of Philosophy in the Department of Materials Science and Engineering.

I certify that I have read this study and that in my opinion it conforms to acceptable standards of scholarly presentation and is fully adequate, in scope and quality, as a dissertation for the degree of Doctor of Philosophy.

Larry Hench

Larry L. Hench, Chair
Graduate Research Professor
of Materials Science and
Engineering

I certify that I have read this study and that in my opinion it conforms to acceptable standards of scholarly presentation and is fully adequate, in scope and quality, as a dissertation for the degree of Doctor of Philosophy.

David E Clark

David E. Clark
Professor of Materials
Science and Engineering

I certify that I have read this study and that in my opinion it conforms to acceptable standards of scholarly presentation and is fully adequate, in scope and quality, as a dissertation for the degree of Doctor of Philosophy.

Fereshteh Ebrahimi

Fereshteh Ebrahimi
Associate Professor of
Materials Science and
Engineering

I certify that I have read this study and that in my opinion it conforms to acceptable standards of scholarly presentation and is fully adequate, in scope and quality, as a dissertation for the degree of Doctor of Philosophy.

E Dow Whitney

E. Dow Whitney
Professor of Materials
Science and Engineering

I certify that I have read this study and that in my opinion it conforms to acceptable standards of scholarly presentation and is fully adequate, in scope and quality, as a dissertation for the degree of Doctor of Philosophy.

Kenneth B Wagener

Kenneth B. Wagener
Associate Professor of
Chemistry

This dissertation was submitted to the Graduate Faculty of the College of Engineering and to the Graduate School and was accepted as partial fulfillment of the requirements for the degree of Doctor of Philosophy.

December, 1991

Winfred M. Phillips
Dean, College of Engineering

Madelyn M. Lockhart
Dean, Graduate School